EFFECT OF CONCENTRATION DIFFERENCE ON THE RATES OF TRANSFER OF URANYL NITRATE BETWEEN WATER AND TBP

By

DALE EDWARD BUSH

Bachelor of Science in Chemical Engineering
Michigan Technological University
Houghton, Michigan
1959

Master of Science in Nuclear Engineering
Michigan Technological University
Houghton, Michigan
1960

Submitted to the Faculty of the Graduate College
of the Oklahoma State University
in partial fulfillment of the requirements
for the Degree of
DOCTOR OF PHILOSOPHY
May, 1966

OKLAHOMA
STATE UNIVERSITY
LIBRARY

NOV 8 1966

EFFECT OF CONCENTRATION DIFFERENCE ON THE

RATES OF TRANSFER OF URANYL NITRATE

BETWEEN WATER AND TBP

Thesis Approval:

John B. West
Thesis Adviser

R. N. Maddox

Kenneth J. Beel

Joyce E. Moore

J. H. Boggs
Dean of the Graduate College

621478

PREFACE

The effect of concentration difference and concentration level on the rates of transfer of uranyl nitrate between water and TBP has been investigated in a stirred cell. The effect of the organic phase stirring rate was greater than that reported in similar studies. However, if the energy transmitted from the aqueous phase stirring was considered, the mass transfer coefficient varied with the square root of the organic phase Reynolds number.

The overall organic phase mass transfer coefficients varied with the concentration driving force and the concentration level of the phase into which the uranyl nitrate was transferred.

The interfacial tension of the uranyl nitrate-water-TBP system indicates that spontaneous interfacial turbulence is not promoted in the system.

I wish to express my sincere thanks to Dr. J. B. West for his guidance in this work and for his continual patience during the time I spent at the University. I also wish to thank Dr. R. N. Maddox for his advice and encouragement.

It is a pleasure to acknowledge the assistance of Mr. Eugene McCroskey, School of Chemical Engineering, for helping in the construction and operation of the mass transfer cell. The great amount of help and the many ideas contributed by my fellow graduate students, particularly Mr. J. Browning Finley, is greatly appreciated.

I wish to express my gratitude for the financial support of the Atomic Energy Commission, under contract AT (11-1) - 846, during my years of graduate study at Oklahoma State University.

TABLE OF CONTENTS

Chapter		Page
I.	INTRODUCTION	1
II.	LITERATURE REVIEW	3
	TBP as an Extracting Agent	3
	Stirred Mass Transfer Cells	5
	Transfer of Uranyl Nitrate Across the Water -TBP Interface	10
	Interfacial Turbulence	12
III.	THEORY	14
	Two-Film Theory of Interphase Mass Transfer	14
	Interfacial Resistance	23
	Interfacial Mass Transfer in Stirred Cells	25
	Interfacial Turbulence	33
IV.	EXPERIMENTAL APPARATUS	36
	Stirred Mass Transfer Cell	36
	Constant Temperature Bath	39
V.	EXPERIMENTAL PROCEDURE	42
	Purification of TBP	42
	Analytical Determination of Uranyl Nitrate	42
	Equilibrium Distribution of Uranyl Nitrate between Water and 30% TBP in Amsco	44
	Unsteady-State Mass Transfer	44
	Steady-State Mass Transfer	45
	Analog Computer Simulation of Mass Transfer Cell	46
VI.	RESULTS AND DISCUSSION	48
	Equilibrium Distribution of Uranyl Nitrate	48
	Benzoic Acid Extraction	48
	Unsteady-State Transfer of Uranyl Nitrate Between Water and TBP	54
	Effect of Stirring Rates on Steady-State Transfer of Uranyl Nitrate	62

Chapter Page

Effect of Driving Force on the Transfer of Uranyl Nitrate Between Water and TBP. 68
Interfacial Tension of the Uranyl Nitrate-Water -TBP System. 85
Analog Simulation of the Stirred Mass Transfer Cell. 89
Accuracy and Experimental Error. 89

VII. CONCLUSION AND RECOMMENDATIONS. 92

BIBLIOGRAPHY 95

NOMENCLATURE. 98

APPENDIX A. 100

Physical Properties of Uranyl Nitrate Solutions. 101

APPENDIX B. 110

Unsteady-State Mass Transfer Data. 111
Steady-State Mass Transfer Data. 119

APPENDIX C. 122

Calculated Quantities. 123
Analog Computer Program. 127

APPENDIX D. 128

Mass Transfer Cell Detailed Drawings. 129

LIST OF TABLES

Table		Page
I.	Physical Properties of TBP.	6
II.	Effect of Stirring Rates on Film Coefficients.	29
III.	Flow Diagram Equipment List.	41
IV.	Physical Properties of Amsco Odorless Mineral Spirits.	43
V.	Unsteady-State Transfer of Benzoic Acid.	52
VI.	Steady-State Transfer of Benzoic Acid.	53
VII.	Geometric Comparison of Cell with Burger's Cell.	55
VIII.	Unsteady-State Mass Transfer Coefficients for Uranyl Nitrate from Aqueous Solutions into 30% TBP-Amsco.	59
IX.	Steady-State Transfer of Uranyl Nitrate from Water to TBP.	70
X.	Molar Flux for Transfer of Uranyl Nitrate from Water to TBP	75
XI.	Molar Flux for Transfer of Uranyl Nitrate from TBP to Water.	84
XII.	Unsteady-State Point Transfer Coefficients.	86
XIII.	Experimental Data-Densities of 30% TBP Uranyl Nitrate Solutions.	102
XIV.	Experimental Data-Viscosities of 30% TBP Uranyl Nitrate Solutions.	104
XV.	Experimental Data-Distribution of Uranyl Nitrate between Water and 30% TBP in Amsco.	107
XVI.	Experimental Data-Interfacial Tension of the Water-Uranyl Nitrate-30% TBP System.	108

Table		Page
XVII.	Uranyl Nitrate Activity Coefficients.	109
XVIII.	Experimental Data-Unsteady -State Transfer of Benzoic Acid.	111
XIX.	Experimental Data Effect of Stirring Rates on Transfer of Benzoic Acid.	112
XX.	Experimental Data-Steady-State Transfer of Benzoic Acid.	113
XXI.	Experimental Data-Unsteady-State Transfer of Uranyl Nitrate A.	114
XXII.	Experimental Data-Unsteady-State Transfer of Uranyl Nitrate B.	117
XXIII.	Experimental Data-Steady-State Transfer of Uranyl Nitrate.	119
XXIV.	Calculated Results-Steady-State Transfer of Uranyl Nitrate.	123
XXV.	Calculated Results - Variation of Mass Transfer Coefficient with Molecular Diffusivity.	126

LIST OF FIGURES

Figure		Page
1.	Two Film Theory of Interphase Mass Transfer.	16
2.	Equilibrium Diagram.	17
3.	Solute Distribution in Turbulent Flow.	22
4.	Roll Cell.	34
5.	Mass Transfer Cell Flow Diagram.	40
6.	Distribution of Uranyl Nitrate Between Water and 30% Tributyl Phosphate in Amsco.	49
7.	Effect of Aqueous Phase Stirring Rate.	51
8.	Unsteady-State Transfer of Uranyl Nitrate as a First-Order Process.	56
9.	Steady-State Mass Transfer Coefficients	65
10.	Flow Patterns Across Interfacial Area.	67
11.	Effect of Driving Force on Mass Transfer Coefficient Divided by Kinematic Viscosity.	71
12.	Effect of Driving Force on Activity-Based Mass Transfer Coefficients.	73
13.	Effect of Driving Force on Activity-Based Mass Transfer Coefficient Divided by Kinematic Viscosity.	74
14.	Effect of Driving Force on Molar Flux.	76
15.	Effect of Driving Force on Mass Transfer Coefficient Divided by Kinematic Viscosity.	78
16.	Effect of Driving Force on Activity-Based Mass Transfer Coefficient.	79
17.	Effect of Driving Force on Activity-Based Mass Transfer Coefficient Divided by Kinematic Viscosity.	80

Figure Page

18a. Effect of Driving Force on $K_{os}/\nu Re_s^{2.8}$ for Transfer from Water to TBP. 81

18b. Effect of Driving Force on $K_{os}/\nu Re_s^{2.8}$ for Transfer from TBP to Water. 82

19. Effect of Aqueous Phase Concentration on Interfacial Tension of the $UO_2(NO_3)_2$-Water-TBP System. 88

20. Analog Computer Simulation of Mass Transfer Cell. 90

21. Effect of Concentration on the Density of Uranyl Nitrate Solutions. 103

22. Effect of Concentration on the Viscosity of Uranyl Nitrate Solutions. 105

23. Analog Computer Simulation Program. 127

24. Stirred Extraction Cell Schematic. 129

25. Cell Bottom Plate Design. 130

26. Cell Top Plate Design. 131

27. Upper Stirrer Bearing Design. 132

28. Fixed and Center Baffle Design. 133

29. Upper and Lower Stirrer Design. 134

LIST OF PLATES

Plate — Page

I. Stirred Mass Transfer Cell. 37

CHAPTER I

INTRODUCTION

At the present time the recovery of uranium from ores and from spent nuclear fuels is generally carried out by liquid-liquid extraction. The most commonly used organic solvent for uranium extraction is tributyl phosphate, TBP. The reaction governing the extraction is written below.

$$UO_{2(Aq)}^{++} + 2(NO_3)_{(Aq)}^{-} + 2TBP_{(org)} \rightleftarrows UO_2(NO_3)_2 \cdot 2TBP_{(org)}$$

Since the extraction of uranium by tributyl phosphate is of such great importance, it is desirable to obtain a better understanding of the process. There have been a few basic studies on the extraction of uranyl nitrate by tributyl phosphate; however, a disagreement has arisen among several of the investigators. Both Lewis (28) and Burger (8) found that in the unsteady-state transfer of uranyl nitrate across the water-TBP interface the transfer rate decreased with time. This decrease of transfer rate was proposed by Lewis (29) to be due to a buildup of an interfacial resistance. Chester (10) using a photographic photometric method of investigating the transfer process concluded that there is no interfacial resistance to transfer and the limiting step is diffusion towards or away from the interface.

In this study a modified Lewis-type stirred extraction cell was used

to investigate both unsteady and steady-state transfer of uranyl nitrate across the water-TBP interface. The results of the unsteady-state transfer were compared to the work performed by Burger (8). The effect of stirring rates was investigated under steady-state conditions. In addition the effect of driving force and concentration level on the mass transfer rate was investigated. The interfacial tension of the water-uranyl nitrate-TBP system was measured in order to predict if spontaneous interfacial turbulence should be observed in this system, according to the theory of Sternling and Scriven (49).

CHAPTER II

LITERATURE REVIEW

Tributyl Phosphate as an Extracting Agent

The recovery of uranium from various aqueous and acidic solutions became of great importance for the separation of uranium from other metallic elements for use in nuclear reactor fuels. In addition, uranium, after being used as a reactor fuel, accumulates fission products which poison the fuel and which must be separated from the uranium.

Although many methods have been investigated for the recovery of uranium, liquid-liquid extraction has become the principal method for separation of uranium from other metallic elements. McKay (37) studied the purification of uranyl nitrate between water and various organic solvents. He found that uranyl nitrate is substantially unionized in the organic phase for most solvents. In a review of the development of the Thorex process, Gresky (22) investigated tributyl phosphate as an extracting agent for both uranyl nitrate and nitric acid. Tributyl phosphate has become the most widely studied organic solvent for the extraction of uranyl nitrate. Alcock, et al., (3, 4, 5,) presented a series of articles on tributyl phosphate as an extracting agent for inorganic nitrates. They noted that with nitric acid tributyl phosphate forms the complexed compound $HNO_3 \cdot TBP$. They also presented a method for purification of tributyl phosphate. The purification of tributyl phosphate, prior to

use as an extracting agent, is necessary since it undergoes slow hydrolysis to form dibutyl and monobutyl phosphates, and butanol. Addition of very small concentrations of these hydrolysis products cause a significant increase in the uranium distribution coefficient. In their publication, Alcock et al., (4) concluded that inorganic nitrates are extracted by TBP in the neutral unionized form and the solute is always hydrated with TBP by a definite number of TBP molecules. Moore (39) proposed the mechanism of uranyl nitrate extraction by tributyl phosphate as follows.

$$UO_{2(Aq)}^{++} + 2NO_{3(Aq)}^{-} + 2TBP_{(org)} \rightleftharpoons UO_2(NO_3)_2 \cdot 2TBP \qquad (1)$$

The uranyl nitrate is complexed in the organic phase with two molecules of tributyl phosphate. Moore further concluded that the extraction of nitric acid involved the formation of a weak, one to one complex with TBP, and that HNO_3 is displaced by uranium in the organic phase due to the more stable uranium complex.

McKay (37) has proposed that the oxygen in the organic solvent acts as an electron donor for the formation of the uranyl nitrate complex. Collopy (14) found that the presence of anions which complex the uranyl ion in aqueous solutions has a detrimental effect on the uranium partition between water and TBP. In addition, Collopy (14) found that nitric acid present in the organic phase in excess of that in the complex exists as a solute.

Sato (48) studied the effect of temperature on the partition of uranyl nitrate between water and TBP. He also found that two molecules of nitric acid were displaced by one molecule of uranyl nitrate in the organic phase. There have been a number of investigations of the

distribution of uranyl nitrate between water and TBP containing different diluents (3, 7, 11, 22, 39, 46). The partition of uranyl nitrate has also been studied where various salting agents, HNO_3, $NaNO_3$, and $Al(NO_3)_3$, were present (5, 12, 15, 20, 48).

Burger and Forsman (9) found that the solubility of pure TBP in water is approximately 0.4 grams per liter at 25° C, and that the solubility decreases when the TBP is diluted with an inert substance which is insoluble in water. The solubility is higher than that which may be predicted by use of mole fractions. The solubility of water in pure TBP is 64 grams per liter (9). The solubility of water drops to 0.66 grams per liter in a pure paraffinic diluent. Burger and Forsman (9) found the solubility of water in 30% TBP in a paraffinic diluent to be 8.0 grams per liter. In another study, Burger (7) found that the distribution of uranyl nitrate varies only slightly with the different diluents normally used in liquid-liquid extraction of uranyl nitrate.

Robinson and Lin (45) have determined the activity coefficients of uranyl nitrate solutions at 25° C. from 0.1 molal to 5.5 molal by isopiestic vapor pressure measurements. Glueckauf, et al, (20) measured the activity coefficient of uranyl nitrate in the presence of sodium nitrate.

The physical properties of tributyl phosphate as reported by Flannery (18) are given in Table I.

Stirred Mass Transfer Cells

Recently several investigators have studied mass transfer across a liquid-liquid interface in stirred cells having a fixed interfacial area. Lewis (27) obtained the following correlation for individual mass transfer coefficients in a stirred mass transfer cell having a fixed annular

TABLE I

Physical Properties of Tributyl Phosphate

Chemical formula	$(C_4H_9)_3\ PO_4$
Molecular weight	266
Color	Water White
Odor	Mildly sweet
Refractive Index (20° C.)	1.4345
Viscosity	
25° C.	3.41 centipoises
85° C.	0.8 centipoises
Boiling point	
760 mm Hg	287° C.
15 mm Hg	173° C.
1 mm Hg	121° C.
Specific gravity at 25° C.	0.973
Freezing point	80° C.
Flash point, cleveland open cup	145° C.
Dielectric constant	7.97
Solubility in water at 25° C.	0.6 vol. %
Solubility of water in TBP at 25° C.	7 vol. %

interfacial area.

$$\frac{60k_1}{\overline{v}} = 6.76 \times 10^{-6}\left[Re_1 + \frac{\mu_2}{\mu_1} Re_2\right]^{1.65} + 1 \qquad (2)$$

where:

k_1 is the film mass transfer coefficient of phase 1

ν_1 is the kinematic viscosity of phase 1

Re_1 is the Reynolds number of phase 1

μ_1 is the viscosity of phase 1.

In later studies Lewis (27,28) measured the overall mass transfer coefficient of various solutes in his stirred cell. He found that in some instances, when a solute was transferred across a liquid-liquid interface, the experimental overall transfer coefficient did not agree with the transfer coefficient predictedby using his previously developed film transfer coefficient correlation. In these cases the experimental coefficient was generally lower than the theoretically predicted value. In order to test the concept of additivity of film resistances for interphase solute transfer between two liquids, Gordon and Sherwood (21) used a stirred cell with a fixed interfacial area. In Gordon and Sherwood's cell the stirrers were not independently adjustable as in the cell designed by Lewis.

The equations giving the overall mass transfer coefficients from the film transfer coefficients are given below.

$$\frac{1}{K_{os}} = \frac{1}{k_s} + \frac{m}{k_w} \qquad (3)$$

$$\frac{1}{K_{ow}} = \frac{1}{k_w} + \frac{1}{mk_1} \qquad (4)$$

where:

K_{os} is the overall mass transfer coefficient of phase s

K_{ow} is the overall mass transfer coefficient of phase w

k_s is the film mass transfer coefficient of phase s

k_w is the film mass transfer coefficient of phase w

m is the slope of the equilibrium relationship between phase s and phase w.

Since there was a disagreement between the experimental and predicted overall mass transfer coefficient, Lewis (27) postulated the difference might be due to an interfacial resistance to mass transfer. Lewis then defined this resistance, $1/k_r$, by the equation given below.

$$\frac{1}{k_r} = \frac{1}{K_{os}} - \frac{1}{k_s} + \frac{m}{k_w} \qquad (5)$$

where:

k_s and k_w are calculated from Lewis's film transfer coefficient correlation.

Blokker (6), using a stirred cell similar to the Lewis cell, studied the transfer of various solutes across liquid-liquid interfaces, and confirmed the interfacial resistance to transfer as reported by Lewis. An improved film transfer coefficient correlation was derived by Mayer (33) in his work using a stirred mass transfer cell.

$$\frac{k_1 L}{D} = 0.00316(Re_1 Re_2)^{1/2}\left(\frac{\mu_2}{\mu_1}\right)^{1.9}\left(0.6 + \frac{\mu_2}{\mu_1}\right)^{-2.9}(Sc)^{5/6} \qquad (6)$$

where:

L is the diameter of the stirrer

D_1 is the diffusivity of the solute in phase 1

μ_1 is the viscosity of phase 1

Sc_1 is the Schmidt number in phase 1, $\frac{\mu}{\rho D}$.

Mayer (34) also used his stirred mass transfer cell to study the effect of surfactants on mass transfer rates. He found that minute quantities of surface active material significantly reduces the mass transfer rate. Mayer concluded that the interfacial resistance concept may be explained by a surface clearing model on the basis of the hydrodynamics of the mass transfer process and the strength of the interfacial film.

McManamey (38) using a stirred cell, measured an interfacial resistance to mass transfer of inorganic nitrates between water and n-butanol and found that the interfacial resistance did not vary with the time of contact of the phases.

Olander (41) used a cell similar to Lewis's, to study nitric acid transfer between water and tributyl phosphate. Olander (41) developed a film mass transfer coefficient model for his cell which has the following form.

$$\frac{k}{v} Sc^{0.44} = 0.046 \left(\frac{\omega}{v}\right)^{0.67} \qquad (7)$$

where:

ω = stirrer speed in radians/sec

A hydrodynamic model of mass transfer was developed by Olander. This model predicted the mass transfer coefficient to be proportional

to the square root of the Reynolds number and the diffusivity raised to the 2/3 power. The model was shown to be unrealistic by Loosemore and Prosser (32). In order to bring the model into agreement with Loosemore and Prosser's data, Olander (44) modified the original model. Recently, Olander (43) studied the effect of the driving force on the transfer of nitric acid between water and tributyl phosphate. He found that the rate of transfer of nitric acid increased with decreasing driving force and that the data agreed with the Sternling and Scriven model of interfacial turbulence (49).

Transfer of $UO_2(NO_3)_2$ across the Water-TBP Interface

Lewis (29) in his studies of solute transfer across liquid-liquid interfaces investigated the transfer of uranyl nitrate across the water-tributyl phosphate interface. He found that the experimental mass transfer coefficients were initially higher than those predicted by his film transfer coefficient model, but after a short period of time an interfacial resistance to transfer appeared. Hahn (24) studied the transfer of uranyl nitrate across a fixed interface in a non-stirred piece of apparatus. He found that the transfer was initially higher than could be calculated from diffusion coefficients. Murdoch and Pratt (40) investigated the transfer of uranyl nitrate between water and methyl isobutyl ketone in a wetted wall column and found that the rate of transfer was partially determined by diffusion and partially by interfacial resistance. The aqueous phase film mass transfer coefficient was found to vary as the square of the uranium concentration. Murdoch and Pratt concluded that mass transfer rate was controlled by a third order chemical reaction at the interface.

Burger (8) has studied the transfer of uranyl nitrate across the water-tributyl phosphate interface in a stirred cell similar to the one used by Lewis. Burger's cell differed from that used by Lewis by having vertical baffling to improve mixing of the phases. He found that the rate of transfer was initially quite rapid but decreased as equilibrium was approached and that the extraction rate was dependent upon the degree of stirring of the phases and on the concentration of the transferring solute. Keish (26) using a very small cell with extremely fast stirring concluded that the transfer was chemical reaction controlled, with the formation of the uranyl nitrate-TBP complex in the organic phase the rate controlling step, and that there was no interfacial resistance to mass transfer.

Chester (10) studied the steady-state transfer of uranyl nitrate between water and tributyl phosphate and was able to obtain point analyses up to the 100 μ of the interface by using a photographic photometer. He concluded that there is no hindrance or interfacial resistance at the interface and that the kinetic data reported by other investigators are simply diffusion measurements in apparatus having various interfacial areas and degrees of mixing.

There is no general agreement concerning the mechanism of transfer of uranyl nitrate between water and TBP. Lewis (29) and Burger (8) found the transfer rate decreased with time. Burger attributed this decrease in transfer rate to a buildup of an interfacial resistance. Murdoch and Pratt (40) found evidence of an interfacial resistance and also concluded that the rate of transfer was controlled by a third order reaction. Keish (26) did not find an interfacial barrier, but concluded that the transfer rate was controlled by the formation of the uranyl nitrate-

TBP complex. Chester (10), on the other hand, could not find any evidence of either a slow chemical reaction at the interface or of an interfacial resistance.

Interfacial Turbulence

During his study of the transfer of uranyl nitrate between water and tributyl phosphate, Lewis (29) observed in some instances an interfacial turbulence occurred at the interface. This was particularly noticeable when the tributyl phosphate had been purified by distillation. In these cases the mass transfer coefficients were abnormally high. Sherwood and Wei (50) observed many liquid-liquid systems which demonstrated spontaneous emulsification and strong agitation of the interface even when there was no stirring of the phases.

Sternling and Scriven (49) presented a mathematical model, starting from the Navier-Stokes equation, which may qualitatively predict the occurrence of interfacial turbulence. The theory assumes the origin of the disturbance is due to random local variations of the interfacial tension with solute composition produced by eddy currents near the interface. This variation of interfacial tension along the interface causes a twitching of the interface which may either damp out or cause reinforcement of the initial disturbance. The conclusion is primarily dependent upon the ratio of the viscosities and the diffusivities of the two phases and the magnitude and sign of the variation of the interfacial tension with composition.

Olander (41), in his study of nitric acid transfer from water to tributyl phosphate, found the mass transfer coefficients to be higher than usual in the instance where the Sternling and Scriven model predicted

the occurrence of interfacial turbulence. It was recommended by Sternling and Scriven that experimenters report observations of the phase interface with their data and that the direction of transfer, and concentration level be noted. In addition, it was recommended that the viscosities, diffusivities, and the variation of interfacial tension with solute concentration be estimated or measured.

CHAPTER III

THEORY

In extraction of a solute across a liquid-liquid interface two insoluble phases are contacted to permit diffusion of the solute between the two phases. This process is more complicated than simple diffusion in liquids since diffusion occurs in both phases simultaneously. Furthermore, in order to properly interpret the process the equilibrium distribution of the solute must be employed.

At a fixed temperature a definite equilibrium exists where there is no net diffusion of the solute between the phases. The equilibrium relationship is generally shown graphically by plotting the equilibrium concentrations of one phase against the other phase. If the system is not in equilibrium, diffusion will occur in such a manner as to bring the system to equilibrium conditions.

Two-Film Theory

The most widely used theory of interphase mass transfer is the Whitman two-film theory (52). Consider a solute, A, diffusing across the interface from phase W to phase S. Since A is diffusing from phase W to S, concentration gradients must exist in each phase in the direction of diffusion. The theory assumes that the concentration gradient must overcome a diffusional resistance within a thin laminar layer

at the interface in both phases. Figure 1 shows the concentration gradients in terms of the distance through each phase.

The average concentration of A in the bulk of phase w is C_w and falls to C_{wi} at the interface. In phase s the concentration falls from C_{si} at the interface to C_s in the bulk of the liquid. A further postulate of the two-film theory is that the two phases are in equilibrium at the interface and that there is no resistance to solute transfer at the interface.

It should be noted that there is a point of discontinuity of the concentration gradient at the interface, and that the discontinuity would still exist even if the two phases were in complete equilibrium. This point of discontinuity is due to the fact that for two phases in equilibrium the concentrations are not equal, whereas the chemical potential of the two phases are equal. Therefore, if chemical potentials are used instead of concentration units, a continuous gradient would exist at the interface.

The concentrations ~~discussed~~ discussed above may be represented by points on the equilibrium diagram (Figure 2). The coordinates of point B are the average bulk solute concentrations in the two phases while the coordinates of point C are the concentrations of the solute at the interface.

When the system is at steady-state, a mole of solute A diffuses into the body of phase S for every mole of A which diffuses from the bulk of phase W to the interface. Letting N represent the moles of solute transferred per unit time per unit area and letting the driving force be represented by the departure from equilibrium, a mass transfer rate equation may be written for each phase and equated.

$$N_A = k_w(C_w - C_{wi}) = k_s(C_{si} - C_s) \qquad (1)$$

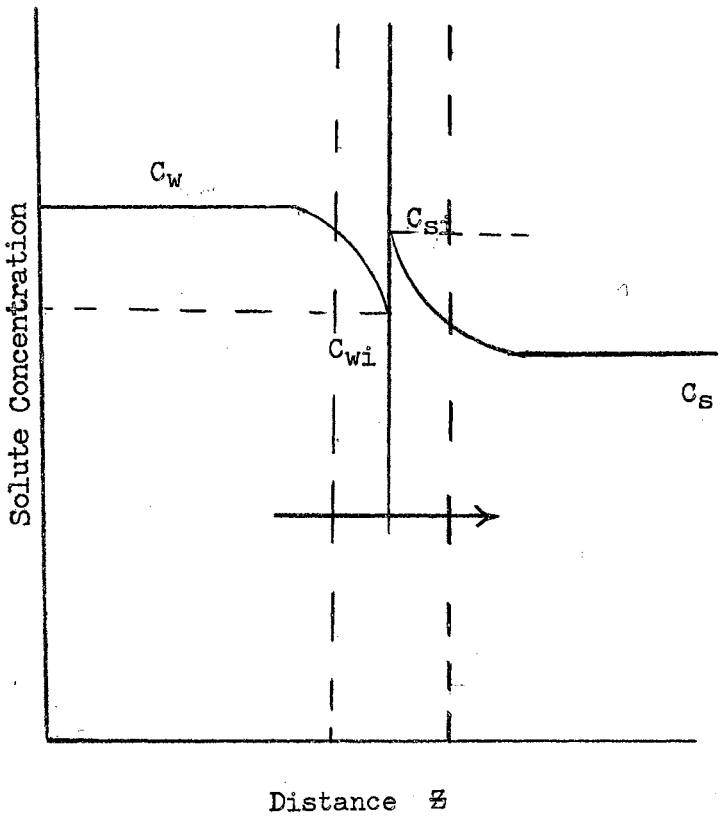

Figure 1

Two-Film Theory of Interphase Mass Transfer

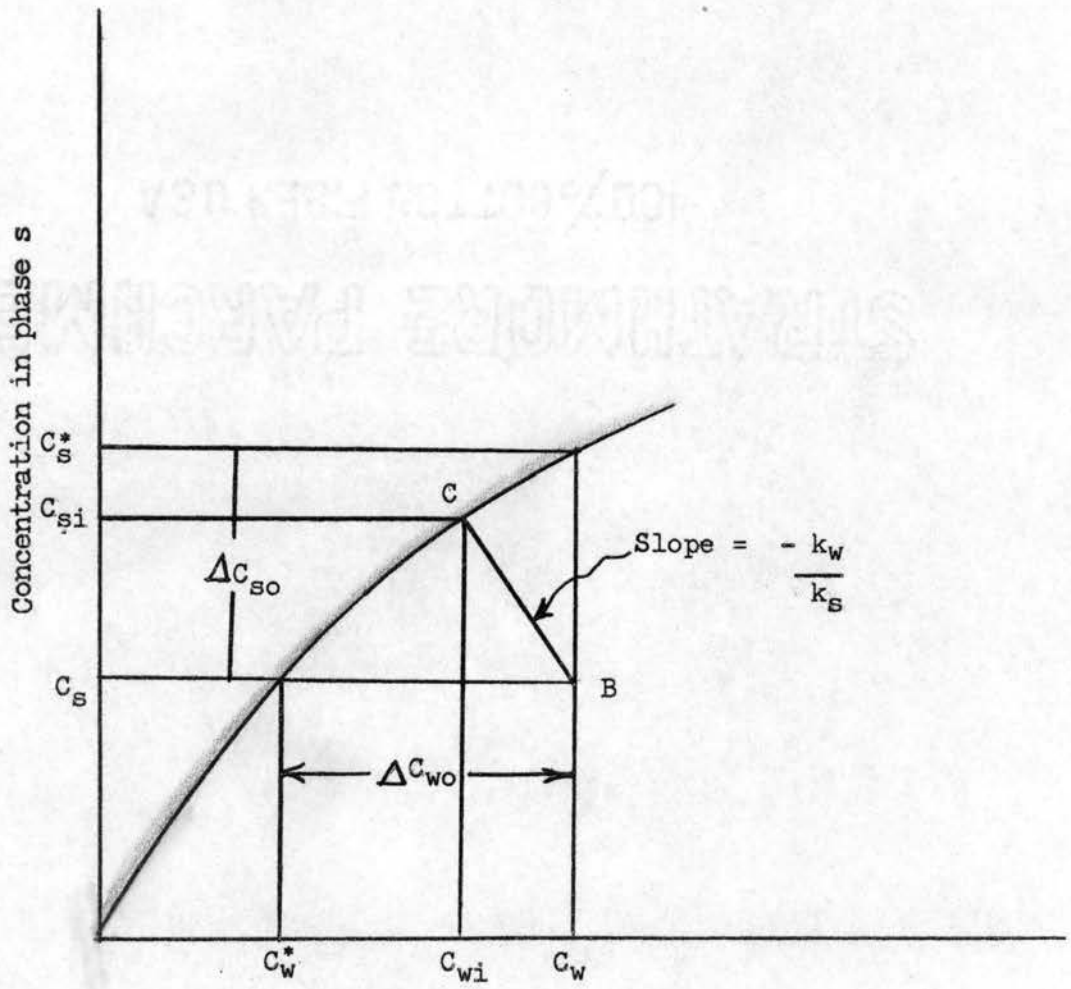

Figure 2.

Equilibrium Diagram

where:

k_w = individual film coefficient for phase w

k_s = individual film coefficient for phase s

The slope of the line BC in Figure 2 may be obtained from Equation (1).

$$\text{Slope of BC} = \frac{C_{si} - C_s}{C_{wi} - C_w} = -\frac{k_w}{k_s} \qquad (2)$$

Thus, if k_s and k_w are known, the value of C_{si} and C_{wi} and the rate of transfer, N, may be obtained by simultaneously solving Equation (2) along with the equilibrium relationship, $C_{si} = f(cw)$.

The individual film coefficients defined by Equation (1) can not be experimentally determined since it is not physically possible to measure the interfacial concentrations. Therefore, since the average bulk concentrations may be readily determined, overall mass transfer coefficients are defined by the following equation.

$$N = K_{ow}(C_w - C_w^*) = K_{os}(C_s^* - C_s) \qquad (3)$$

where:

K_{ow} = overall transfer coefficient for phase w

K_{os} = overall transfer coefficient for phase s

C_w^* = concentration of C_w which is in equilibrium with C_s

C_s^* = concentration of C_s which is in equilibrium with C_w

The overall coefficients account for the diffusion resistances in both phases. The values of C_s^* and C_w^* are shown in Figure 2 and the overall driving forces, $(C_w - C_w^*)$ and $(C_s^* - C_s)$, are shown as ΔC_{wo}

and ΔC_{so} respectively.

The relationship between the overall and the individual film mass transfer coefficients may be obtained from Equations (1) and (3). First to find K_{os} as a function of k_s and k_w rewrite Equation 3 as follows

$$\frac{N}{K_{os}} = C_s^* - C_s \tag{4}$$

Next add and subtract C_{si} from the right hand side of Equation 4 and regroup the terms

$$\frac{N}{K_{os}} = (C_s^* - C_{si}) + (C_{si} - C_s) \tag{5}$$

Now from Equation (1) the following expressions are obtained.

$$C_{si} - C_s = \frac{N}{k_s} \tag{6}$$

$$C_s^* - C_{si} = \frac{N}{k_w} \frac{(C_s^* - C_{si})}{(C_w - C_{wi})} \tag{7}$$

Substituting Equations (6) and (7) into Equation (5) and dividing both sides by N yields:

$$\frac{1}{K_{os}} = \frac{1}{k_w} \frac{(C_s^* - C_{si})}{(C_w - C_{wi})} + \frac{1}{k_s} \tag{8}$$

Let:

$$H = \frac{(C_s^* - C_{si})}{(C_w - C_{wi})} \tag{9}$$

Then:

$$\frac{1}{K_{os}} = \frac{H}{k_w} + \frac{1}{k_s} \tag{10}$$

Following the above procedure it can be shown that:

$$\frac{1}{K_{ow}} = \frac{1}{k_s} + \frac{1}{H' k_s} \tag{11}$$

where:

$$H' = \frac{(C_{si} - C_s)}{(C_{wi} - C_w^*)} \tag{12}$$

It should be noted that in this derivation the usual assumption of the equilibrium relation being linear was not required. In general H and H' are not equal. H and H' are the slopes of the chords connecting the points (C_{si}, C_{wi}) with (C_s^*, C_w) and (C_s, C_w^*) respectively. When the equilibrium relationship is linear, H and H' are both equal to the slope of the equilibrium line.

In two-film theory, the transfer is assumed to be controlled by molecular diffusion and the film mass transfer coefficient is equal to the diffusivity divided by the effective film thickness, δ.

$$k_w = \frac{D_w}{\delta_w} \tag{13}$$

$$k_s = \frac{D_s}{\delta_s} \tag{14}$$

Equations (13) and (14) are obtained by assuming that the liquids

on both sides of the interface are static.

Higbie (25) has developed a theory of interphase mass transfer which he named penetration theory. This theory is based on the concept of unsteady-state penetration of a solute into a liquid during its time of exposure to a diffusing solute. The film coefficients in this case are proportional to the square root of the diffusivity instead of the diffusivity as in classical film theory.

In two-film theory the two phases are assumed to be in equilibrium at the interface as discussed above. Recently, Abramzon and Ostrovskii (1) have questioned this assumption. They note several instances where investigators have found marked discrepancies between measured and theoretically calculated quantities of materials transferred between two phases in both gas absorption and liquid-liquid extraction. Although Higbie (25) accepted the assumption of equilibrium at the interface, he noted discrepancies between measured and calculated quantities of CO_2 absorbed in water.

When the bulk of the fluid is not static, eddy diffusion must be considered along with molecular diffusion. The combination of the mechanisms of molecular and eddy diffusion is generally called convective diffusion. In convective diffusion it is assumed that the liquid may be nominally divided into two regions. The first region has a constant concentration and is far from the interface while the second region has a rapidly changing concentration in the immediate vicinity of the interface. Since there is a high concentration gradient in this second region, molecular diffusion must be taken into account and, therefore, the region is termed the diffusion boundary layer. Levich (31) has shown that the diffusion boundary layer is about one-tenth of the Prandtl

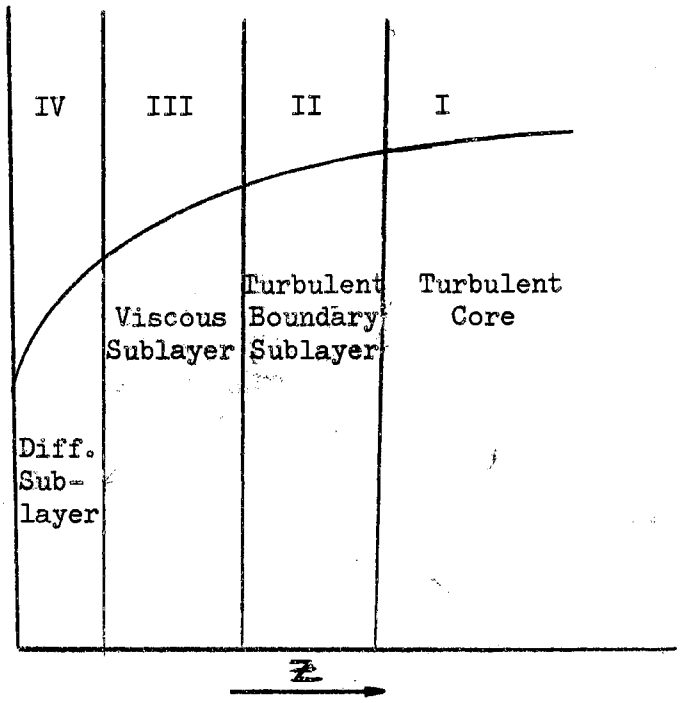

Figure 3

Solute Distribution in Turbulent Flow

hydrodynamic boundary layer.

When turbulent flow occurs there are four regions to be considered for diffusion across an interface (Fig. 3). First, far from the interface, a turbulent zone occurs in which the concentration remains constant. In the next zone, the turbulent boundary layer, both the average concentration and the average fluid velocity decrease very slowly and both momentum and material are transported by turbulent eddies. Closer to the interface is the viscous sublayer where the eddies become so small that momentum transfer is controlled by molecular viscosity; however, solute transfer is still controlled by eddy diffusion. Finally, very close to the interface molecular diffusion becomes the controlling mechanism of solute transfer.

Interfacial Resistance

Several investigators (6, 28, 33) have observed an interfacial resistance to mass transfer in some systems. Lewis (28) defined the interfacial transfer coefficients, k_{rs}, for phase s as:

$$N = k_{rs}(C_{si}^{*} - C_{si}) \tag{15}$$

In this case C_{si}^{*} is the solute concentration which would be in equilibrium with C_{wi}, the w phase interfacial concentration. If k_{rs} is very small, indicating a very small resistance, C_{si} and C_{wi} are in equilibrium as assumed in two-film theory. When an interfacial resistance occurs the equation for additivity of film resistances is different from Equation 10. Following the procedure used above the following expression can be derived.

$$\frac{1}{K_{os}} = \frac{H}{k_w} + \frac{1}{k_s} + \frac{1}{k_{rs}} \tag{16}$$

where:

$$H = \frac{(C_{si}^* - C_s^*)}{(C_{wi} - C_w)} \tag{17}$$

The existence of interfacial resistance to mass transfer has been disputed by Abramzon and Ostrovskii (2). Both Chester (10) and Keisch (26) were unable to detect any interfacial resistance to the transfer of uranyl nitrate between TBP and water. Ward and Brooks (51) were unable to detect interfacial resistance for the transfer of the lower aliphatic acids between water and toluene. Thus, there does not seem to be any general agreement on the existence of interfacial resistance to interfacial mass transfer.

When the equilibrium relationship is based on activities, there is no point of discontinuity at the interface. The equation defining the activity based mass transfer coefficients for transfer from phase w to phase s is given below.

$$N = k'_w (a_w - a_{wi}) = k'_s (a_{si} - a_s) \tag{18a}$$

$$= K'_{os} (a_w - a_s) = K'_{ow} (a_s - a_w) \tag{18b}$$

where:

a_w = activity of phase w

a_{wi} = activity of phase w at the interface

a_s = activity of phase s

a_{si} = activity of phase s at the interface

The values of K'_{ow} and K'_{os} are equal when the driving force is expressed in terms of activities, and the relationship between the individual coefficients and the overall coefficient becomes:

$$\frac{1}{K'_{os}} = \frac{1}{K'_{ow}} = \frac{1}{k'_{w}} + \frac{1}{k'_{s}} \tag{19}$$

Interfacial Mass Transfer in Stirred Cells

Lewis (27, 28, 29) studied the unsteady-state mass transfer of solutes across liquid-liquid interfaces in a cell where the degree of turbulence and the interfacial area were accurately controlled. Initially, he investigated the rate of saturation of partially miscible binary systems in order to determine individual film mass transfer coefficients. The effect of turbulence and diffusivities on the individual coefficients were studied. The interfacial area in the stirred cell was restricted to an annular gap between a central baffle and a circumferential wall baffle in order to minimize cavitation and irregular wall effects.

For a binary system the rate of transfer is given by:

$$N = kA\ (C^* - C_i) \tag{20}$$

where:

N = moles transferred per unit time

A = interfacial area

K = film mass transfer coefficient

C_i = interfacial concentration

C = concentration in the liquid

C* is essentially equal to the saturation value.

The rate of transfer is also given by:

$$N = v \frac{dC}{dt} \tag{21}$$

where: v = volume of the liquid.

Therefore:

$$k = \frac{v}{A} \left[\frac{dC}{(C^* - C)dt} \right] \tag{22}$$

Integrating and applying the initial condition c = o at t = o gives:

$$- k' = \frac{v}{A_t} \ln \left[\frac{C^* - C}{C^*} \right] \tag{23}$$

The results of several binary systems were correlated by the following equation.

$$60 \frac{K_1}{V_1} = 6.76 \times 10^{-6} \left[Re_1 + \frac{\mu_2}{\mu_1} Re_2 \right]^{1.65} + 1 \tag{24}$$

where:

R_e = Reynolds number for mixing, $\frac{NL^2}{\nu}$

ν = Kinematic viscosity

μ = Viscosity

This correlation shows the individual coefficients to be independent of the diffusivities of either phase and is only dependent on the Reynolds number and the viscosities of either phase.

Olander (41, 43) used a mass transfer cell, similar to the one built by Lewis, to study interphase transfer across the water-tributyl phosphate

interface. A correlation for film coefficients was developed and is presented below.

$$\frac{k}{\nu} = 0.046 \left(\frac{\omega}{\nu}\right)^{.67} (S_c)^{-.44} \qquad (25)$$

where:

ω = stirrer rate in radians per second

S_c = Schmidt number

This correlation states that the individual coefficients are proportional to the 0.44 power of the diffusivity and to the 0.67 power stirring rate.

Mayers (33) used a modified Lewis type cell and developed an improved correlation for individual coefficients using both his and Lewis' data. The correlation proposed by Mayers has the following form:

$$\frac{k_1 L}{D} = 0.00316(Re_1 Re_2)^{1/2} \left(\frac{\mu_2}{\mu_1}\right)^{1.9} \left(0.6 + \frac{\mu_2}{\mu_1}\right)^{-2.9} (S_c)^{5/6} \qquad (26)$$

where: L is the stirrer diameter.

This correlation predicts that the individual coefficients are proportional to the 1/6 power of diffusivity and to the 0.5 power of the product of the Reynolds number in both phases.

A hydrodynamic model of mass transfer in a stirred extractor was developed by Olander (42). In the model the stirred extractor was an unbaffled cylindrical vessel with equal volumes in the two phases with stirring provided by rotating stirrer bars connected to a common shaft. Olander defined two parts of the interface as the core, the area

within the vertically projected sweep of the stirrer, and the annulus. The model was derived by starting with the Navier-Stokes equation and Ficks second law of diffusion. The conclusion was reached that there was essentially no transfer across the core interfacial region. The model had a form very similar to Olander's previously developed correlation.

$$\frac{k}{D} = 0.4 \left(\frac{\omega}{\nu}\right)^{1/2} (S_c)^{-2/3} \qquad (27)$$

The assumption that there was no mass transfer in the core region of Olander's model was disputed by Loosemore and Prosser (32) after comparing the model to experimental data. Olander (44) later modified the model to include transfer in the core region of the interface. This model agreed with the data of Loosemore and Prosser.

It is interesting to note the effect of diffusivity on the individual film mass transfer coefficients as presented by the various correlations. According to classical film theory, the coefficients should be directly proportional to diffusivity while penetration theory predicts a square root dependency. There appears to be no general agreement among investigators on the effect of diffusivity. The effect reported varied from no dependence to the 0.67 power of the diffusivity.

Table II gives the dependency of the individual film coefficients on the diffusivity in the various published correlations.

Lewis (29) has studied the unsteady-state transfer of uranyl nitrate across liquid-liquid interfaces using dibutoxy diethyl ether, methyl isobutyl ketone, and 20% tributyl phosphate solutions as solvents. The experimental overall mass transfer coefficients were compared to the

TABLE II

Effect of Diffusivity
on
Film Transfer Coefficients

Power dependency of D on film coefficients	References	
0	Lewis	(27)
1/6	Mayer	(33)
0.37	McManamey	(38)
0.44	Olander	(41)
0.5	Gordon and Sherwood	(21)
0.67	Olander	(42)

values predicted by Equations (10) and (20). Some systems gave larger values than predicted and in these cases interfacial turbulence was observed. In other systems there was initially fair agreement between the calculated and observed values; however, the experimental transfer rates decreased with time. The decrease was proposed to be due to the build-up of an interfacial barrier. The build-up of the barrier depended only on the duration of the experiment and was independent of the concentration. The experimental mass transfer coefficient was calculated by graphically integrating the equation:

$$N = V\frac{dC}{dt} = K_{os}A(C_s^* - C_s) \tag{28}$$

Burger (8) studied the transfer of uranyl nitrate across the water-TBP interface in a stirred batch extractor which differed from the Lewis type cell by having internal baffling to improve mixing. The data obtained were analyzed on the basis of reaction kinetics. Consider the transfer of uranyl nitrate from the aqueous phase to TBP.

$$UO_{2(Aq)}^{++} + 2NO_{3(Aq)}^{-} + 2\ TBP_{(org)} \rightleftharpoons UO_2(NO_3)_2 \cdot 2TBP_{(org)}$$

If the organic phase initially contains no uranium, then the initial rate equation is:

$$\frac{dC_s}{dt} = k_1(C_{wo})^n \tag{29}$$

where:

n is the reaction rate order and k_1 the forward rate constant. After a short interval the reverse transfer must be considered and the rate equation becomes:

$$\frac{dC_s}{dt} = k_1(Cw)^n - k_2(C_s)^m \tag{30}$$

Here m is the order of the reverse reaction and k_2 is the rate constant. When m and n are unity Equation (30) becomes:

$$\frac{dC_s}{dt} = k_1C_w - k_2C_s \tag{31}$$

If it is assumed that at equilibrium:

$$\frac{k_1}{k_2} = \frac{C_{seq}}{C_{weq}} \tag{32}$$

where:

C_{seq} = equilibrium value of c_s

C_{weq} = equilibrium value of c_w

Then Equation (26) may be integrated.

$$t = \int \frac{dC}{k_1C_w - k_2C_s} \tag{33}$$

Since in Burger's cell the volumes of both phases were equal, the following equations may be written:

$$C_w = C_{wo} - C_s \tag{34}$$

and

$$C_{weq} = C_{wo} - C_{seq} \tag{35}$$

Using Equations (32), (34), and (35), Equation (33) may be rewritten as:

$$t = \int \frac{dC_s}{k_1(C_{wo} - C_s) - k_1 C_{weq} \frac{C_s}{C_{seq}}} \tag{36}$$

Integrating and applying the initial condition $C_s = 0$ at $t = 0$, and rearranging gives:

$$\ln \left(\frac{(C_{seq} - C_s)}{C_{seq}} \right) = - \frac{C_{wo}}{C_{seq}} k_1 t \tag{37}$$

In his work Burger found that initially the transfer from water to TBP followed first order kinetics, but the transfer rate decreased with time. This effect was attributed to the blockage of the interface with impurities.

The effect of surfactants on the rate of transfer was investigated by Mayer (34). He found that the presence of an interfacial film reduced the rate of transfer by damping out the eddies coming from the stirrers and by reducing the transfer of momentum across the interface. Lewis (29) has investigated the buildup of an interfacial film at the interface as the mechanism for the buildup of an interfacial resistance in the uranyl nitrate-water-TBP system. He concluded that the decrease in transfer rate with time could not be attributed to surface blockage.

Interfacial Turbulence

A mathematical model of interfacial turbulence has been developed by Sternling and Scriven (49). The model was developed in terms of classical flow, diffusion, and surface processes. It was proposed that ever present, small, random fluctuations about an interface may cause the onset of hydrodynamic instability, or interfacial turbulence.

Consider a solute diffusing from phase A to phase B, and assume a small roll cell brings solute rich liquid from phase A towards the interface and that another roll cell brings solute lean liquid from phase B towards the interface (Figure 4).

When a disturbance is developing the rates of convection differ in the two phases, being higher in the phase of greater kinematic viscosity. Thus, the net change in solute content at point 1 will depend in part on the viscosity ratio. In addition the net change in solute concentration depends upon the ratio of the diffusivities of the two phases, since molecular diffusion alters the composition of each roll cell as liquid moves toward the interface.

Consider the case where the viscosity is higher in phase A and the diffusivity is lower in phase A than in phase B. Then the convection current is stronger in phase A and the concentration gradient is less affected by diffusion than in phase B. This causes the upset to be greater in phase A and the concentration at point 1 is increased. The concentration at point 2 will be lower than at point 1 due to the symmetry and conservation of solute. Thus, variations in concentration are set up along the interface. If, as in many systems, the interfacial tension decreases with solute concentration, then the interface will stretch at

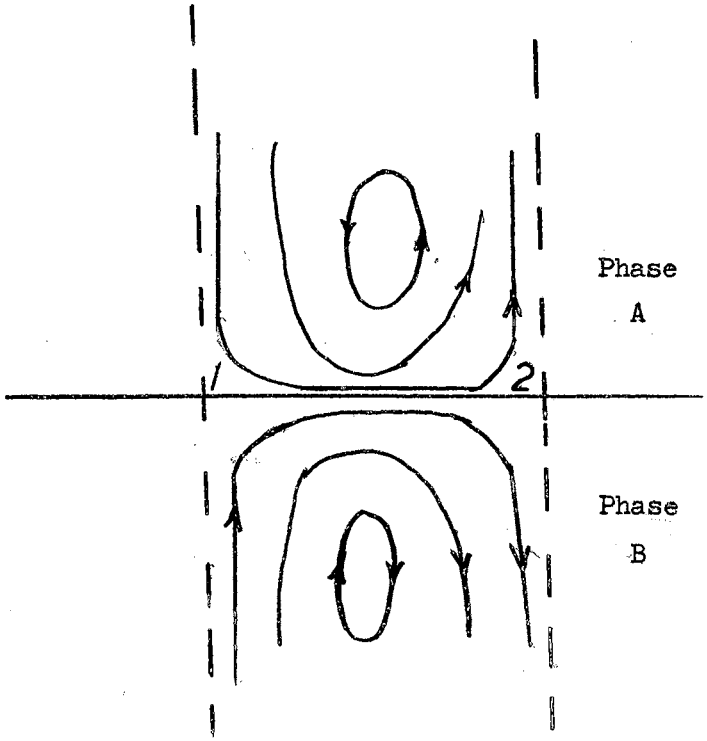

Figure 4.

Roll Cell

point 1 and contract at point 2. This then causes a reinforcement of the original disturbance. If the interfacial tension increases with solute composition, then the interface will contract at point 1 and stretch at point 2 causing the original disturbance to be damped out. From this analysis it is seen that interfacial turbulence is likely to occur when a solute is being transferred out of the phase of higher viscosity and lower diffusivity.

CHAPTER IV

EXPERIMENTAL APPARATUS

The experimental apparatus for this work consisted of a stirred mass transfer cell with its flow lines and auxiliary equipment.

Stirred Mass Transfer Cell

The mass transfer cell, shown in Plate I, was patterned after the design of Burger. A cross-sectional view of the transfer cell is shown in Figure 24. The cell was four inches high and two and one-eighth inches in internal diameter. The cell was constructed of a four-inch length of heavy wall glass tubing. In order to prevent leakage around the gaskets at the ends of the cell, the ends of the glass tubing were ground flat.

The bottom plate was machined from one-fourth inch stainless steel to a four-inch diameter and had two one-fourth inch Swagelok fittings installed for the heavy phase inlet and outlet flow lines. The top plate was also machined from one-fourth inch stainless steel to a four inch diameter. This plate had four Swagelok one-fourth inch fittings installed, two of which were used for upper and lower cell compartment sampling probe tubes, the other two fittings were for the light phase inlet and outlet flow lines. Gaskets for the two end plates were cut from one-sixteenth inch teflon. A three-fourth inch rod of polyethylene was machined and press fitted into the top end plate for the upper stirrer bearing.

PLATE I. Stirred Mass Transfer Cell

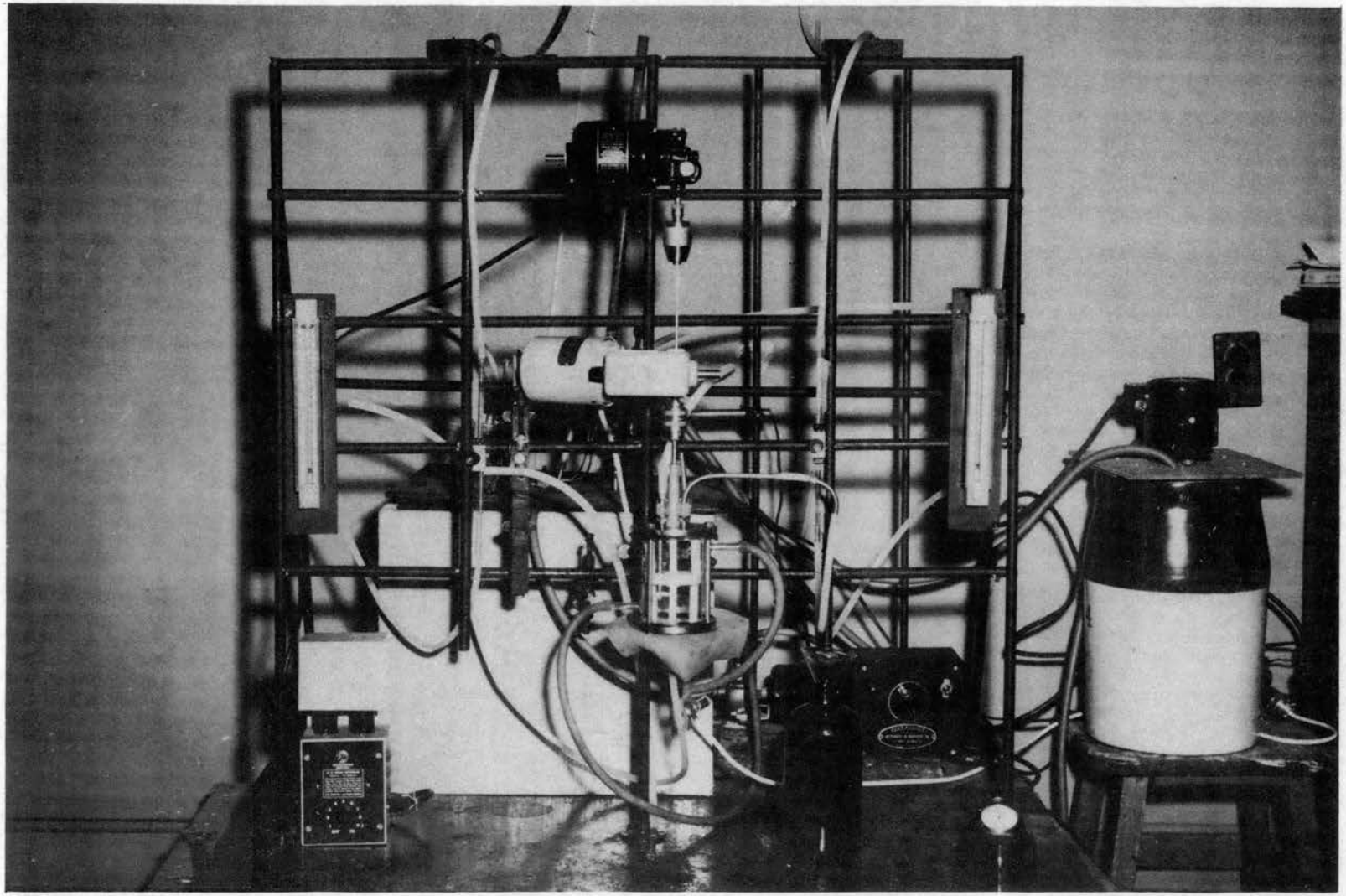

The mass transfer area was confined to an annular space of 0.75 inches inner diameter and 1.125 inches outer diameter. This annular area was formed by a baffle ring and a center baffle. The baffle ring was two and one-eighth inches in outer diameter and was machined from a sheet of one-half inch teflon. The ring was tapered to a one-fourth inch thickness at its inner surface. The 0.75 inch center baffle was machined from one-half inch teflon and serves as a bearing for both the upper and lower phase stirrer. This center baffle is held in the center of the baffle ring by six, one-sixteenth inch, stainless steel pins. Three vertical baffles constructed of one-eighth inch teflon rod were used to prevent swirling of the solutions in the cell.

The upper stirrer was constructed of one-fourth inch stainless steel tubing fitted with two 2.86 cm by .714 cm thin stainless steel paddles at right angles to each other. The lower stirrer was constructed from a one-sixteenth inch stainless steel rod fitted with two stainless steel paddles of the same size as the upper stirrer paddles.

A two and seven-eighths inch glass jacket, which surrounds the glass cell, was used for controlling the cell temperature. The lower stirrer was operated by a G. K. Keller electronic controlled motor. A La Pine variable-speed hollow-shaft cone-drive motor was used for operating the upper stirrer. The height of the interface was controlled by adjusting the height of the lower phase outlet line. The feed lines were constructed of glass and one-fourth inch stainless steel tubing and all joints were made with polyethylene tubing. The feed supply bottles were allowed to siphone into constant head feed tanks at a rate approximately equal to the feed flow rate. The flow rates were controlled by one-fourth inch Ideal needle valves. Matheson rotameters, Tube No. 602, were

used to indicate the flow rate. A flow diagram of the apparatus is shown in Figure 5. Detailed drawings of the cell components are presented in Appendix D.

Constant Temperature Bath

The constant temperature bath consisted of a glass cylinder twelve inches in diameter and twelve inches high surrounded by cork insulation and was inserted in a wood box. A Lionel Type TRC, AC-DC motor was used for the stirring of the water bath. The speed of this motor was controlled by a Superior electric type 116 powerstat. A Cutler-Hammer model 15053H114A, 500 watt immersion heater was controlled by a Fenwal adjustable controller. A copper cooling coil was immersed in the bath and an Eastern model 100 pump was used for circulating the cooling water. The cooling water was cooled to 15° C. by a Laird Engineering Company refrigeration unit. This arrangement allowed the constant temperature bath to operate at 25 ± 0.3° C.

A small centrifugal pump was used to circulate water from the constant temperature bath through the glass cell temperature jacket. Stainless steel coils were immersed in the temperature bath through which the feed passed prior to entering the cell in order to ensure that the inlet solutions were at the same temperature as the solutions in the cell.

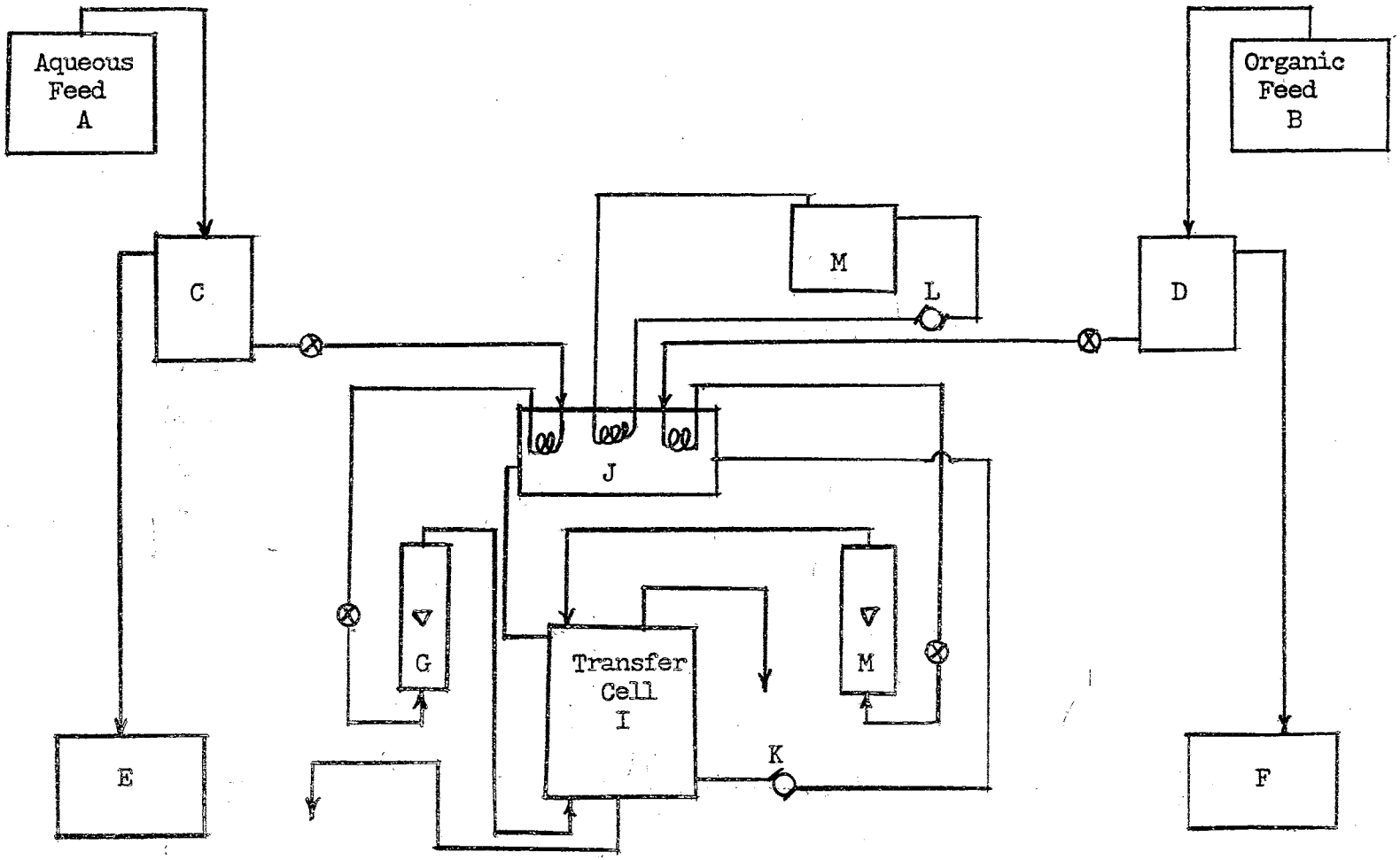

Figure 5.

Mass Transfer Cell Flow Diagram

TABLE II

Flow Diagram Equipment List

A. Heavy phase feed container

B. Light phase feed container

C. Heavy phase constant head feed tank

D. Light phase constant head feed tank

E. Heavy phase overflow container

F. Light phase overflow container

G. Heavy phase rotameter

H. Light phase rotameter

I. Mass transfer cell

J. Constant temperature bath

K. Cell jacket water pump

L. Cooling water pump

M. Refrigeration unit

CHAPTER V

EXPERIMENTAL PROCEDURE

Purification of TBP

The tributyl phosphate used in this work was commercial grade purchased from Commercial Solvents Corporation. The tributyl phosphate was purified by boiling one liter of TBP with one-half liter of 0.5 molar NaOH at total reflux for ten hours. The mixture was then allowed to boil without refluxing for one hour. The resulting mixture was poured into a three liter separatory funnel and the aqueous NaOH solution decanted. Next, the residual tributyl phosphate was washed with demineralized water until neutral, as indicated by litmus paper.

The solvent used for diluent was Amsco odorless mineral spirits (W-7) purchased from Missouri Solvents and Chemicals Company. The physical properties of the solvent are given in Table III. When the mixture of 30% by volume tributyl phosphate in Amsco was mixed a water emulsion formed. This occurred because water saturated TBP holds about 64 grams of water per liter while 30% TBP holds about eight grams per liter. The emulsion was broken by filtering the 30% TBP solution.

Analytical Determination of Uranyl Nitrate

The uranyl nitrate solutions were prepared from A. C. S. reagent grade uranyl nitrate purchased from the General Chemical Division of

TABLE III

Physical Properties of Amsco Odorless Mineral Spirits

(W-7)

API Gravity at 60° F	54.5
Specific Gravity at 60° F	.7608
Aniline Cloud point, ° F	184.5
Kari-Butanol No., cc	27.0
Flash point, ° F	123

Allied Chemical Co.

Analysis for uranyl nitrate concentrations of both aqueous and organic solutions were performed by the potassium ferrocyanide method of Dizdar and Obernovic (14). First, a volume of the solution to be analyzed, containing between 1.20 and 2.38 mg. of uranium was pipetted into a 25 ml. volumetric flask. Then about 10 to 15 ml. of demineralized water and 3 ml. of 10% potassium ferrocyanide solution were added. The volumetric flask was filled to the calibration mark and the solution mixed by shaking. The solution was allowed to stand for ten minutes to allow the color to develope, and its optical absorbance was measured on a Beckman DU Spectrophotometer at 480 mμ. The reference solution for the measurements was demineralized water. A calibration curve was prepared by following the above procedure using a standard 0.01 molar solution of uranyl nitrate. The 0.01 molar uranyl nitrate solution was prepared by weighing uranyl nitrate crystals on a Voland and Sons Inc. analytical balance and dissolving in demineralized water in a volumetric flask. The 30% tributyl phosphate-uranyl nitrate solutions were analyzed in the

same manner, but the 25 ml. volumetric flasks were filled with water until the interface between the aqueous and organic phases, reached the calibration mark.

Equilibrium Distribution of Uranyl Nitrate

Uranyl nitrate distribution data were necessary for calculating the mass transfer coefficients. The distribution data were obtained by the following procedure: Different volumes of 30% TBP and aqueous uranyl nitrate solutions were stirred for twelve hours with a magnetic stirrer, or the two phases were shaken manually for ten minutes in a 60 ml. separatory funnel. The phases were then allowed to separate and each phase was analyzed for uranyl nitrate. The distribution data were fitted to a polynomial using the least squares criteria on an IBM 1620 computer.

Unsteady-State Mass Transfer

The unsteady-state mass transfer runs were performed according to the following procedure: First, the constant temperature bath stirrer and the cooling water pump were turned on; then, the cooling water refrigeration unit, the constant temperature bath heater, and the circulating water pump were started. The temperature of the water bath was allowed to reach 25 $\pm$ 0.3° C. Next, the lower and upper phase stirrers were started and adjusted to the desired speeds. Then the upper phase stirrer was turned off. The aqueous phase solution was then pipetted into the cell through the lower phase sampling tube until the liquid height reached the center of the annular transfer area. Then the organic phase was pipetted into the cell through the upper phase sampling tube. Care was taken in filling the upper cell compartment to

avoid agitating the interface by directing the liquid stream onto the fixed baffle ring. As soon as the upper phase compartment was filled, the time was recorded and the upper stirrer started. One milliliter samples of the aqueous and organic phases were taken at various time intervals. In order to keep the total cell volume constant one milliliter of the starting feed solutions were added. This caused little error since each cell compartment contained 100 ml. and at the most seven samples were taken. After each run the cell was disassembled, thoroughly cleaned, rinsed with demineralized water and allowed to dry before reassembly.

Some unsteady state runs were made with benzoic acid being transferred across the water-toluene interface. In these runs the concentration levels were so low that almost the entire cell content was required for analysis. Therefore, after a period of operation the stirrers were turned off and the cell quickly emptied.

Steady-State Mass Transfer

Steady state mass transfer runs were performed according to the following procedure. The constant temperature bath was started accordint to the procedure given above. The feed bottles were put in place and the constant head tanks were filled by siphoning the solution from the feed supply bottle. The aqueous phase valves were opened and the lower compartment filled. While the lower cell compartment was being filled, the lower phase stirrer was started and its speed adjusted. The stirrer speed was determined by timing with a stop watch 50 revolutions of the stirrer motor shaft. If the desired speed was greater than 100 rpm, a stroboscope was used. The height of the lower phase

outlet line was adjusted to the approximate position required to maintain the interface in the annular area. When the lower compartment was filled the needle control valve was closed. Next the organic phase valves were opened and the upper compartment filled. While filling the upper cell compartment, the height of the interface was controlled by raising or lowering the aqueous phase outlet line. When the cell was completely filled the aqueous and organic feed control valves were adjusted to provide the desired flow rates, with indication of the flow rate being obtained from the rotameters. The upper phase stirrer was then started. Next, the height of the interface was adjusted to the center of the annular transfer area. Then the flow rates were checked by using a stop watch to obtain the time required to fill a 10 ml. volumetric flask. The flow rates were checked periodically throughout the run and the control valves readjusted if necessary.

After three and one-half hours a sample of the phase having the greatest change in concentration was analyzed. Steady-state conditions were determined by analyzing samples every 15 minutes until three consecutive readings were constant within the experimental error of the analytical procedure.

Analog Computer Simulation of Transfer Cell

The mass transfer cell was simulated on a Donner Model 3400 Analog Computer. This simulation allowed the estimation of the time required to reach steady state. Two experimental runs were compared to the analog simulation using the experimental value of the mass transfer coefficient.

The resistors and capaciters used for the simulation were 0.1%

precision components and the potentiometers used were 10 turn helipots. The following equations describe the physical situation and were programed as shown in Figure 23.

$$V \frac{dXo}{dt} = F_w(Xi - Xo) + K_{os}A(Yo - Yo^*) \quad (1a)$$

$$V \frac{dYo}{dt} = F_s(Yi - Yo) - K_{os}A(Yo - Y^*) \quad (1b)$$

where:

Xi = aqueous phase inlet concentration

Xo = aqueous phase outlet concentration

Yi = organic phase inlet concentration

Yo = organic phase outlet concentration

CHAPTER VI

RESULTS AND DISCUSSION

Equilibrium Distribution of Uranyl Nitrate

The uranyl nitrate distribution data were obtained as discussed in Chapter IV. The two methods of equilibrating the phases gave identical results within the experimental error of determining the concentration of uranyl nitrate. The equilibrium data were then fitted to a polynomial equation on an IBM 1620 digital computer.

The data were correlated in two regions by the following equations.

$$C_s = 9.36 \times 10^{-4} - 0.248C_w + 10.4\,C_w^2 - 29.1C_w^3 + 23.76\,C_w^4 \qquad (1)$$

$$0 \leq C_w \leq 0.35M$$

Standard deviation = 0.00894 M

and for $0.35M \leq C_w \leq 1.7M$

$$C_s = 0.184 + 0.38C_w - 0.13C_w^2 \qquad (2)$$

Standard deviation = 0.013M

The equilibrium distribution curve is shown in Figure 6. These data agree quite well with the data reported by Burger (8).

Benzoic Acid Extraction

Transfer of benzoic acid between toluene and water was performed

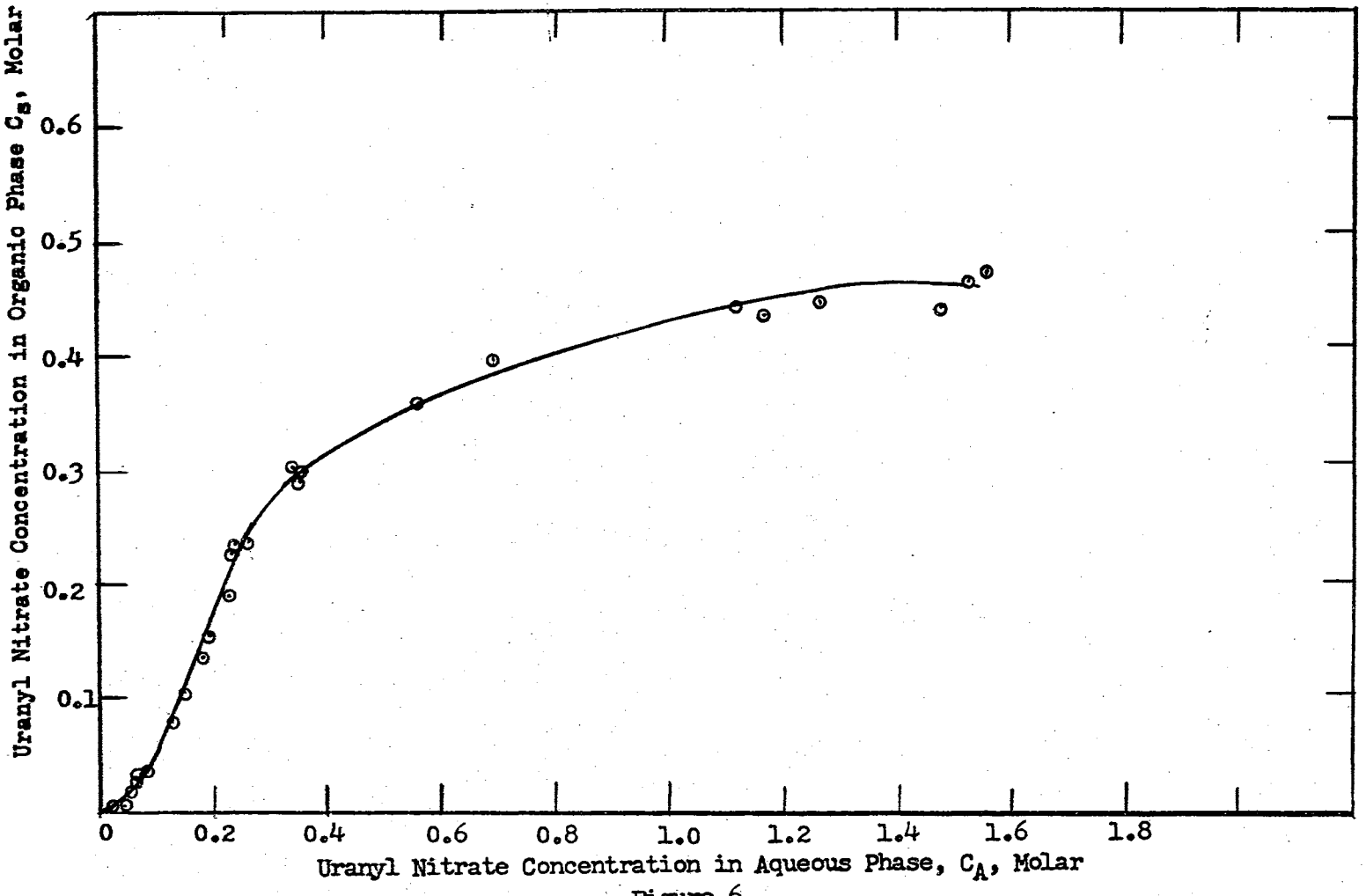

Figure 6.

Distribution of Uranyl Nitrate Between Water and 30% Tributyl Phosphate in Amsco

in the mass transfer cell in order to compare the cell with the ones used by Blokker (6) and Lewis (28), and also to become familiar with the operation of the cell. The benzoic acid concentrations were determined by titration with NaOH. The procedure for the unsteady-state transfer of benzoic acid is discussed in Chapter IV.

When the Whitman two-film theory is applied to unsteady-state mass transfer the overall mass transfer coefficient is defined as:

$$K_{ow} = \frac{\int \frac{dc_w}{(C_w^* - C_w)}}{\frac{A}{V} t} \qquad (3)$$

The mass transfer coefficients were evaluated by graphically integrating a plot of $1/(C_w^* - C_w)$ versus C_w.

Initially, several runs were carried out to learn how to properly operate the apparatus. Next the effect of stirring rates was studied. An upper stirring rate of 43.5 rpm was chosen as this was the maximum rate at which no visible motion of the interface was observed. The lower stirring speed was then varied and runs of two hours duration were carried out. The concentration of the aqueous phase after two hours of operation was plotted versus the stirring rate (Figure 7), in order to determine the aqueous phase stirring rate at which the rate of mass transfer becomes independent of the stirring rate. The mass transfer rate increased with the stirring rate, becoming relatively constant at stirring rates greater than 70 rpm.

A series of runs were then performed with stirring rates of 43.5 rpm and 70 rpm for the upper and lower stirrers respectively. Table V gives a comparison of the experimentally determined mass transfer coefficient with the data reported by Lewis (28) and Blokker (6).

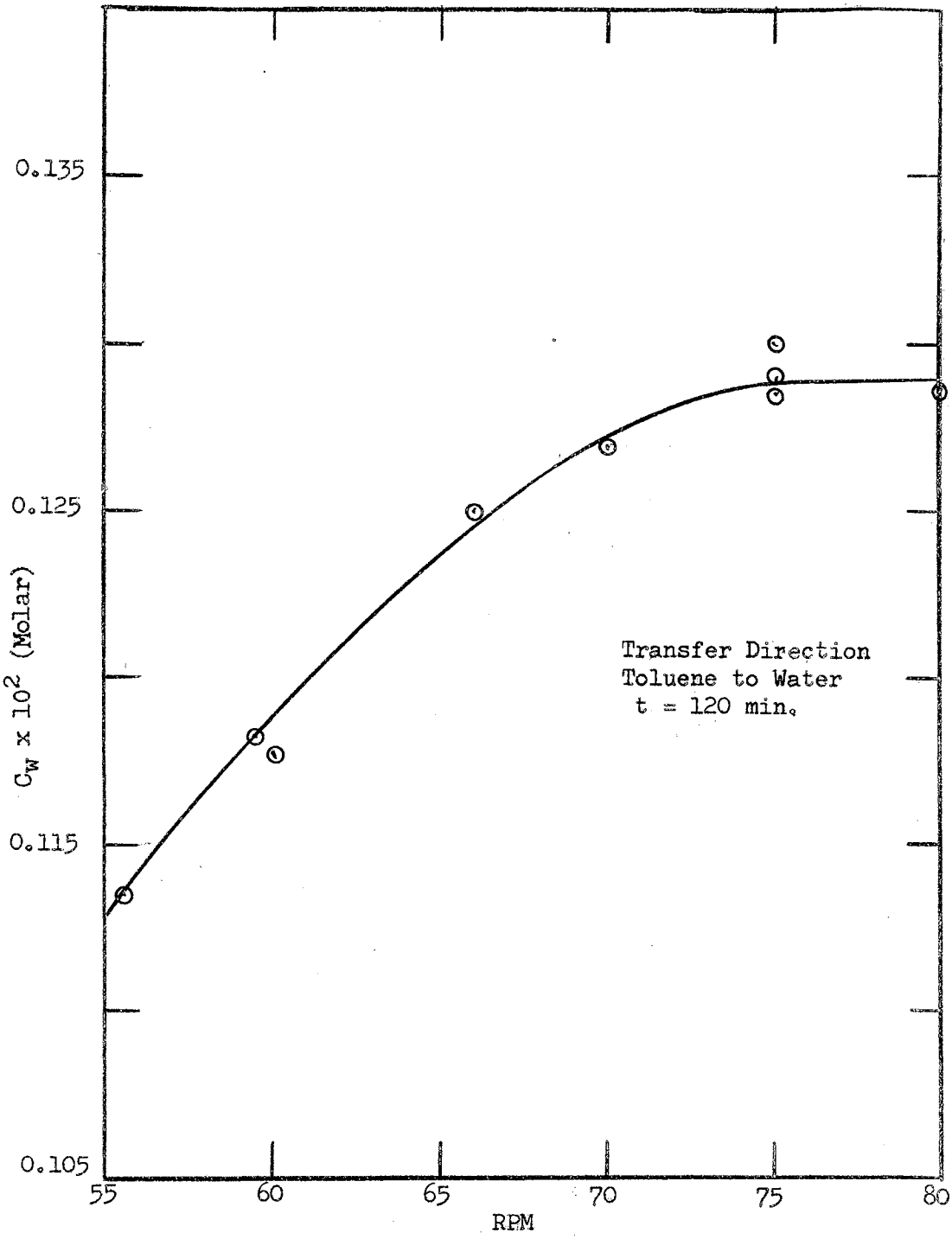

Figure 7.

Effect of Aqueous Phase Stirring Rate

TABLE V

Unsteady-State Transfer of Benzoic Acid

Concentration (toluene phase) gm/l		Benzoic Acid Transfer direction	K_{ow} x 10^3 cm/sec	Reference
initial	final			
2.0	1.85	Toluene to Water	1.06	This work
2.0	1.79	" "	1.11	This work
1.95	1.86	" "	1.30	Lewis (28)
2.04	1.94	" "	1.17	Lewis (28)
2.00	1.77	" "	0.73	Blokker (6)
(Aqueous phase) gm/l				
1.5	1.081	Water to Toluene	0.996	This work
1.79	1.460	" "	1.77	Lewis (28)
0.62	0.45	" "	1.08	Lewis (28)
1.5	0.5	" "	0.64	Blokker (6)

Several steady-state mass transfer runs were performed with transfer of benzoic acid from toluene to water to become familiar with the steady-state operating procedure of the cell.

Since the interface was observed to be in visible motion at organic phase stirring rates greater than 43.5 rpm, producing an unknown interfacial area, the stirring rates used in these runs were 43.5 rpm and 70 rpm for the toluene and aqueous phases respectively.

The mass transfer coefficients for steady-state operation were calculated from the following equation.

$$K_{ow} = \frac{Fw}{A} \frac{(C_{wo} - C_{wi})}{(C_w^* - C_w)} \qquad (4)$$

Table VI presents a summary of the results of the steady-state runs. The mass transfer coefficients for these steady-state runs were lower than the values obtained for unsteady-state. Tables V and VI are not directly comparable, since the driving force and concentration levels were continuously changing in the unsteady-state runs.

TABLE VI

Steady-State Transfer of Benzoic Acid

Flow Rates cc/min.		Benzoic Acid concentration (toluene phase) gm/l		K_{ow} cm/sec x 10^3
Toluene	Water	in	out	
2.13	2.05	1.5	1.39	0.817
2.00	2.00	1.5	1.388	0.820
1.66	1.70	1.5	1.368	0.828
1.31	1.37	1.5	1.340	0.853

A comprehensive investigation of the toluene-benzoic acid water

system was not undertaken, since the main object was to compare the mass transfer cell with cells used by Blokker (6) and Lewis (28) and to become familiar with the operating characteristics of the Cell. The unsteady-state mass transfer coefficients obtained compare fairly well with those reported by Lewis (28), but were higher than those reported by Blokker (6).

Unsteady-State Transfer of Uranyl Nitrate Between Water and TBP

The unsteady-state transfer of uranyl nitrate across the water-TBP interface was undertaken to check the results of Burger (8) and Lewis (29). These runs were performed according to the procedure discussed in Chapter IV. Several runs were made with the aqueous stirrer set at 75 rpm and an organic stirrer rate of 60 rpm. Since the 30% TBP solutions were rather viscous, the organic phase stirrer could be operated at stirring rates higher than those used for the benzoic acid-water-toluene system. The data were compared to Burger's work.

Burger analyzed his data on a kinetic basis. If the transfer is assumed to follow first order kinetics then the following equation applies.

$$\ln \frac{(C_{seq} - C_s)}{C_{seq}} = \frac{-C_{wo}}{C_{seq}} k_1 t \qquad (5)$$

Thus, a plot of $\ln\frac{(C_{seq} - C_s)}{C_{seq}}$ as a function of t should yield a straight line. Applying the above equation, Burger found that an initial linear relationship was obtained and that the rate of transfer decreased with time.

The unsteady-state data in this work were initially compared to

Burger's results by plotting $\frac{\ln(C_{seq} - C_s)}{C_{seq}}$ versus time. Figure 8 shows a typical result. It is immediately noted that the rate of transfer obtained is considerably less than that obtained Burger, however, a tailing off of the transfer rate with time, similar to that found by Burger, is observed. The discrepancy between these results and Burger's data is probably due to the difference in geometric and dynamic similarity between the two transfer cells, since the degree of turbulence depends on the stirring rates, the cell geometry, and the cell baffling. Table VII presents a comparison of the volume to surface area, ratio of the cell diameter to stirrer diameter, and the stirrer width to stirrer diameter for the two cells.

TABLE VII

GEOMETRIC COMPARISON OF CELL USED IN THIS STUDY AND BURGER'S CELL

	This work	Burger
Volume/surface area, cm.	24.6	19.45
Cell diameter/stirrer diameter	1.89	1.588
Stirrer width/stirrer diameter	0.36	0.6

Two runs were made where the organic phase volume was reduced to 65.7cc to decrease the volume to surface area in an attempt to increase the apparent rate of transfer. The results of these runs are shown in Figure 8. Although the transfer rate was increased, the results were still low in comparison to Burger's data.

Further unsteady-state runs were made on the transfer of uranyl nitrate from water to TBP, in order to check for build-up of an interfacial resistance with time as reported by Lewis (29). In most of these runs stirring rates of 150 rpm and 175 rpm were used for the aqueous and organic phases, respectively. These stirring rates of 150 rpm and 175

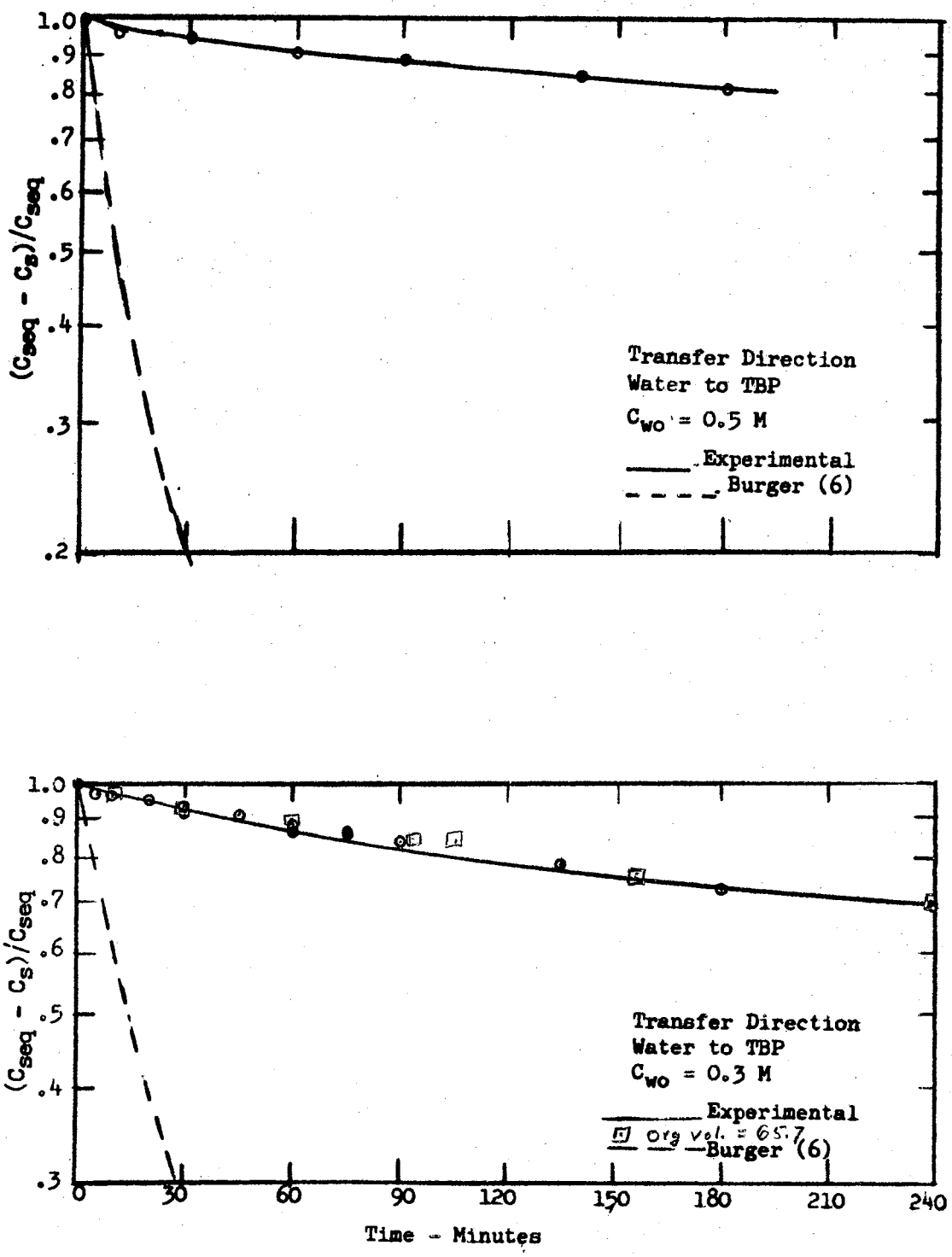

Figure 8.

Unsteady-State Transfer of Uranyl Nitrate
as a First Order Process

rpm were chosen, since they were the limiting stirring rates above which the interface was observed to be disrupted and in violent motion. Individual film mass transfer coefficients were calculated using the correlation developed by Mayer (33). A theoretical overall mass transfer coefficient was calculated by using the equation for additivity of film resistances.

$$\frac{1}{K_{os_{Theor.}}} = \frac{H}{k_w} + \frac{1}{k_s} \tag{6}$$

where:

$$H = \frac{C_{si} - C_s^*}{C_{wi} - C_w} \tag{7}$$

The experimental mass transfer coefficient was calculated from the equation.

$$K_{os} = \frac{\int \frac{dC_s}{C_s - C_s}}{\frac{A}{V} t} \tag{8}$$

An apparent interfacial resistance may then be calculated from the following equation:

$$\frac{1}{k_{rs}} = \frac{1}{K_{os}} - \frac{1}{K_{os\ Theor.}} \tag{9}$$

These calculations were carried out on an IBM 1410 digital computer. In addition, a point mass transfer coefficient was calculated by the following equation.

$$K'_{os} = \frac{dC_s}{dt} \left(\frac{1}{C_s^* - C_s}\right) \frac{v}{A} \qquad (10)$$

Table VIII presents the results of these runs. In some cases a negative interfacial resistance was obtained, indicating more rapid transfer than that predicted by the individual film correlations reported in the literature. This could be due to: (1) High transfer rates from turbulence induced in filling the cell, (2) Interfacial turbulence during the early stages of extraction, although transfer was in the opposite direction to that in which turbulence would be predicted, and (3) inapplicability of the correlations to predict the individual film coefficients in the cell used in this study.

The most probable cause for the calculation of a negative interfacial resistance is the inapplicability of Mayer's correlation (33) to adequately predict film coefficients in the mass transfer cell used. In the next section, the effect of stirring rates on the mass transfer coefficients is shown to be much larger than that predicted by Mayer's correlation. Even Lewis (29) has reported the calculation of a negative interfacial resistance during the early stages of transfer of uranyl nitrate between water and TBP. The effect of turbulence generated in filling the cell should lead to negative interfacial resistances only during the first five to ten minutes of operation. Thus, it is concluded that the negative resistances are due to the use of inadequate correlations. The overall point mass transfer coefficients were lower than the integral coefficients. This is probably due to the fact that these coefficients were evaluated by using $\frac{dC_s}{dt}$. Therefore, the point coefficients were not greatly influenced by turbulence generated in filling the cell.

The decrease of the mass transfer coefficients could be caused by an

TABLE VIII

Unsteady-State Mass Transfer Coefficients for Uranyl Nitrate

from Aqueous Solution into 30% TBP-Amsco

Uranyl Nitrate Concentration		Stirrer Speed		Time (min)	Calculated Overall Mass Transfer Coefficient	Experimental Integral Mass Transfer Coefficient	Hypothetical Interfacial Resistance	Experimental Point Overall Coefficient
Initial Aqueous Phase, M	Initial Organic Phase, M	Aqueous Phase, RPM	Organic Phase, RPM		$\times 10^3$ cm/sec	$\times 10^3$ cm/sec	sec/cm	$\times 10^3$ cm/sec
0.3	0.0	214	250	8	1.352	2.165	-2.775×10^2	1.618
"	"	"	"	16	"	1.951	-2.269×10^2	1.538
"	"	"	"	25	"	1.719	-1.579×10^2	1.425
"	"	"	"	38	"	1.432	-4.109×10	1.198
"	"	"	"	55	"	1.244	6.396×10	0.847
"	"	"	"	80	"	1.151	1.288×10^2	0.212
0.3	0.0	155	176	5	0.9657	1.218	-2.151×10^2	0.397
"	"	"	"	10	"	0.738	3.196×10^2	0.393
"	"	"	"	20	"	0.518	8.944×10^2	0.384
"	"	"	"	30	"	0.433	1.273×10^3	0.374
"	"	"	"	45	"	0.428	1.303×10^3	0.362
"	"	"	"	75	"	0.386	1.556×10^3	0.321
"	"	"	"	123	"	0.324	2.051×10^3	0.264
"	"	"	"	180	"	0.317	2.111×10^3	0.182
0.3	0.0	154	173	5	0.9574	1.860	-5.068×10^2	0.629
"	"	"	"	10	"	1.418	-3.392×10^2	0.622
"	"	"	"	20	"	0.958	-0.733	0.602
"	"	"	"	36	"	0.785	2.288×10^2	0.572

TABLE VII (continued)

Uranyl Nitrate Concentration		Stirrer Speed		Time (min)	Calculated Overall Mass Transfer Coefficient	Experimental Intergral Mass Transfer Coefficient	Hypothetical Interfacial Resistance	Experimental Point Overall Coefficient
Initial Aqueous Phase, M	Initial Organic Phase, M	Aqueous Phase, RPM	Organic Phase, RPM		$\times 10^3$ cm/sec	$\times 10^3$ cm/sec	sec/cm	$\times 10^3$ cm/sec
0.3	0.0	154	173	58	0.9574	0.656	4.798×10^2	0.524
"	"	"	"	80	"	0.510	9.199×10^2	0.456
"	"	"	"	120	"	0.507	9.269×10^2	0.354
"	"	"	"	180	"	0.452	1.168×10^3	0.144
0.5	0.0	154	175	11	1.011	3.984	-7.380×10^2	0.702
"	"	"	"	20	"	2.287	-5.512×10^2	0.674
"	"	"	"	35	"	1.694	-3.987×10^2	0.643
"	"	"	"	55	"	1.145	-1.158×10^2	0.576
"	"	"	"	81	"	0.861	1.728×10^2	0.491
"	"	"	"	180	"	0.645	5.610×10^2	0.307
0.5	0.0	148	176	5	0.9941	4.090	-7.614×10^2	0.928
"	"	"	"	10	"	2.277	-5.668×10^2	0.904
"	"	"	"	20	"	1.587	-3.762×10^2	0.865
"	"	"	"	35	"	1.204	-1.751×10^2	0.798
"	"	"	"	55	"	0.865	1.197×10^2	0.672
"	"	"	"	81	"	0.779	2.763×10^2	0.547
"	"	"	"	120	"	0.574	7.360×10^2	0.221
"	"	"	"	180	"	0.531	8.750×10^2	
0.5	0.0	147	175	5	0.9879	5.908	-8.430×10^2	1.161
"	"	"	"	10	"	3.248	-7.04×10^2	1.137
"	"	"	"	21	"	2.010	-5.48×10^2	1.096
"	"	"	"	36	"	1.543	-3.655×10^2	1.035
"	"	"	"	55	"	1.180	-1.651×10^2	0.933

TABLE VIII (continued)

Uranyl Nitrate Concentration		Stirrer Speed		Time (min)	Calculated Overall Mass Transfer Coefficient X 10^3 cm/sec	Experimental Integral Mass Transfer Coefficient X 10^3 cm/sec	Hypothetical Interfacial Resistance sec/cm	Experimental Point Overall Coefficient X 10^3 cm/sec
Initial Aqueous Phase, M	Initial Organic Phase M	Aqueous Phase, RPM	Organic Phase, RPM					
0.5	0.0	147	175	80	0.9879	0.983	5.489	0.793
"	"	"	"	133	"	0.781	2.670×10^2	0.457
0.8	0.0	146	175	10	0.9845	2.470	-6.110×10^2	1.229
"	"	"	"	20	"	1.830	-4.694×10^2	1.124
"	"	"	"	35	"	1.331	-2.645×10^2	0.927
"	"	"	"	56	"	1.005	-2.108×10^2	0.623
"	"	"	"	80	"	0.827	1.934×10^2	0.253
"	"	"	"	120	"	0.713	3.864×10^2	
0.8	0.0	148	175	5	1.121	3.344	-5.926×10^2	2.138
"	"	"	"	10	"	3.901	-6.353×10^2	2.085
"	"	"	"	20	"	2.596	-5.060×10^2	1.866
"	"	"	"	38	"	1.765	-3.251×10^2	1.419
"	"	"	"	55	"	1.541	-2.926×10^2	0.977
"	"	"	"	81	"	1.156	-2.073×10^2	0.209
"	"	"	"	120	"	0.978	1.299×10^2	
"	"	"	"	180	"	0.791	3.310×10^2	

interfacial surface blockage. Mayers and Davies (34) have investigated the effect of interfacial films and found that mass transfer rates are significantly reduced by interfacial films. An interfacial film tends to damp out eddies coming from the stirrers in the organic phase and also damps out momentum transfer across the interface. Lewis (29) has shown that the decrease of the transfer rate of uranyl nitrate between water and TBP with time is not due to interfacial contamination. Therefore, surface blockage does not appear to be the mechanism which causes the decrease of the transfer rate with time, provided care is taken to prevent the occurence of surfactants in the experimental apparatus and solutions.

The driving force for mass transfer, in the unsteady-state runs, decreased with time. The effect of the varying driving force is discussed in the steady-state section and the unsteady-state and steady-state data compared.

Effect of Stirring Rates on the Steady-State Transfer of Uranyl Nitrate

Steady-state mass transfer runs, with uranyl nitrate transferring from water to TBP, were made to study the effect of stirring on the transfer rate. After several runs it became evident that the uranyl nitrate analysis had to be improved to obtain good material balances. The uranium analysis was improved such that the concentrations could be reproduced to $\pm$ 0.3%, and the material balance error was reduced to about $\pm$ 1.0%.

The following equations describe the transfer of uranyl nitrate when the cell is operating under flow conditions with transfer from water to TBP.

$$v \frac{dC_{w_2}}{dt} = F_w(C_{w_1} - C_{w_2}) - K_{os} A(C^*_{s_2} - C_{s_2}) \quad (11)$$

and

$$v \frac{dC_{s_2}}{dt} = F_s(C_{s_1} - C_{s_2}) + K_{os} A(C^*_{s_2} - C_{s_2}) \quad (12)$$

where:

F_w = Aqueous feed rate

F_s = Organic feed rate

C_{w_1} = Aqueous feed concentration

C_{w_2} = Aqueous outlet concentration

C_{s_1} = Organic feed concentration

C_{s_2} = Organic outlet concentration

$C^*_{s_2}$ = Concentration of organic phase in equilibrium with the aqueous outlet concentration.

At steady-state conditions, $\frac{dC_w}{dt}$ and $\frac{dC_s}{dt}$ are identically zero. Thus the overall mass transfer coefficient may be calculated from either of the following equations.

$$K_{os} = \frac{F_w}{A} \frac{(C_{w_1} - C_{w_2})}{(C^*_{s_2} - C_{s_2})} \quad (13a)$$

and

$$K_{os} = \frac{F_s}{A} \frac{(C_{s_2} - C_{s_1})}{(C^*_{s_2} - C_{s_2})} \quad (13b)$$

The stirring rate runs were made with the aqueous phase stirring rate maintained at 100 rpm while the organic phase stirring rate was varied. The maximum rate of stirring used in the TBP phase was 175 rpm, since at higher stirring rates the interface was broken up. One run was made with no stirring in the organic phase in order to investigate

whether the flow rate was causing any significant turbulence or mixing in the cell. After eight hours of operation, the organic phase stream did not contain a detectable uranyl nitrate content. This indicates that the organic phase flow rate was sufficiently low to prevent any significant turbulence or mixing of the two phases and that the rate of solute transfer was controlled by molecular diffusion. The results of these runs are shown in Figure 9.

A least-means-square regression analysis of the steady-state mass transfer coefficient in the cell gives the following relationship.

$$\frac{K_{os}}{\nu} = 3.57 \times 10^{-10} Re_s^{2.8} \qquad (14)$$

This curve fit was obtained based on the linearized equation:

$$\ln \frac{K_{os}}{\nu} = A + B \ln Re_s \qquad (15)$$

The standard deviation of the linearized equation is 0.489.

This analysis gives a substantially higher exponent for the Reynolds number than that reported by Lewis $\left(\frac{k}{\nu} \times Re^{1.65}\right)$, and greater than five times the exponent recommended by Mayers (33) and Olander and Benedict (41). These data were also curve fitted to Mayers' model. The result of this correlation is:

$$K_{os} = 1.54 \times 10^{-18} (Re_s \cdot Re_w)^{2.45} \qquad (16)$$

The standard deviation of the linearized model is 0.5329. If it is assumed that the organic phase resistance is controlling so that the overall organic phase mass transfer coefficient is approximately equal

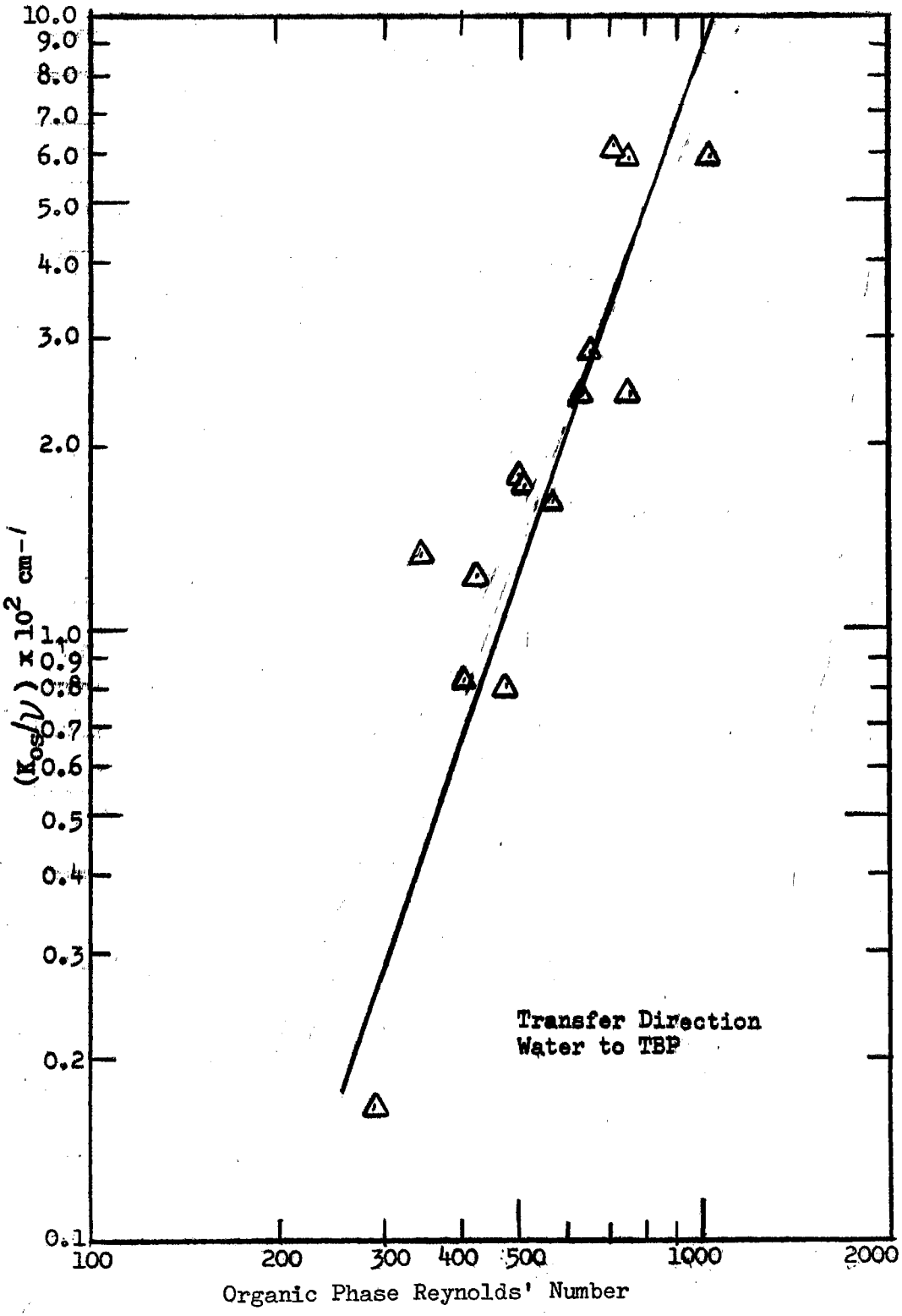

Figure 9.

Steady-State Mass Transfer Coefficients

to the individual film coefficient, then it must be concluded that the correlation proposed by Mayers is not valid for estimating film coefficients in our equipment. In Burger's work, (6), the effect of the organic phase stirring rate on the first order rate constant was proportional to the stirring rate raised to the 3.81 power.

The high exponent on the Reynolds number is probably due to the geometric configuration of the cell, including the cell baffling and the spacing of the stirrers relative to the interface, as these factors would have a significant effect on the hydrodynamic conditions in the cell.

The high exponent may be partially attributed to the fact that stirring in the aqueous phase transmits energy to the interface. Therefore, the data were investigated assuming the following equation.

$$\frac{K_{os}}{\nu} = A\,(Re_s)^{0.5}\left(1 + \frac{Re_w}{Re_s}\right)^{Z} \tag{17}$$

Here, the term $(1 + \frac{Re_w}{Re_s})$ is assumed to be a correction factor which accounts for the energy transmitted from the other phase. This correction factor seems reasonable since the correlation presented by Lewis contained the term $(Re_1 + \frac{\mu_2}{\mu_1} Re_2)^{Z}$.

Treating the data in this manner, the following correlation was obtained.

$$\frac{K_{os}}{\nu} = 6.52 \times 10^{-5} Re_s^{0.5}\left(1 + \frac{Re_w}{Re_s}\right)^{2.02} \tag{18}$$

The standard deviation of this model is 0.657.

The data were also curve fitted to the Lewis model and the following correlation obtained.

$$K_{os} = 3.68 \times 10^{-22}\left(Re_s + \frac{\mu_2}{\mu_1} Re_w\right)^{6.26} \tag{19}$$

The standard deviation of this model is 0.6117. Thus, the model using only the organic phase Reynolds numbers best represents the experimental data.

The aqueous or lower phase has a much lower kinematic viscosity than the TBP phase and thus the diffusional boundary layer is probably quite thin. On the other hand, the organic phase has a rather high kinematic viscosity in addition to a low diffusivity. Thus, if it is assumed that the solute transfer is by eddy or turbulent diffusion the viscous sublayer and the diffusion sublayer contribute the major resistances to uranyl nitrate transfer. If a section of the transfer area is examined the flow patterns will probably be as shown in Figure 10.

Since the TBP phase is more viscous the eddies do not approach the interface as close as in the aqueous phase. Furthermore, the eddies sweeping across the interface as pictured may lead to operation in a

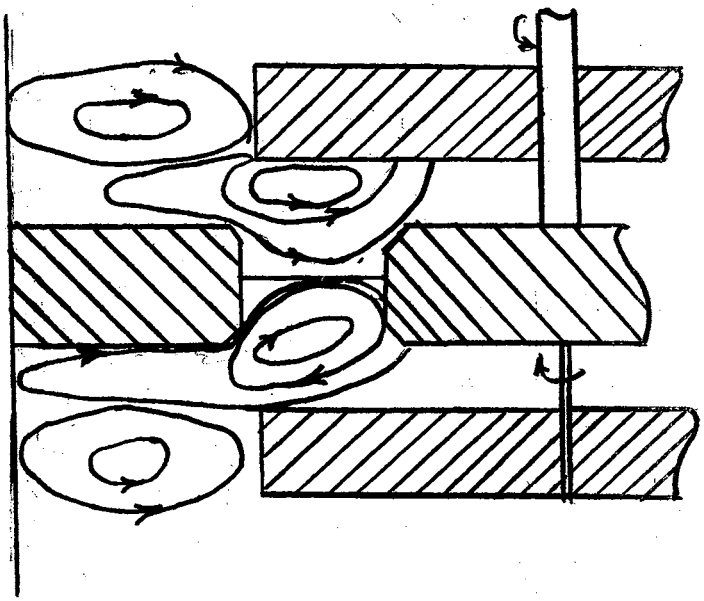

Figure 10.

Flow Patterns Across Interfacial Area

transition regime causing a higher dependency on the Reynolds number than the direct relationship usually assumed for turbulent diffusion.

Effect of Driving Force on the Transfer of Uranyl Nitrate Between Water and TBP

Most studies of mass transfer have assumed that the rate of solute transfer is independent of concentration level or concentration driving force. However, under some circumstances the effect of physical property variations may affect the mass transfer coefficients. Two possible mechanisms which immediately come to mind are:

1. A chemical reaction occurring at the interface.
2. Interfacial turbulence due to transfer of a solute from a liquid phase of high viscosity to a phase of low viscosity.

Murdoch and Pratt (40) predict that the aqueous phase film coefficient for the transfer of uranyl nitrate between water and methyl isobutyl ketone varies as the square of uranium concentration, suggesting a third order chemical reaction at the interface. The theory of interfacial turbulence as presented by Sternling and Scriven (42) also suggests a mechanism whereby the transfer of a solute between two liquid phases may be controlled by the concentration driving force. Olander and Reddy (43) have shown that the rate of transfer of nitric acid between various organic solvents and water is a function of the driving force.

The effect of the driving force on the rate of transfer of uranyl nitrate across the water TBP interface was investigated by operating the cell at steady-state. The stirrer speeds selected for these runs were 100 rpm for both the aqueous and organic stirrers. The driving force for transfer in both directions was varied from about 0.09 Molar to about 0.43 Molar.

The mass transfer coefficients were calculated as discussed under the stirring rate data. The results of the transfer coefficients for transfer from water to TBP are reported in Table IX. The ratio of the overall organic phase mass transfer coefficient to the kinematic viscosity is plotted as a function of the driving force. In these runs the organic feed contained no uranium and thus the concentration level varied. From Figure 11, it is observed that the transfer rate increases rapidly as the driving force decreases. The data for these runs are tabulated in Table XXII. A regression analysis of this data gave the following correlation.

$$\frac{K_{os}}{\nu Re^{2.8}} = 0.2169 \times 10^{-9}(C_s^* - C_s)^{-0.549} \qquad (20)$$

The organic phase Reynolds numbers were about 615 for the runs with organic phase stirring rates of 100 rpm. Since a considerable number of steady-state runs were performed for the investigation of the effect of stirring rates on the mass transfer rate, these stirring rate data were normalized to a Reynolds number of 615 and are shown in Figure 11. The normalization was performed by using Equation (14).

The activity-based mass transfer coefficients were calculated since activities provide a better definition of driving force. The driving force based on activities is simply the activity in phase W minus the activity in phase S. Robinson (45) has published the molal activity coefficient for aqueous uranyl nitrate solutions. These values were converted to molar activity coefficients and the activity was then plotted as a function of the aqueous phase molarity. It should be noted that the assumption of equilibrium at the interface in two film transfer theory is not relaxed by using activities in place of concentrations.

TABLE IX

Steady-State Transfer From Water to TBP

C_w Molar	C_s Molar	Re_w	Re_s	$(C_s^* - C_s)$ Molar	K_{ow} x 10^3 cm/sec	K_{os}/ν x 10 cm
0.4899	0.0254	1360	615.5	0.3135	0.5698	0.257
0.4229	0.0340	1388	610.4	0.2874	0.8366	0.374
0.7180	0.0391	1257	610.3	0.3557	0.678	0.304
0.9489	0.0289	1148	613.7	0.3991	0.494	0.222
0.5568	0.0281	1331	613.9	0.3271	0.6112	0.2752
0.9266	0.0267	1158	614.7	0.3977	0.467	0.2106
0.1448	0.0157	1479	621.2	0.0894	1.250	0.5707
0.1831	0.0185	1470	619.6	0.1336	0.987	0.448
0.2975	0.0204	1409	650	0.2476	0.609	0.280
0.292	0.0187	1410	625	0.2463	0.535	0.295

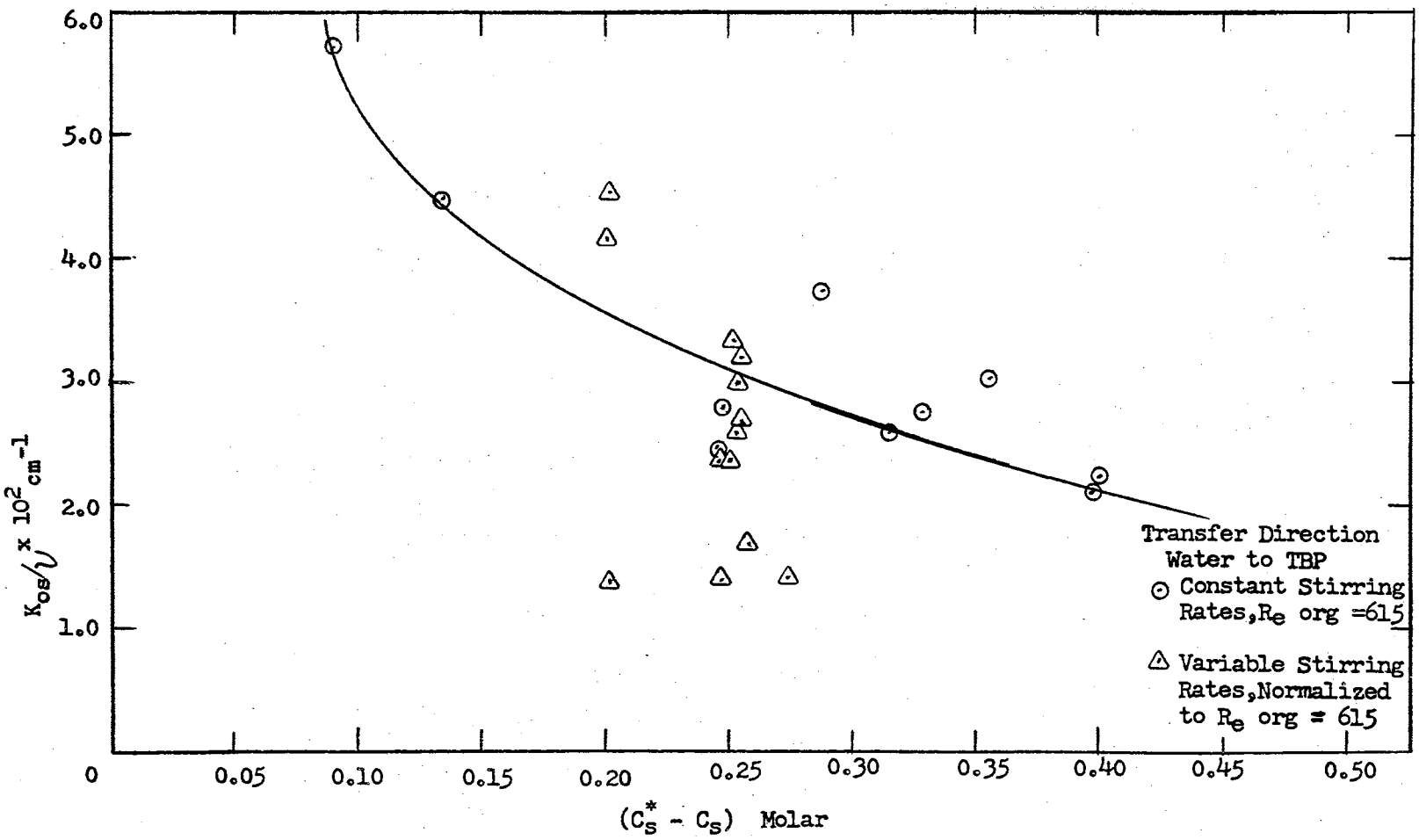

Figure 11.

Effect of Driving Force on Mass Transfer Coefficient Divided by Kinematic Viscosity

In this case the assumption of equilibrium at the interface means that the chemical potential of the two phases are equal at the interface. Since when two phases are in equilibrium the chemical potentials of the two phases are equal, the activity of TBP-uranyl nitrate solutions may be calculated from the aqueous phase activity and the molar equilibrium relationship. Figure 12 shows the activity-based transfer coefficient, K'_{os}, as a function of the activity driving force while Figure 13 presents the relationship between K'_{os}/ν and the driving force. When the mass transfer coefficients are converted to activity-based coefficients the scatter of the data is reduced. However, the activity-based coefficients also increase as the driving force decreases.

Since the mass transfer coefficients increased rapidly with decreasing driving force, the molar flux, j, was calculated for these runs in order to check whether the transfer of uranyl nitrate remains finite at low driving forces. Table X and Figure 14 gives the molar flux for these runs and it is seen that although the transfer coefficients increase with decreasing driving force, the molar flux decreases slowly with the driving force. Therefore, the mass flux remains finite as the driving force approaches zero although the mass transfer coefficient tends to increase very rapidly.

The steady-state transfer of uranyl nitrate from TBP to water was investigated as a function of both the driving force and concentration level in the aqueous phase. In these runs, the stirring rates were again operated at 100 rpm in both phases. The driving force in these runs varied from 0.1 molar to approximately 0.44 molar, while the aqueous phase concentration level varied from 0.025 molar to 0.23 molar. The overall mass transfer coefficients divided by the kinematic viscosity

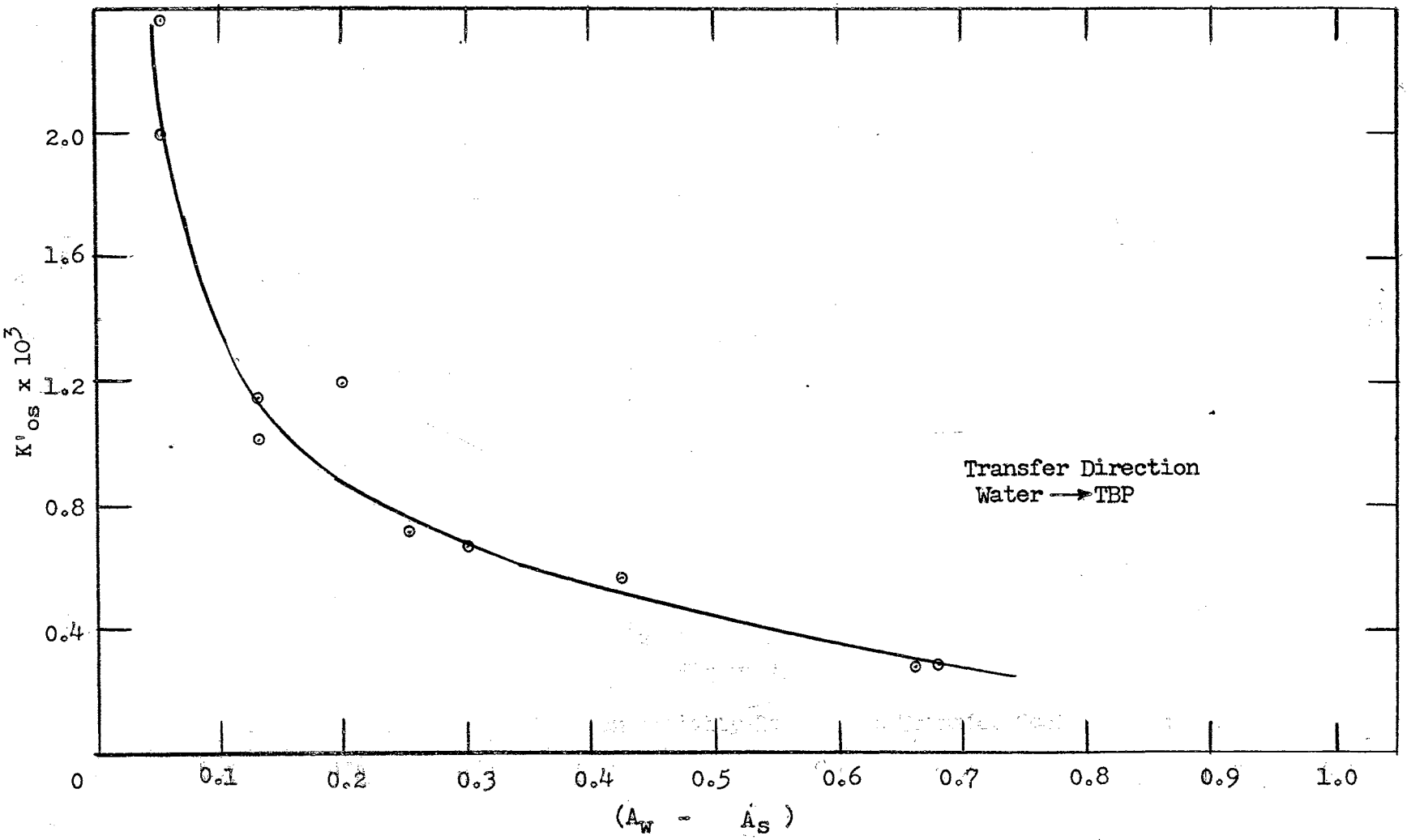

Figure 12.

Effect of Driving Force on Activity-Based Mass Transfer Coefficients

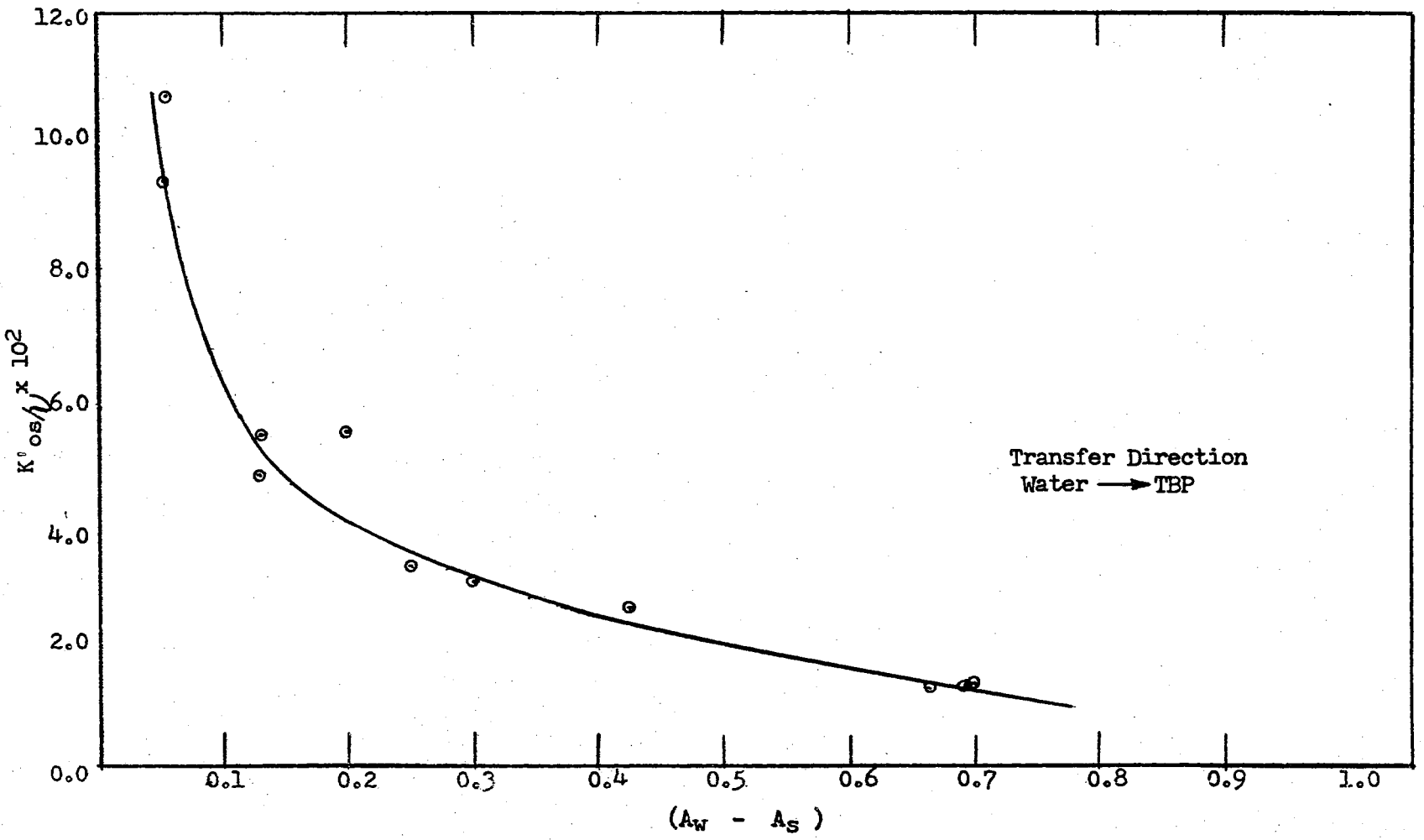

Figure 13.

Effect of Driving Force on Activity-Based Mass Transfer Coefficient Divided by Kinematic Viscosity

TABLE X

Molar Flux for Transfer
from Water to TBP

$j \times 10^3$ $\frac{\text{gm moles}}{\text{cm.}^2\text{sec}}$	$(C_s^* - C_s)$ Molar
.1786	.3135
.2405	.2874
.24137	.3557
.2022	.3991
.1858	.3977
.1999	.3271
.1119	.0894
.1318	.1336

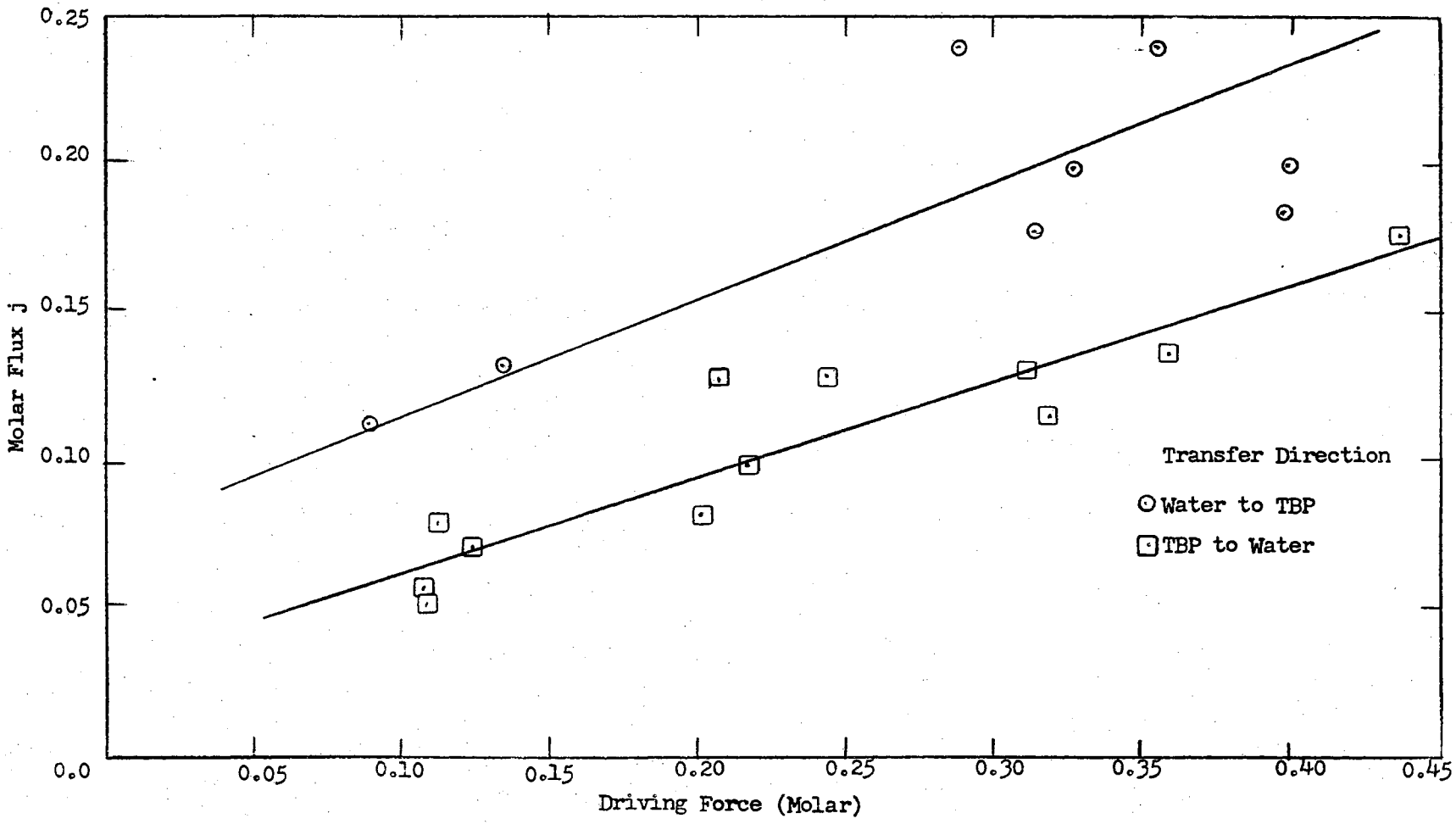

Figure 14.

Effect of Driving Force on Molar Flux

are plotted versus the molar driving force in Figure 15. It appears that for uranyl nitrate transfer from 30% TBP to water the effect of the aqueous phase concentration level is small. However, as discussed below, further analysis shows that concentration level is a significant variable. The effect of driving force on the activity-based mass transfer coefficients and the activity-based mass transfer coefficients divided by kinematic viscosity is shown in Figure 16 and 17, respectively. A least-means-square-analysis of this data was performed and the following correlation obtained:

$$\frac{K_{os}}{R_{es}^{2.8}} = 0.259 \times 10^{-10}(C_s - C_s^*)^{0.3056} \qquad (21)$$

This correlation does not agree with that obtained for transfer from water to TBP, since it indicates the transfer rate increases with the driving force. It should be noted that aqueous phase concentration level varied by a factor of 20 for these steady-state runs with transfer from TBP to water. Therefore, $K_{os}/\nu Re_s^{2.8}$ was plotted versus $(C_s - C_s^*)$ for various parameters of C_w (Figure 18b). This plot shows that the term $K_{os}/\nu Re_s^{2.8}$ increases with driving force and is also a function of the aqueous phase concentration. This plot indicates that Equation 21 does not adequately describe the transfer of uranyl nitrate from TBP to water. The data for transfer from water to TBP are shown in Figure 18a for two parameters of C_s. Figures 18a and 18b show that the transfer of uranyl nitrate between water and TBP is a function of the driving force and the concentration level of the phase into which the uranyl nitrate is being transferred. At a fixed driving force, the rate of transfer of uranyl nitrate from water to TBP increases with decreasing organic phase

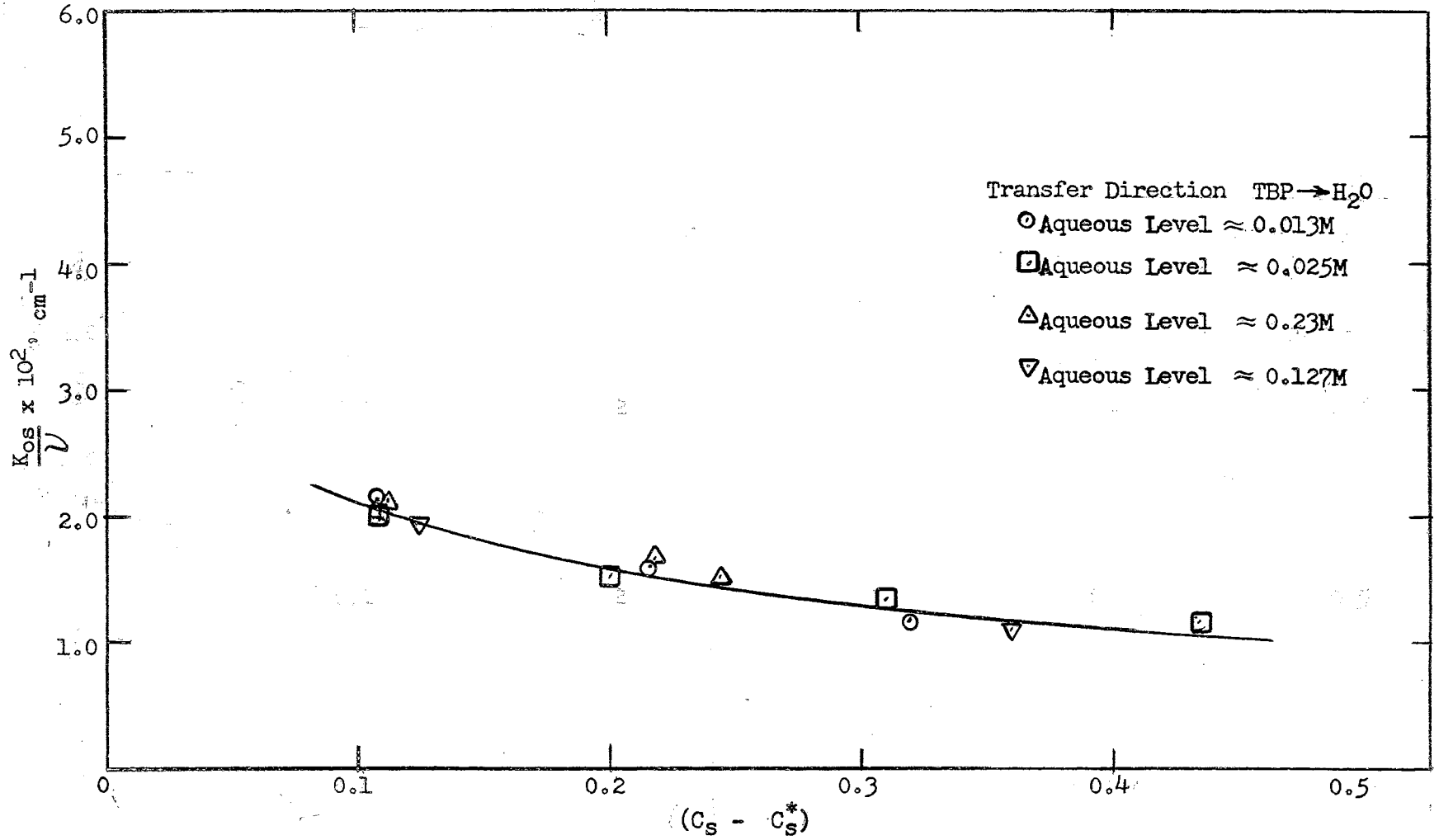

Figure 15.

Effect of Driving Force on Mass Transfer Coefficient Divided by Kinematic Viscosity

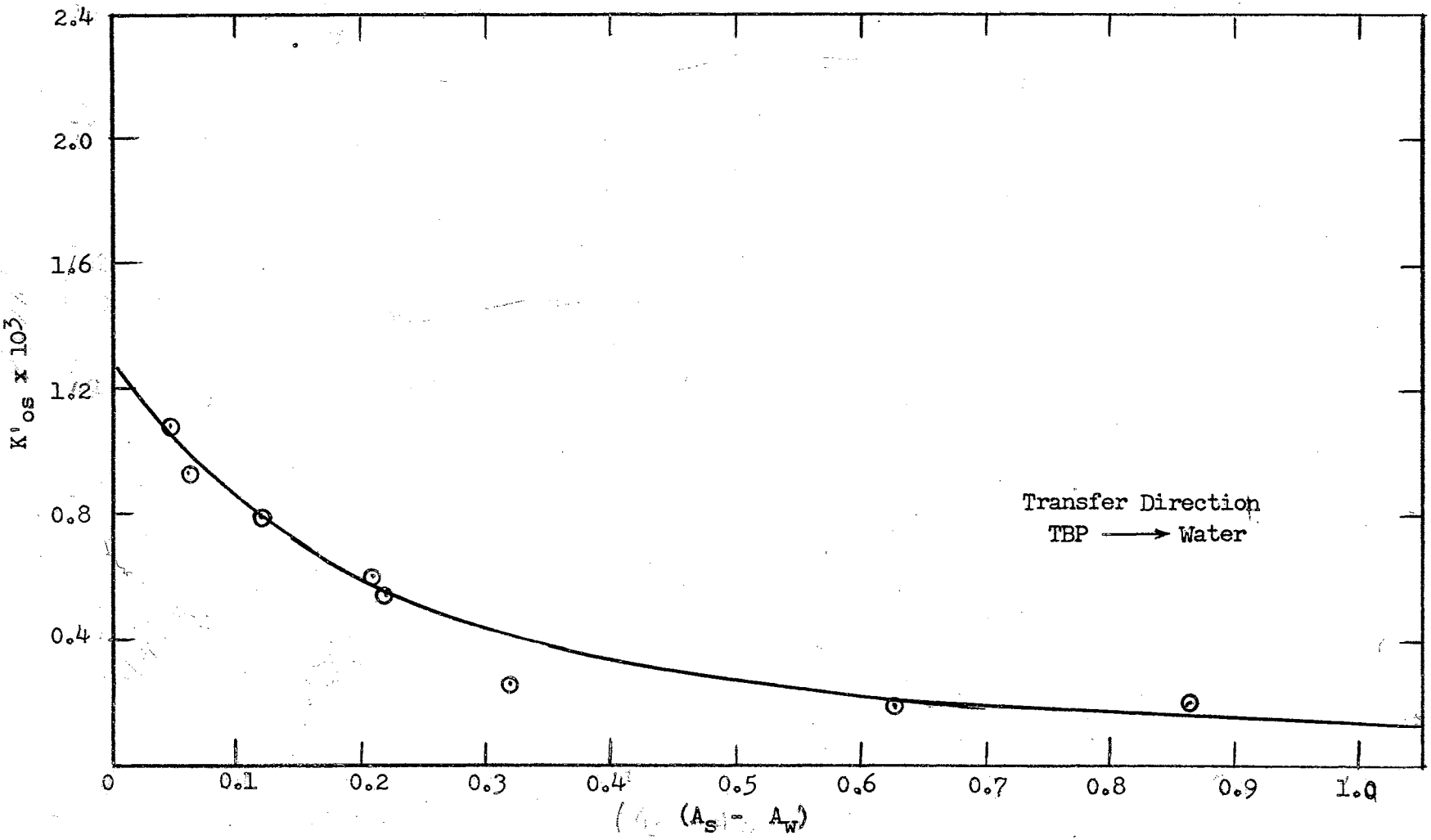

Figure 16.

Effect of Driving Force on Activity-Based Mass Transfer Coefficient

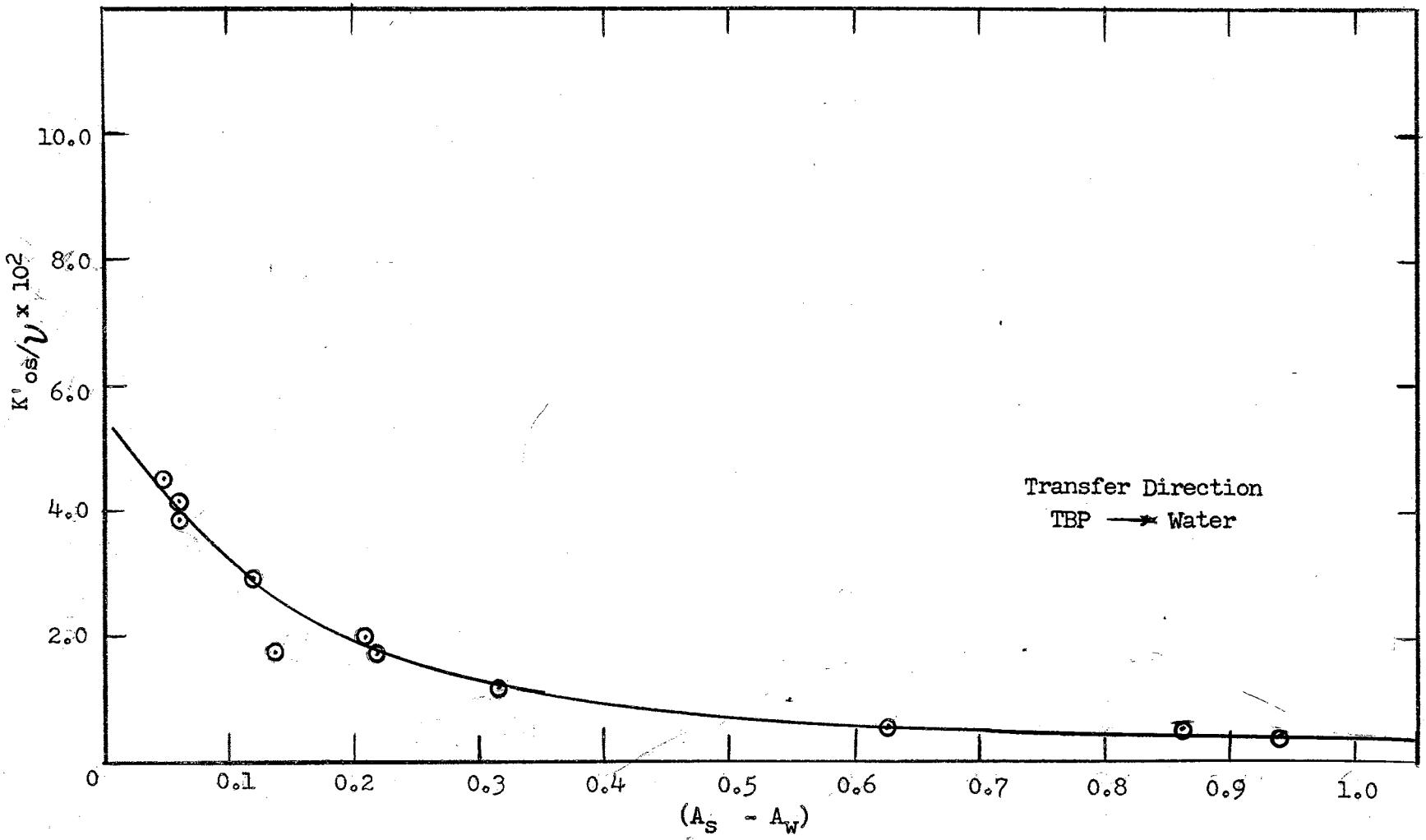

Figure 17.

Effect of Driving Force on Activity-Based Mass Transfer Coefficient Divided by Kinematic Viscosity

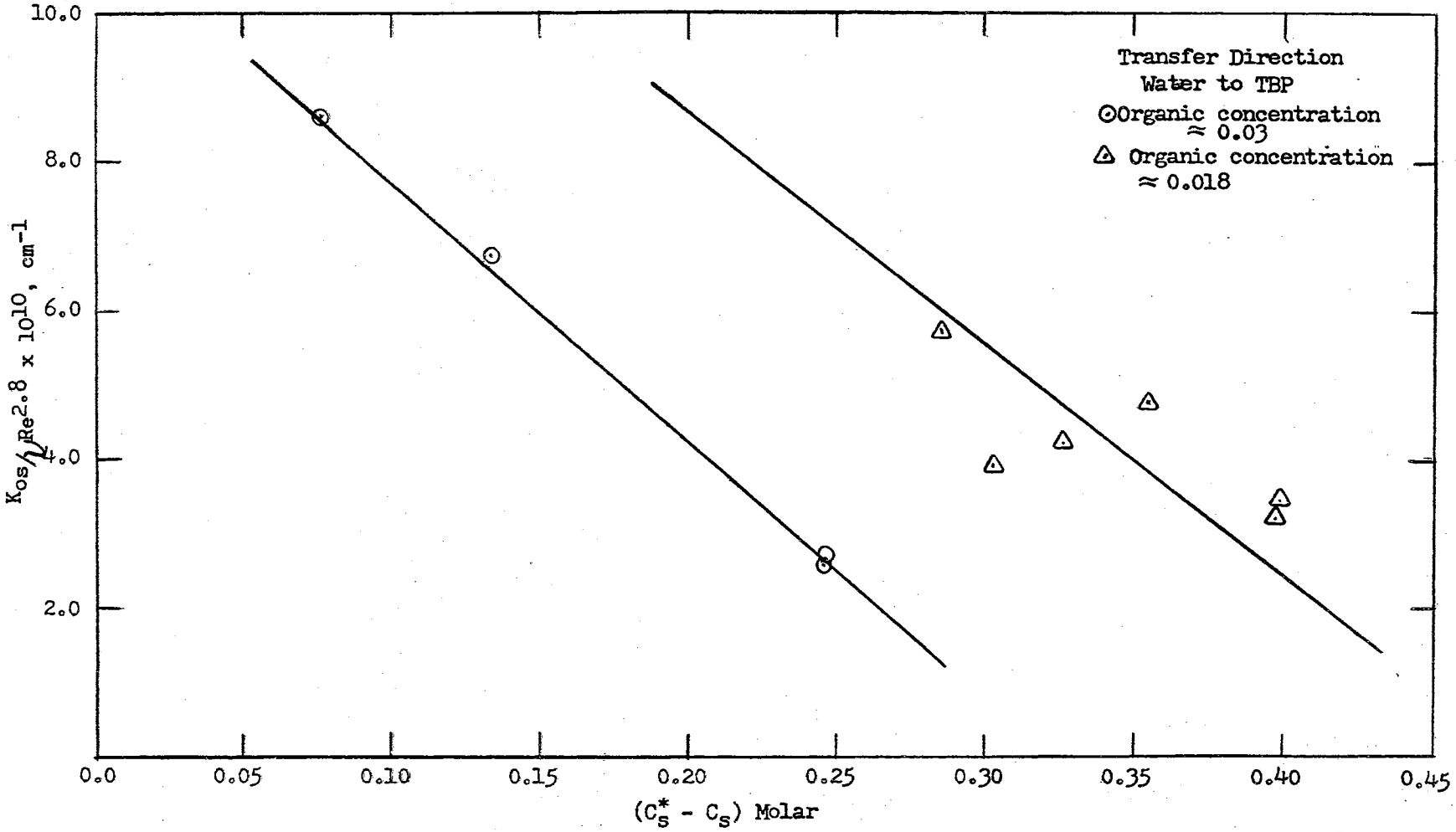

Figure 18a.

Effect of Driving Force on $K_{os}/\mu Re_s^{2.8}$ for Transfer from Water to TBP

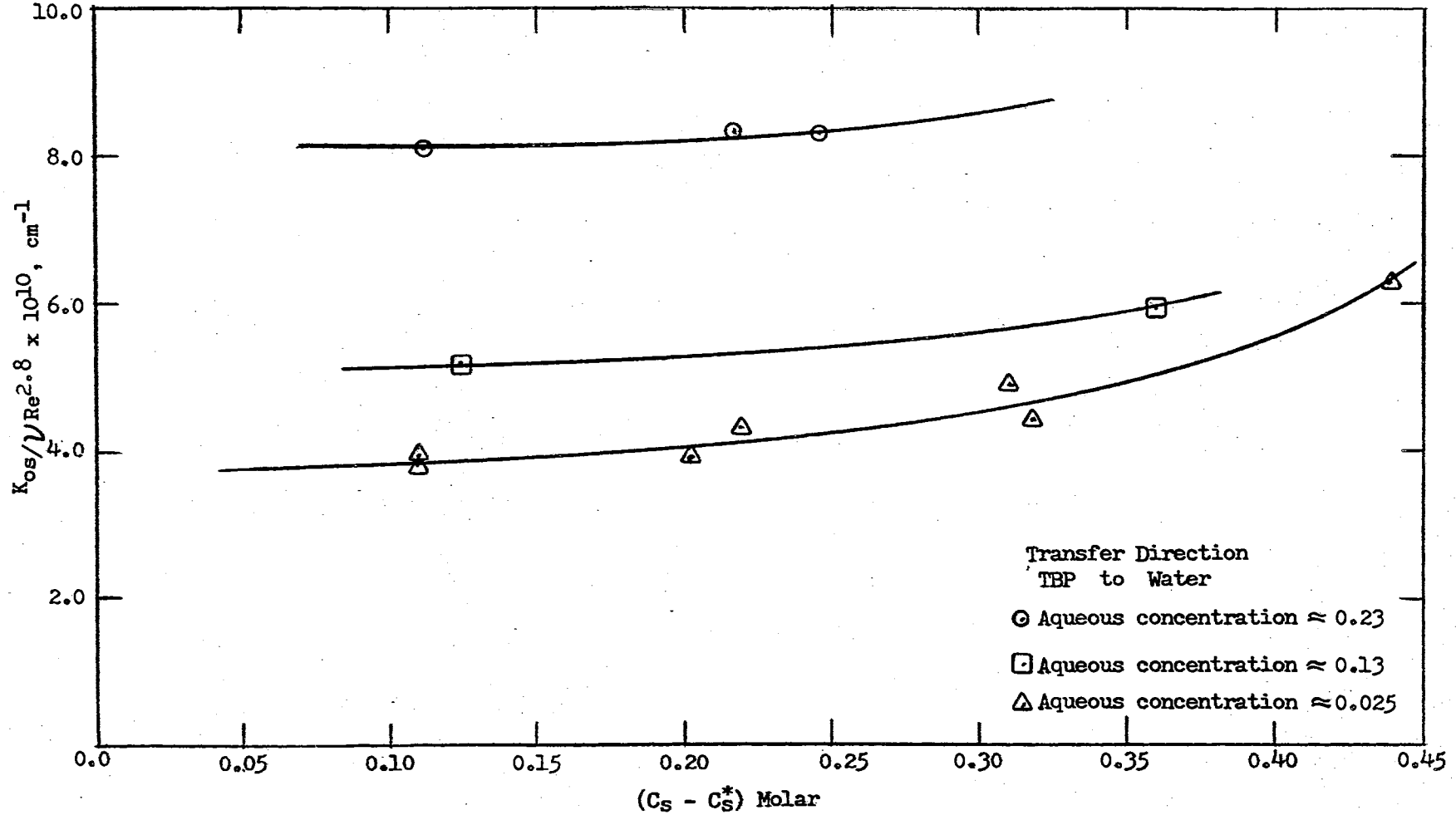

Figure 18b.

Effect of Driving Force on $K_{os}/\nu Re_s^{2.8}$ for Transfer from TBP to Water

concentration level. The rate of transfer of uranyl nitrate from TBP to water at a fixed driving force increases with increasing aqueous phase concentration level.

In order to determine whether the molecular diffusion coefficient had any effect on the relationship between the concentration level and the mass transfer coefficients, the term $\frac{K_{os}}{\nu(c_s - c_s^*)}$ was compared to the differential molecular diffusion coefficient of uranyl nitrate in water as reported by Finley (19) for the steady-state transfer of uranyl nitrate from TBP to water. The results are tabulated in Table XXV in the appendix. The factor $\frac{K_{os}}{\nu(c_s - c_s^*)}$ did not correlate with the aqueous phase diffusion coefficients. The diffusion coefficient for uranyl nitrate in 30% TBP in Amsco as reported by Finley (19) does not vary significantly with concentration. Therefore, the mass transfer coefficients appear to be controlled by convective or turbulent diffusion rather than by molecular diffusion. This appears to be consistent with the data on the effect of stirring rates and indicates that the diffusion boundary layer must be very small in the organic phase. Therefore, the primary mechanism of transfer is due to hydrodynamic turbulence. Figures 16 and 17 show the relation between the activity driving force and K'_{os} and $\frac{K'_{os}}{\nu}$ respectively. Table XI presents the molar flux and it is seen that the flux decreases as the driving force decreases as was observed or transfer in the reverse direction.

The unsteady-state mass transfer data for transfer of uranyl nitrate from water to TBP were not consistent with the steady-state data, since the unsteady-state mass transfer coefficients decreased with time, equivalent to decreasing driving force. The steady-state coefficients for transfer from water to TBP increased with decreasing driving force.

TABLE XI

Molar Flux for Transfer from TBP to Water

$j \times 10^3$ $\frac{gm - moles}{cm^2 sec}$	$(C_s - C_s^*)$ Molar
.1768	.436
.1159	.3193
.0984	.2169
.0560	.10803
.1311	.3121
.0819	.2017
.0520	.1085
.1275	.2177
.1281	.2439
.0794	.1125
.1367	.3589
.0708	.1242

However, in the unsteady-state experiments the concentration level was continuously decreasing. Table XII presents the instantaneous driving forces for unsteady-state transfer of uranyl nitrate from water to TBP. The mass transfer rates presented in Table XII have been normalized to stirring rates of 100 rpm in both phases. This normalization was performed by using Equation 18. It should be noted that in most cases the unsteady-state point mass transfer coefficients divided by the kinematic viscosity, $\frac{K'_{os}}{\nu}$, are less than those obtained in the steady-state experiments, when compared at the same driving force.

Interfacial Tension of the Uranyl Nitrate TBP System

The interfacial tension of the water-uranyl nitrate-TBP system was measured in order to use the Sternling and Scriven's (49) model of interfacial turbulence to qualitatively predict whether interfacial turbulence should exist in this system. The Sternling and Scriven model predicts interfacial turbulence will occur when a solute transfers out of the phase of higher viscosity and lower diffusivity, if the interfacial tension decreases with increasing solute concentration. The viscosity of 30% TBP uranyl nitrate solutions is much higher than the viscosity of aqueous uranyl nitrate solutions. Therefore, the Sternling and Scriven theory predicts that interfacial turbulence might be observed for transfer of uranyl nitrate from TBP. The interfacial tension of the water-uranyl nitrate-TBP system as a function of the aqueous phase concentration is given in Figure 19. Since the interfacial tension increases with uranyl nitrate concentration, the Sternling and Scriven theory predicts that any disturbances at the interface will be damped out.

If equilibrium does not exist at the interface, interfacial turbulence

TABLE XII

Unsteady-State Point Transfer Coefficients

Transfer Direction: $H_2O \longrightarrow TBP$

$(C_s^* - C_s)$ molar	C_s molar	C_w molar	$\frac{K'_{os}}{v} \times 10^2$
.2502	.00950	.292	5.910
.238	.01700	.289	5.550
.2241	.02390	.272	5.120
.2086	.02840	.265	4.26
.1958	.03420	.255	2.93
.2545	.00348	.290	1.31
.2538	.00420	.290	1.285
.2522	.00585	.290	1.255
.2477	.00729	.287	1.215
.2364	.01065	.278	1.172
.2313	.01570	.277	1.025
.2449	.00609	.281	1.890
.2413	.00771	.2782	1.860
.2381	.01036	.2775	1.80
.2299	.01507	.275	1.70
.2223	.01994	.272	1.57
.2167	.02128	.267	1.36
.1966	.03043	.251	1.05
.3328	.03020	.494	2.04
.3104	.03160	.489	1.96
.3001	.04090	.4875	1.84
.2973	.04270	.485	1.64
.2900	.04700	.470	1.37

TABLE XII (continued)

$(C_s^* - C_s)$ molar	C_s molar	C_w molar	$\frac{K'_{os}}{\nu} \times 10^2$
.2755	.05950	.459	0.845
.3303	.0147	.501	2.52
.3287	.0163	.502	2.44
.3224	.0226	.501	2.34
.3131	.0294	.491	2.14
.3121	.0294	.489	1.80
.3058	.0347	.483	1.46
.3220	.0210	.495	3.18
.3188	.0232	.492	3.10
.3125	.0295	.492	2.97
.3031	.0386	.489	2.75
.2965	.0445	.483	2.48
.2860	.0530	.479	2.09
.2692	.0678	.474	1.18
.3280	.0152	.497	3.32
.3217	.0213	.495	3.02
.3173	.0307	.495	2.48
.3032	.0388	.492	1.69
.3952	.0118	.816	6.0
.3780	.0270	.806	5.71
.3649	.0356	.779	5.16
.3997	.0453	.745	3.88
.3387	.0563	.745	2.62

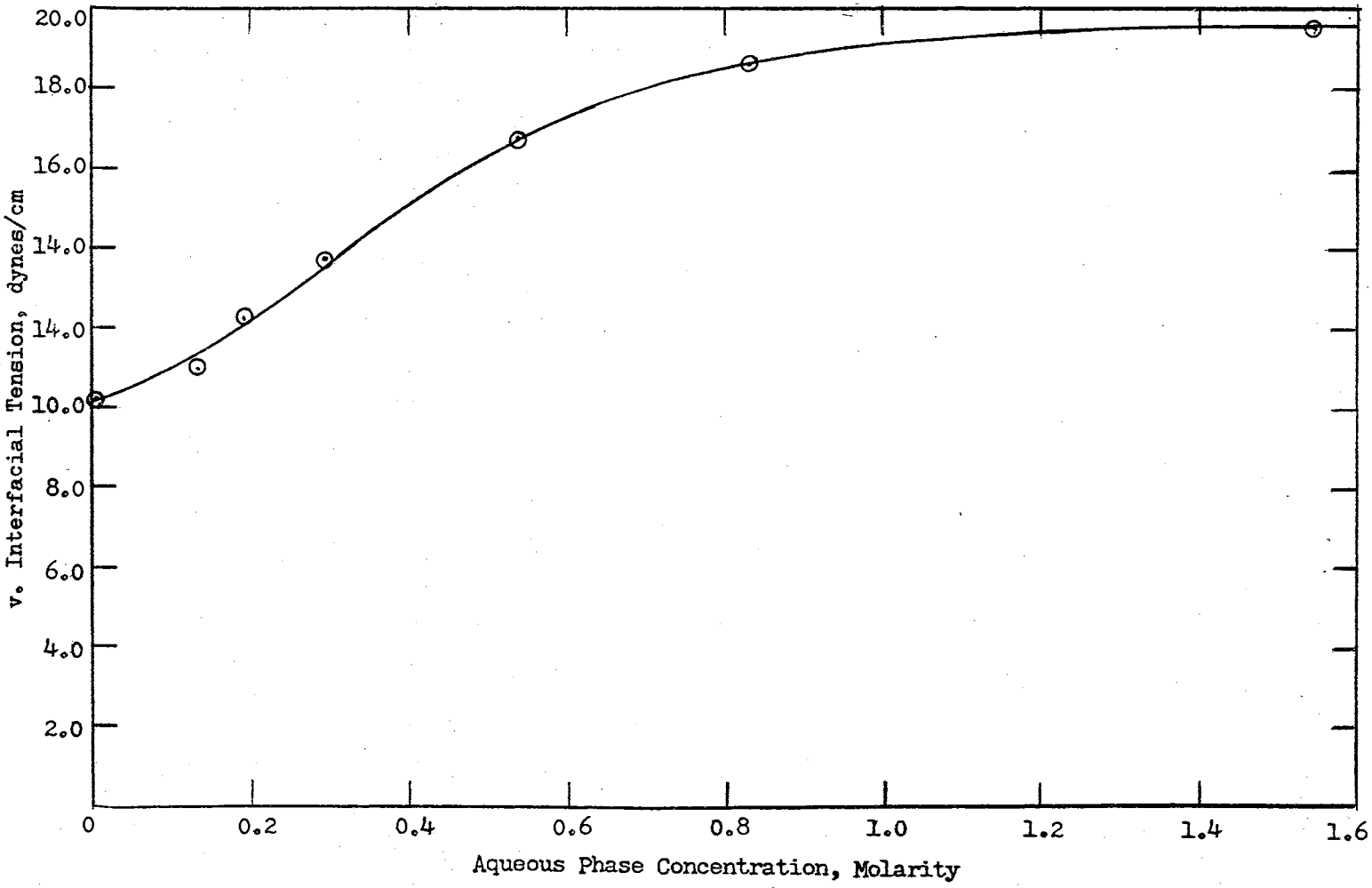

Figure 19.

Effect of Aqueous Phase Concentration on Interfacial Tension of the $UO_2(NO_3)_2$-Water-TBP System

might account for the effect of aqueous phase concentration level and driving force on the mass transfer coefficients. It should be noted that the rate of change of interfacial tension decreases with the concentration level. Interfacial tension data for the $UO_2(NO_3)_2$ - H_2O - TBP system at non-equilibrium conditions are necessary in order to further pursue this phenomenon.

Analog Simulation of Mass Transfer Cell

An analog simulation of the mass transfer cell is compared to the approach to steady-state for a run where uranyl nitrate is being transferred from TBP to water. Equations 11 and 12 were used as the mathematical model. The steady-state values for the simulation and the experimental run were equal. However, the experimental run approached steady-state conditions much faster than the model. This is in agreement with the unsteady-state data which showed that transfer rate decreased with time. The experimental run and the result of the mathematical model are shown in Figure 20.

Accuracy and Experimental Error

The accuracy of the mass transfer experimental data is affected by several factors. One of the more probable causes of experimental error is the purity of tributyl phosphate. Tributyl phosphate undergoes slow hydrolysis with time producing dibutyl and monobutyl phosphates and butanol. These hydrolysis products significantly affect the distribution coefficient. Dibutyl phosphate froms strong complexes with uranyl nitrate. In order to minimize this effect only one to two liters of TBP were purified at any one time. However, this degradation of TBP certainly may

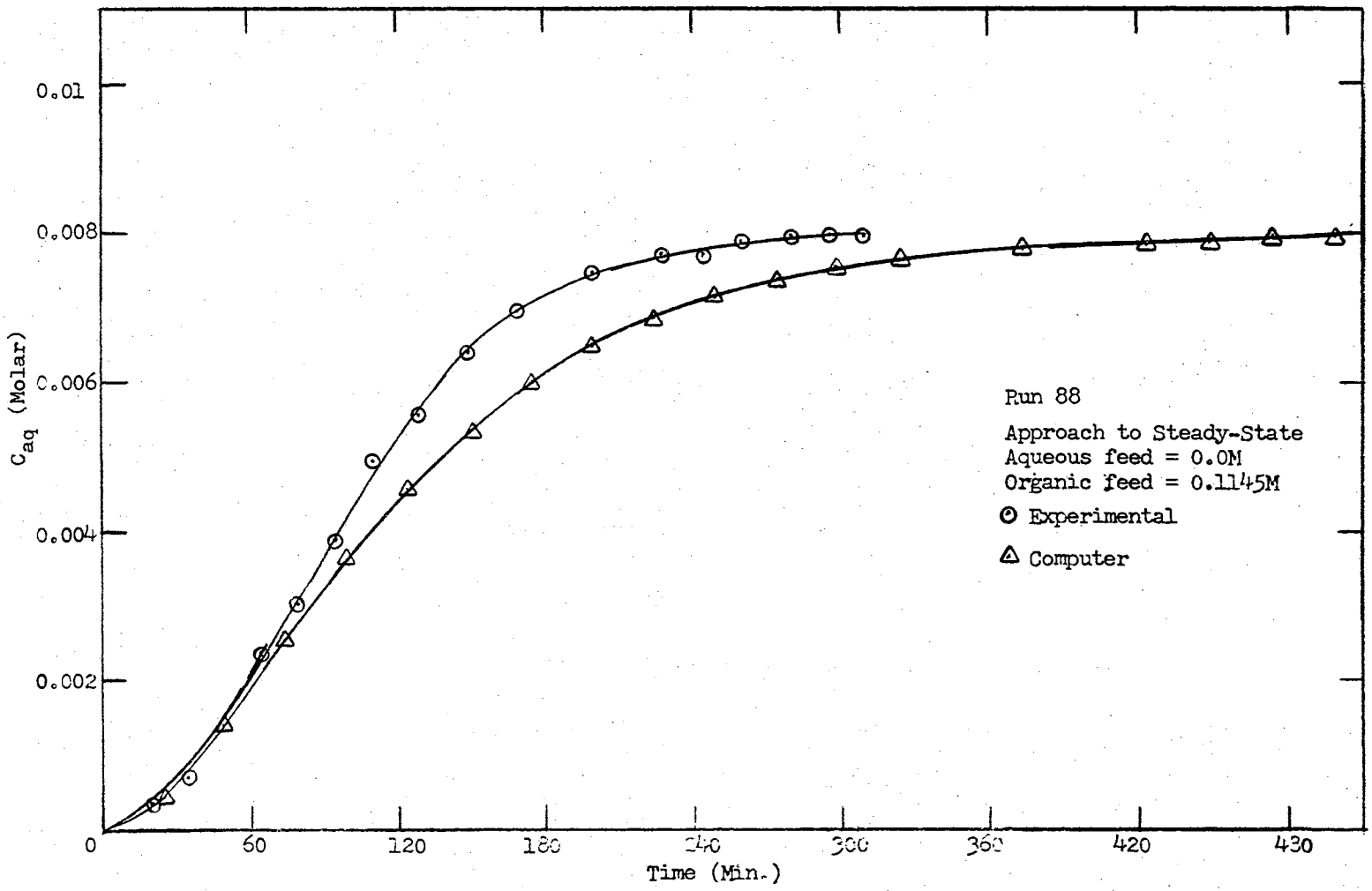

Figure 20.

Analog Computer Simulation of Mass Transfer Cell

partially account for the scatter of the experimental data.

The measurement of the stirring rates were with ± 1 rpm and thus the error was generally less than ± 1.0%.

The flow rates were measured to an accuracy of about ± 0.01 cc/min. This corresponds to ± 0.6%, which should not significantly affect the data.

The uranyl nitrate concentration was measured to an accuracy of ± 0.3%.

The material balance error was generally within ± 1.0%.

Another possible source of error is the movement or vibration of the mass transfer cell due to improper alignment of the stirring shafts and motors.

It is concluded that the two major sources of experimental error are:

1. Slow degradation of TBP.
2. Variations of the flow rates preventing the reaching of a "true" steady-state condition.

CHAPTER VII

CONCLUSIONS AND RECOMMENDATIONS

The interfacial transfer of uranyl nitrate across the water-TBP interface has been studied under unsteady and steady-state conditions in a stirred extraction cell.

The unsteady-state mass transfer coefficient for transfer of uranyl nitrate from water to TBP decreased with time. This cannot be explained on the basis of the build-up of an interfacial resistance with time.

The correlations presented in the literature do not properly predict the individual film coefficients for the transfer of uranyl nitrate across the water-TBP interface in the stirred extractor used in this study. The effect of the stirring rates on the transfer rate was much greater than is normally predicted. The mass transfer coefficient increased with the organic phase Reynolds number according to the following equation.

$$\frac{K_{os}}{v} = 3.56 \times 10^{-10} \, Re_s^{2.8}$$

By considering the energy transferred from the aqueous phase, the mass transfer coefficient was found to vary with $Re_s^{0.5}$ according to the relationship:

$$\frac{K_{os}}{v} = 6.529 \times 10^{-5} \, Re_s^{0.5} \left(1 + \frac{Re_w}{Re_s}\right)^{2.02}$$

The term, $(1 + \frac{Re_w}{Re_s})^{2.02}$, may be considered as a correction factor for the energy transmitted from the aqueous phase.

The steady-state transfer of uranyl nitrate from water to TBP was found to increase as the driving force was reduced. Furthermore, the rate of transfer was found to depend upon the organic phase concentration level, decreasing with the organic phase concentration level.

The steady-state transfer of uranyl nitrate from TBP to water increased with the driving force provided the data were adjusted for the organic phase Reynolds number. The rate of transfer was also found to increase with the aqueous phase concentration level. The effect of concentration driving force and concentration level might be due to interfacial turbulence if the two phases are not in equilibrium at the interface. In order to examine the hypothesis, data on the interfacial tension of the uranyl nitrate-water-TBP system are required at non equilibrium conditions.

The molar flux for transfer of uranyl nitrate between water and TBP decreased with decreasing driving force.

The mass transfer coefficients were dependent on convective diffusion rather than simple molecular diffusion.

Interfacial turbulence does not occur in the transfer of uranyl nitrate across the water-TBP interface due to the interfacial tension increasing with uranyl nitrate concentration.

The transfer rate from water to TBP is greater than for transfer in the reverse direction.

The steady-state transfer coefficients could not be adequately predicted from the unsteady-state data.

Recommendations

The steady-state transfer of uranyl nitrate should be studied in the presence of other inorganic nitrates such as nitric acid and aluminum nitrate.

The mass transfer cell should be modified to produce a larger surface area to volume ratio in order to increase the accuracy of the results.

The effect of temperature on the steady-state transfer of uranyl nitrate should be studied.

The flow patterns close to the interface should be investigated in order to better understand the hydrodynamics of the transfer cell.

A method should be developed to accurately determine the interfacial tensions of the uranyl nitrate-water-TBP system at non-equilibrium conditions and the data then used to predict whether the effect of concentration level and concentration driving force might be due to interfacial turbulence.

The uranyl nitrate solutions should be enriched with U-235 or U-233 and small solid state detectors be installed in the outlet flow lines to allow the continuous monitoring of the concentration and to improve the accuracy.

The effect of concentration level and concentration difference should be studied on other systems.

A correlation of the data by a chemical kinetic analysis approach, as done by Murdoch and Pratt, should be attempted.

BIBLIOGRAPHY

1. Abramzon, A. A. and M. V. Ostrovskii, Zhurnal Prikladnoi., 36; 789 (1963).

2. Abramzon, A. A. and M. V. Ostrovskii, Zhurnal Prikladnoi., 36; 793 (1963).

3. Alcock, K., G. F. Best, E. Hesford and H. A. C. McKay, J. Inorg. and Nuc. Chem., 4; 304 (1957).

4. Alcock, K., S. Grimley, T. Healey, J. Kennedy and H. A. C. McKay, Trans. Faraday Soc., 52; 39 (1956).

5. Alcock, K., W. H. Hardwick and H. A. C. McKay, J. Inorg. and Nuc. Chem., 4; 100 (1957).

6. Blokker, P. C., Proceedings of the Second International Congress of Surface Activity, Vol. 1, p 503 - 506. Academic Press, Inc., New York, 1957.

7. Burger, L. L.,
U. S. Atomic Energy Commission Document. HW - 19065 (1950).

8. Burger, L. L.,
U. S. Atomic Energy Commission Document. HW - 62087 (1959).

9. Burger, L. L. and R. C. Forsman,
U. S. Atomic Energy Commission Document. HW - 20936 (1951).

10. Chester, C. V.,
U. S. Atomic Energy Commission Document. ORNL - 3109 (1961).

11. Clagett, F.,
U. S. Atomic Energy Commission Document. HW - 17179 (1950)

12. Codding, J. W.,
U. S. Atomic Energy Commission Document. IDO - 14454 (1958).

13. Codding, J. W., W. Haas and F. K. Heumann, Ind. Eng. Chem., 50; 145 (1958).

14. Collopy, T. J.,
U. S. Atomic Energy Commission Document. NLCO - 749 (1958).

15. Collopy, T. J. and D. A. Stock,
U. S. Atomic Energy Commission Document. NLCO - 801 (1959).

16. Davies, J. T., Advances in Chemical Engineering, Vol. 4, p 20-33.
Academic Press, Inc., New York, 1963.

17. Dizdar, F. I. and I. D. Obrenovic, Proc. of Int. Conf. on the Peaceful Uses of Atomic Energy, 28; United Nations, New York, 1958.

18. Flannery, J. R., Proc. of Int. Conf. on the Peaceful Uses of Atomic Energy, 9; 258, United Nations, New York, 1956.

19. Finley, J. B., "Diffusion in Concentrated Uranyl Nitrate Solutions.," Ph. D. Thesis, Oklahoma State University, (1964).

20. Glueckhauf, E., H. A. C. McKay and A. R. Mathieson, J. Chem. Soc., S 299; (1949).

21. Gordon, K. F. and T. K. Sherwood, Chem, Eng. Prog. Symposium Series No. 10, Vol. 50, p 15. 1954.

22. Gresky, A. T.,
U. S. Atomic Energy Commission Document. ORNL - 1367 (1952).

23. Granquist, D. P. and E. T. Merrill,
U. S. Atomic Energy Commission Document. HW - 17747 (1951).

24. Hahn, H. T.,
U. S. Atomic Energy Commission Document. HW - 32626 (1954).

25. Higbie, R., Trans. Am. Inst. Chem. Eng., 31; 365 (1935).

26. Keisch, B.,
U. S. Atomic Energy Commission Document. IDO - 14490 (1959).

27. Lewis, J. B., AERE CE/R 1118 (1954).

28. Lewis, J. B., Chem. Eng. Sci., 3; 260 (1958).

29. Lewis, J. B., Chem. Eng. Sci., 8; 295 (1958).

30. Lewis, J. B., "An Interfacial Barrier Observed During Liquid - Liquid Extraction of Uranyl Nitrate," Nature, Vol. 178, 224 (1956).

31. Levitch, G. V., Physicochemical Hydrodynamics, Prentice Hall, Inc. N. J., 1962.

32. Loosemore, M. J. and A. P. Prosser, Chem. Eng. Sci., 18; 555 (1963).

33. Mayer, G. R. A., Chem. Eng. Sci., 16; 69 - 75 (1961).

34. Mayer, G. R. A. and J. T. Davies, Chem. Eng. Sci., 16; 55 - 66 (1961).

35. McKay, H. A. C. and A. R. Mathieson, Trans. Faraday Soc., 47; 248 (1951).

36. McKay, H. A. C., Chem. and Ind., 51; 1549 (1954).

37. McKay, H. A. C., J. Inorg. and Nuc. Chem., 4; 100 (1957).

38. McManamey, W. J., Chem. Eng. Sci., 15; 210 (1961).

39. Moore, R. L.,
U. S. Atomic Energy Commission Document. AECD - 3196 (1951).

40. Murdoch, R., and H. R. C. Pratt, AERE CE/R - 907 (1953).

41. Olander, D. R., and Manson Benedict, Nuclear Science and Engineering, 15; 359 (1963).

42. Olander, D. R., Chem. Eng. Sci., 18; 123 (1963).

43. Olander, D. R., and L. B. Reddy, Chem. Eng. Sci., 19; 67 (1964).

44. Olander, D. R., Chem. Eng. Sci., 19; 275 (1964).

45. Robinson, R. A., and C. K. Lim, J. Chem. Soc., 5; 1840 (1951).

46. Rodden, C. J.,
U. S. Atomic Energy Commission Document. TID - 10161 (1951).

47. Sato, T., J. Inorg. and Nuc. Chem., 6; 334 (1958).

48. Sato, T., J. Inorg. and Nuc. Chem., 9; 188 (1959).

49. Sternling, C. V., and L. E. Scriven, A. I. Ch. E. J., 5; 514 (1959).

50. Sherwood, T. K., and J. C. Wei, Ind. Eng. Chem., 49; 1030 (1957).

51. Ward, F. H., and L. H. Brooks, Trans. Faraday Soc., 48; 1124 (1952).

52. Whitman, W. G., Chem. Met. Eng., 29; 147 (1923).

NOMENCLATURE

a = activity

A = interfacial area - cm^2

C_s = concentration of organic phase - molar

C_w = concentration of aqueous phase - molar

C_s^* = concentration of organic phase in equilibrium with aqueous phase - molar

D = molecular diffusivity - $cm^2 sec^{-1}$

F = flow rate - cc/min

H = distribution coefficient

k_s = organic phase film transfer coefficient - cm/sec

k_w = aqueous phase film transfer coefficient - cm/sec

K_{os} = organic phase overall transfer coefficient - cm/sec

K_{ow} = aqueous phase overall transfer coefficient - cm/sec

K'_{os} = activity based organic phase overall transfer coefficient - cm/sec

L = stirrer diameter - cm

N = stirrer rate revolutions per second

n = stirrer rate - r.p.m.

Re = Reynolds Number - $\frac{NL^2}{\gamma}$

S_c = Schmidt Number $\frac{\mu}{\rho D}$

t = time - seconds

v = cell compartment volume - cc.

Greek Symbols

γ = activity coefficient

ρ = density of solution - gm/cc

μ = viscosity - centipoises

ν = kinematic viscosity - cm^2/sec

ω = stirrer rate -radians per second

APPENDIX A

Physical Properties of Uranyl Nitrate Solutions

The densities of 30% TBP uranyl nitrate solutions were determined by multiple weighting of 25 ml. volumetric flasks which were filled at 25° C. ± 0.05°C. The data are reported in Table XIII and Figure 21. In order to facilitate the use of this data in digital computer programs, the data were curve-fitted and the following relationship obtained.

$$\rho_s = 0.823 + 0.33C_s$$

Where:

ρ_s = density of solution, gm/cc

C_s = concentration of solution, mole/liter

The aqueous uranyl nitrate solution densities as determined by Finley (19) are given in Figure 21. The following equation was obtained by a regression analysis of the data.

$$\rho_w = 1.0 + 0.318\ C_w$$

Where:

ρ_w = density of solution, gm/cc

C_w = concentration of solution, mole/liter

The viscosities of 30% TBP uranyl nitrate solutions were determined using stand five milliliter Ostwald viscosimeters at 25° C ± 0.05°C. The data are reported in Table XIV and Figure 22. These data along with those reported by Finley (19) for aqueous uranyl nitrate solutions were curve-fitted to yield the following equations.

TABLE XIII

EXPERIMENTAL DATA

Densities of 30% TBP Uranyl Nitrate Solutions

Temp. 25°C ± 0.2°C

Uranyl Nitrate Concentration Molar	Weight of 25 cc. gm.	Density gm/cc
0.0	20.29765	0.8119
0.0814	21.03446	0.8414
0.1628	21.77097	0.8708
0.2442	22.48726	0.8995
0.3256	23.19734	0.9278
0.4070	23.93679	0.9575

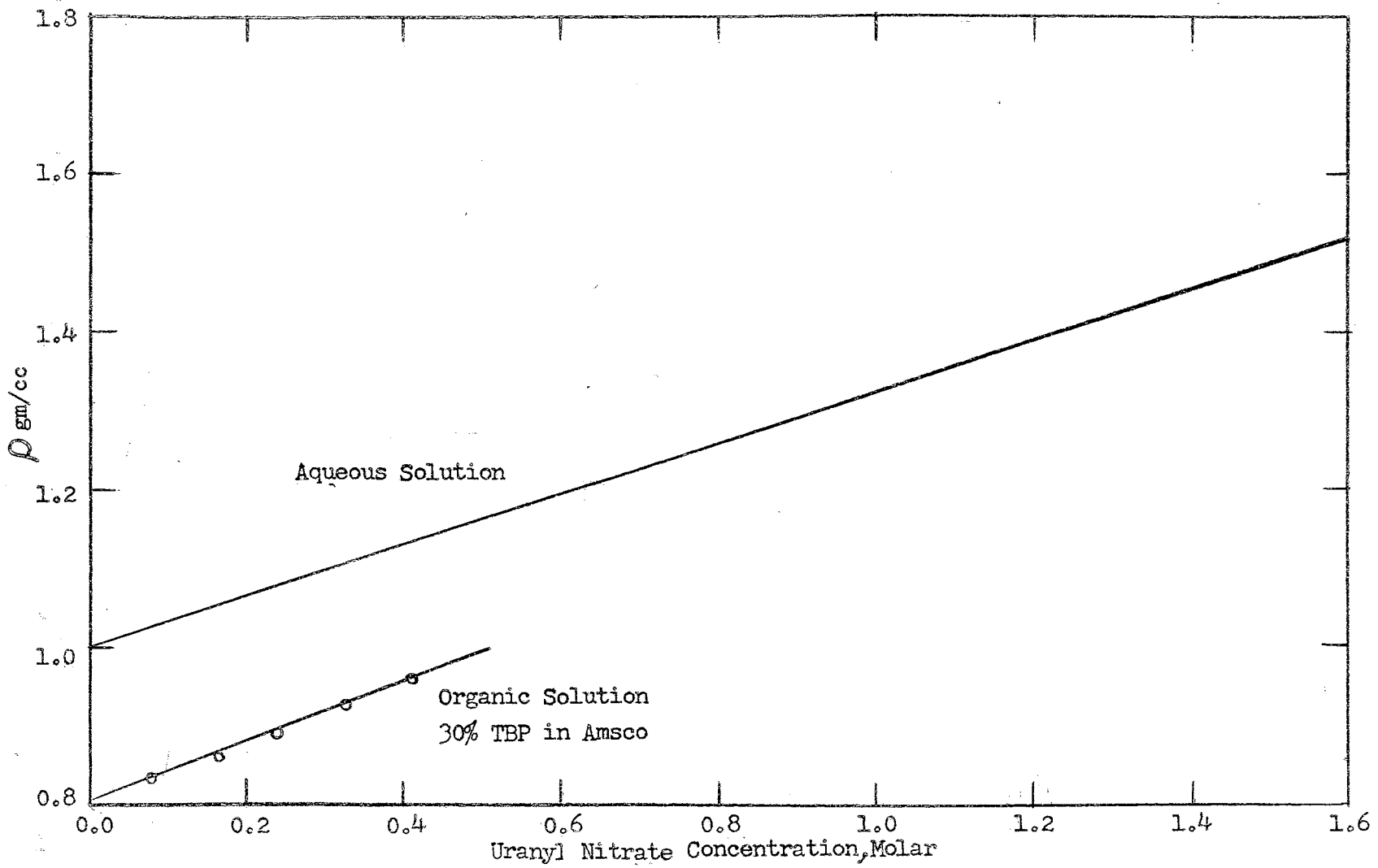

Figure 21.

Effect of Concentration on the Density of Uranyl Nitrate Solutions

TABLE XIV

EXPERIMENTAL DATA

Viscosities of 30% TBP Uranyl Nitrate Solutions

Temp. = 25° ± 0.2°C.

Solution	Oswald Tube No.	Number of Determinations	Average Flow Time Seconds	Viscosity Millipoise
Water	1	4	91.87	8.95
Water	2	3	98.66	8.95
30%TBP	1	3	222.22	17.60
0.0814M $UO_2(NO_3)_2$	2	3	255.73	19.60
0.1628M $UO_2(NO_3)_2$	1	4	264.93	22.50
0.2442M $UO_2(NO_3)_2$	1	3	286.66	25.10
0.3256M $UO_2(NO_3)_2$	2	3	330.60	28.10
0.407M $UO_2(NO_3)_2$	1	3	343.83	32.05

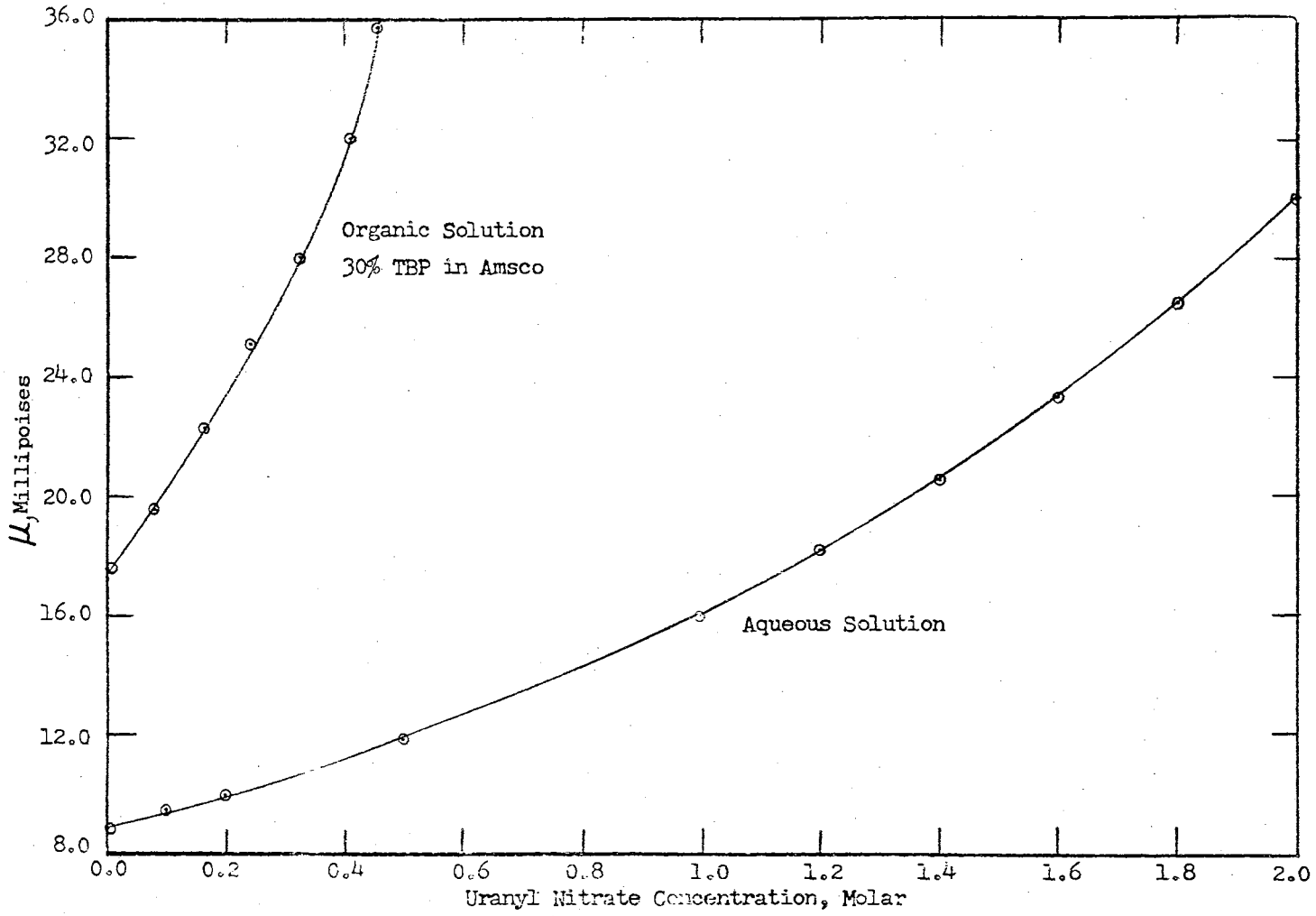

Figure 22.

Effect of Concentration on the Viscosity of Uranyl Nitrate Solutions

$$\mu_w = 9.069 + 3.411C_w + 3.504C_w^2$$

$$\mu_s = 17.562 + 24.08C_s + 27.623C_s^2$$

Where:

μ_i = viscosity of solution i, millipoises

Ci = concentration of solute in phase i, molar

Table XV presents the equilibrium distribution data for uranyl nitrate-water-TBP system.

The interfacial tension between water and 30% TBP uranyl nitrate solutions was determined using a Central Scientific Tensiometer at 25° C. In measureing the interfacial tension with a tensiometer, it is very important that the ring be cleaned and flamed between each determination. The data are reported in Table XVI.

Table XVII presents the activity coefficients for aqueous uranyl nitrate solutions.

TABLE XV

EXPERIMENTAL DATA

Distribution of Uranyl Nitrate between Water and 30% TBP in Amsco

Temp. = 25°C ± 0.3°C

Aqueous Phase Concentration Molar	Organic Phase Concentration Molar
0.0667	0.0276
0.0777	0.0342
0.0846	0.0358
0.0597	0.0180
0.0680	0.0274
0.0409	0.0079
0.0226	0.0018
0.0808	0.0362
0.1310	0.0880
0.2460	0.2390
0.3550	0.2910
0.2610	0.2600
0.3470	0.3020
0.5760	0.4080
1.1190	0.4430
0.1522	0.1100
0.2310	0.1413
0.6930	0.3980
1.5570	0.4780
0.1960	0.1570
0.5670	0.3600
0.2456	0.2355
0.1870	0.1366
0.0730	0.0342
1.1680	0.4363
1.4780	0.4460
0.6860	0.4000
1.5300	0.4680
1.2680	0.4470
0.3530	0.2960
0.2430	0.2280

TABLE XVI

EXPERIMENTAL DATA

Interfacial Tension of the
Water, Uranyl Nitrate, 30% TBP System

Temp. = 25°C ± 0.3°C

Uranyl Nitrate Concentration Molar		Apparent Interfacial Tension	Correction Factor	Interfacial Tension
Aqueous Phase	Organic Phase	Dyne/cm	F	Dyne/cm
0.0	0.0	11.15	0.918	10.23
0.1318	0.0987	12.00	0.917	11.00
0.1960	0.1629	13.20	0.926	12.21
0.2960	0.2710	14.69	0.936	13.75
0.5400	0.3740	17.83	0.939	16.75
0.831	0.4360	19.85	0.939	18.60
1.545	0.4700	21.60	0.905	19.55

TABLE XVII

Uranyl Nitrate Activity Coefficients

Density (gm/cc)	Molar	Gamma (molar)	Molal	Gamma (molal)	Activity
1.03152	.09923	.54715	.10000	.54300	.05429
1.06258	.19699	.51981	.20000	.51200	.10239
1.09317	.29328	.52168	.30000	.51000	.15299
1.12331	.38813	.53382	.40000	.51800	.20719
1.15300	.48159	.55440	.50000	.53400	.26699
1.18225	.57368	.58046	.60000	.55500	.33299
1.21110	.66449	.60888	.70000	.57800	.40459
1.23953	.75395	.64513	.80000	.60800	.48639
1.26754	.84213	.68504	.90000	.64100	.57689
1.29516	.92905	.73084	1.00000	.67900	.67899
1.34924	1.09929	.83071	1.20000	.76100	.91319
1.40182	1.26479	.94640	1.40000	.85500	1.19699
1.45300	1.42587	1.05815	1.60000	.94300	1.50879
1.50278	1.58256	1.23179	1.80000	1.08300	1.94939
1.55124	1.73509	1.40395	2.00000	1.21800	2.43599
1.66698	2.09942	1.90766	2.50000	1.60200	4.00499
1.77550	2.44100	2.45799	3.00000	2.00000	5.99999
1.87753	2.76216	3.00308	3.50000	2.37000	8.29499
1.97356	3.06440	3.44601	4.00000	2.64000	10.55999
2.06418	3.34963	3.82877	4.50000	2.85000	12.82499
2.14974	3.61897	4.15863	5.00000	3.01000	15.04999
2.23071	3.87382	4.54331	5.50000	3.20000	17.59999

APPENDIX B

TABLE XVIII

EXPERIMENTAL DATA

Unsteady-State Transfer
of Benzoic Acid

Temp. = 25°C ± 0.3°C

Transfer Direction
Toluene → Water

Run Series	Time Min.	Stirring Rates Aqueous Phase RPM	Organic Phase RPM	Organic Phase Conc. Molar	Aqueous Phase Conc. Molar	$K_{ow} \times 10^3$ cm/sec
1	0	58	40	2.000	0.0	
	60	58	40	1.955	0.0598	
	120	58	40	1.924	0.0989	
	180	58	40	1.892	0.1276	
	240	58	40	1.862	0.1509	
	300	58	40	1.831	0.1710	
						0.578
2	0	57	52	2.000	0.0000	
	30	57	52	1.945	0.0456	
	60	57	52	1.918	0.0753	
	120	57	52	1.869	0.1291	
	180	57	52	1.850	0.1615	
	240	57	52	1.827	0.1852	
						0.819
3	0	68	46	2.000	0.0000	
	30	68	46	1.958	0.0509	
	60	68	46	1.900	0.0906	
	120	68	46	1.844	0.1345	
	180	68	46	1.778	0.1803	
	240	68	46	1.740	0.2150	
						1.010

TABLE XIX

EXPERIMENTAL DATA

Effect of Stirring Rates on Transfer of Benzoic Acid

Temp. = 25°C. ± 0.3°C
Transfer Direction Toluene → Water

Time Min.	Stirring Rates Aqueous Phase RPM	Organic Phase RPM	Aqueous Phase Conc. Molar
120	70	43.5	0.001268
120	70	43.5	0.00128
120	75	43.5	0.001284
120	75	43.5	0.001302
120	75	43.5	0.001292
120	80	43.5	0.001284
120	80	43.5	0.001291
120	65	43.5	0.001253
120	66	43.5	0.001253
120	55.5	43.5	0.001135
120	60.6	43.5	0.001170

TABLE XX

EXPERIMENTAL DATA

Steady-State Transfer
of Benzoic Acid

Temp. = 25°C ± 0.3°C

Transfer Direction
Water → Toluene

Run	Flow Rates		Stirring Rates		Aqueous Phase Conc.		K_{ow}
	Aqueous	Organic	Aqueous	Organic			
	cm^3/min	cm^3/min	RPM	RPM	gm/liter in	gm/liter out	cm/sec x 10^3
	2.05	2.13	75	43.5	1.5	1.39	0.817
	2.00	2.00	75	43.5	1.5	1.388	0.820
	1.70	1.66	75	43.5	1.5	1.368	0.828
	1.37	1.31	75	43.5	1.5	1.340	0.853

TABLE XXI

EXPERIMENTAL DATA

Unsteady-State Transfer
of Uranyl Nitrate - A

Temp. = 25.0°C ± 0.3°C

Transfer Direction
Water ⟶ TBP

Run	Time Min.	Uranyl Nitrate Conc. Molar Aqueous	Organic	Stirring Rates Aqueous RPM	Organic RPM	$(C_{seq} - C_s)/C_{seq}$
20	0	0.300	0.000	75	60	1.000
	5	0.295	0.00291	75	60	0.973
	10	0.295	0.00323	75	60	0.970
	20	0.290	0.00518	75	60	0.952
	30	0.290	0.00734	75	60	0.934
	45	0.287	0.00978	75	60	0.914
	60	0.292	0.01320	75	60	0.884
	75	0.290	0.01510	75	60	0.866
21	0	0.300	0.000	75	60	1.000
	10	0.297	0.00352	75	60	0.968
	30	0.290	0.00928	75	60	0.918
	60	0.285	0.01470	75	60	0.868
	90	0.281	0.0179	75	60	0.840
	135	0.276	0.024	75	60	0.786
	180	0.269	0.0307	75	60	0.729
	240	0.254	0.0346	75	60	0.695
22	0	0.300	0.0000	75	60	1.000
	10	0.283	0.00475	75	60	0.964
	30	0.278	0.00761	75	60	0.935
	60	0.270	0.01575	75	60	0.860
	90	0.263	0.02063	75	60	0.816
	135	0.269	0.02940	75	60	0.740
23	0	0.300	0.0000	75	60	1.000
	30	0.283	0.00684	75	60	0.940
	60	0.282	0.01300	75	60	0.885
	120	0.278	0.02095	75	60	0.815
	180	0.274	0.03050	75	60	0.731
	240	0.263	0.03960	75	60	0.652
	300	0.243	0.05130	75	60	0.546

TABLE XXI (continued)

Run	Time Min.	Uranyl Nitrate Conc. Molar Aqueous	Organic	Stirring Rates Aqueous RPM	Organic RPM	$(C_{seq} - C_s)/C_{seq}$
24	0	0.300	0.0000	75	60	1.000
	30	0.298	0.00325	75	60	0.970
	60	0.288	0.00775	75	60	0.931
	120	0.293	0.01310	75	60	0.876
	180	0.283	0.0208	75	60	0.816
	240	0.277	0.0284	75	60	0.750
	300	0.273	0.0299	75	60	0.735
25	0	0.520	0.0000	75	60	1.000
	10	0.513	0.00606	75	60	0.970
	30	0.507	0.0109	75	60	0.950
	60	0.505	0.01775	75	60	0.920
	90	0.507	0.02290	75	60	0.900
	135	0.513	0.03650	75	60	0.840
26	0	0.527	0.0000	75	60	1.000
	10	0.520	0.00714	75	60	0.967
	30	0.517	0.01235	75	60	0.944
	60	0.515	0.02060	75	60	0.909
	90	0.507	0.02520	75	60	0.890
	135	0.505	0.03530	75	60	0.845
	180	0.488	0.04310	75	60	0.812
	240	0.462	0.05210	75	60	0.772
28	0	0.800	0.0000	75	60	1.000
	10	0.798	0.00710	75	60	0.978
	30	0.795	0.00873	75	60	0.973
	60	0.791	0.01375	75	60	0.958
	90	0.795	0.01705	75	60	0.947
	135	0.795	0.02110	75	60	0.936
	180	0.795	0.0332	75	60	0.900
	240	0.784	0.0414	75	60	0.873
29	0	0.800	0.0000	75	60	1.000
	10	0.791	0.00917	75	60	0.971
	36	0.796	0.01610	75	60	0.954
	60	0.791	0.01940	75	60	0.940
	95	0.791	0.02480	75	60	0.925
	135	0.795	0.0277	75	60	0.916
	180	0.797	0.0331	75	60	0.900
	240	0.784	0.0355	75	60	0.894

TABLE XXI (continued)

Run	Time Min.	Uranyl Conc. Aqueous	Nitrate Molar Organic	Stirring Rates Aqueous RPM	Stirring Rates Organic RPM	$(C_{seq} - C_s)/C_{seq}$
30	0	0.300	0.0000	75	60	1.000
	10	0.294	0.00410	75	60	0.971
	30	0.289	0.00672	75	60	0.954
	60	0.285	0.01365	75	60	0.907
	90	0.268	0.01870	75	60	0.873
	136	0.268	0.02010	75	60	0.864
	180	0.264	0.03740	75	60	0.743
	240	0.259	0.04350	75	60	0.701
	300	0.244	0.05130	75	60	0.649
31*	0	0.300	0.0000	75	60	1.000
	10	0.298	0.00446	75	60	0.970
	25	0.293	0.00620	75	60	0.959
	55	0.281	0.01040	75	60	0.928
	92	0.275	0.01460	75	60	0.901
	130	0.275	0.01760	75	60	0.880
	180	0.275	0.02255	75	60	0.847
	240	0.259	0.02860	75	60	0.805
32	0	0.300	0.0000	78	60	1.000
	10	0.280	0.00473	78	60	0.965
	25	0.289	0.00706	78	60	0.945
	55	0.276	0.01225	78	60	0.904
	90	0.263	0.01780	78	60	0.864
	135	0.256	0.02150	78	60	0.843
	180	0.250	0.02700	78	60	0.784
	300	0.244	0.03520	78	60	0.729

* Volume of organic phase was 65.7 cc.

TABLE XXII

EXPERIMENTAL DATA

Unsteady-State Transfer of Uranyl Nitrate - B

Temp. = 25°C. ± 0.3° C.

Transfer Direction Water ⟶ TBP

Run	Time Min.	Initial Conc. Aqueous Molar	Initial Conc. Organic Molar	Stirring Rates Aqueous RPM	Stirring Rates Organic RPM	Transfer Integral cm/sec x 10^3	Coefficient Point cm/sec x 10^3
34	8	0.3	0.0	214	250	2.167	1.618
	16	0.3	0.0	214	250	1.951	1.538
	25	0.3	0.0	214	250	1.719	1.425
	38	0.3	0.0	214	250	1.432	1.198
	55	0.3	0.0	214	250	1.244	0.847
	80	0.3	0.0	214	250	1.151	0.212
36	5	0.3	0.0	155	176	1.218	0.397
	10	0.3	0.0	155	176	0.738	0.393
	20	0.3	0.0	155	176	0.518	0.384
	30	0.3	0.0	155	176	0.433	0.374
	45	0.3	0.0	155	176	0.428	0.362
	75	0.3	0.0	155	176	0.386	0.321
	123	0.3	0.0	155	176	0.324	0.264
	180	0.3	0.0	155	176	0.317	0.182
37	5	0.3	0.0	154	173	1.860	0.629
	10	0.3	0.0	154	173	1.418	0.622
	20	0.3	0.0	154	173	0.958	0.602
	36	0.3	0.0	154	173	0.785	0.572
	58	0.3	0.0	154	173	0.656	0.524
	80	0.3	0.0	154	173	0.510	0.456
	120	0.3	0.0	154	173	0.507	0.354
	180	0.3	0.0	154	173	0.452	0.144
38	11	0.5	0.0	154	175	3.984	0.702
	20	0.5	0.0	154	175	2.287	0.674
	35	0.5	0.0	154	175	1.694	0.643
	55	0.5	0.0	154	175	1.145	0.576
	81	0.5	0.0	154	175	0.861	0.491
	180	0.5	0.0	154	175	0.645	0.307

TABLE XXII (continued)

Run	Time Min.	Initial Conc. Aqueous Molar	Organic Molar	Stirring Rates Aqueous RPM	Organic RPM	Transfer Integral cm/sec x 10^3	Coefficient Point cm/sec x 10^3
39	5	0.5	0.0	148	176	4.090	0.928
	10	0.5	0.0	148	176	2.277	0.904
	20	0.5	0.0	148	176	1.587	0.865
	35	0.5	0.0	148	176	1.204	0.789
	55	0.5	0.0	148	176	0.865	0.672
	81	0.5	0.0	148	176	0.779	0.547
	120	0.5	0.0	148	176	0.574	0.221
	180	0.5	0.0	148	176	0.531	
40	5	0.5	0.0	147	175	5.908	1.161
	10	0.5	0.0	147	175	3.248	1.127
	21	0.5	0.0	147	175	2.010	1.096
	36	0.5	0.0	147	175	1.543	1.035
	55	0.5	0.0	147	175	1.180	0.933
	80	0.5	0.0	147	175	0.983	0.793
	133	0.5	0.0	147	175	0.781	0.457
41	10	0.8	0.0	146	175	2.470	1.229
	20	0.8	0.0	146	175	1.830	1.124
	35	0.8	0.0	146	175	1.331	0.927
	56	0.8	0.0	146	175	1.005	0.623
	80	0.8	0.0	146	175	0.827	0.253
	120	0.8	0.0	146	175	0.713	
42	5	0.8	0.0	148	175	3.344	2.138
	10	0.8	0.0	148	175	2.901	2.085
	20	0.8	0.0	148	175	2.596	1.866
	38	0.8	0.0	148	175	1.765	1.419
	55	0.8	0.0	148	175	1.541	0.977
	81	0.8	0.0	148	175	1.156	0.209
	120	0.8	0.0	148	175	0.978	
	180	0.8	0.0	148	175	0.791	

TABLE XXIII

EXPERIMENTAL DATA

Steady-State Transfer of Uranyl Nitrate

Temp. = 25° C ± 0.3° C

Transfer Direction Water ⟶ TBP

Run	Flow Rate cc/min		Uranyl Nitrate Concentration Molar		Stirring Rates RPM		Driving Force Molar	Overall Mass Transfer Coefficient $K_{os} \times 10^3$ cm/sec
	Aqueous	Organic	Aqueous	Organic	Aqueous	Organic		
43	1.80	1.70	0.289	0.0214	153	175	0.221	0.745
44	1.27	1.88	0.273	0.0153	150	175	0.225	0.600
45	1.50	1.50	0.260	0.0388	150	175	0.191	1.425
46	1.50	1.50	0.258	0.0650	150	175	0.165	2.770
47	1.50	1.48	0.292	0.0238	153	175	0.211	0.753
49	1.49	1.50	0.261	0.0261	150	175	0.213	0.861
50	1.50	1.51	0.268	0.0281	151	175	0.214	0.925
51	1.49	1.50	0.264	0.0259	151	175	0.219	0.830
56	1.62	1.77	0.242	0.0461	150	175	0.176	2.140
57	1.98	2.00	0.253	0.0461	150	175	0.184	2.330
60	1.73	2.06	0.269	0.0293	150	175	0.219	1.325
62	1.52	1.50	0.286	0.0094	100	60	0.231	0.263
63	1.52	1.48	0.258	0.0370	100	110	0.203	1.267
64	1.52	1.48	0.258	0.0370	100	130	0.203	1.267
65	1.493	1.523	0.3048	0.00136	100	45	0.2706	0.036
66	1.51	1.55	0.300	0.0063	100	75	0.2637	0.174

TABLE XXIII (continued)

EXPERIMENTAL DATA

Steady-State Transfer of Uranyl Nitrate

Temp. = 25° C ± 0.3° C

Transfer Direction
Water ⟶ TBP

Run	Flow Rates cc/min		Uranyl Nitrate Concentration Molar		Stirring Rates RPM		Driving Force Molar	Overall Mass Transfer Coefficient $K_{os} \times 10^3$ cm/sec
	Aqueous	Organic	Aqueous	Organic	Aqueous	Organic		
67	1.51	1.525	0.294	0.01264	100	90	0.2599	0.354
68	1.56	1.58	0.2975	0.02038	100	105	0.2442	0.605
69	1.56	1.58	0.3015	0.0144	100	80	0.2520	0.395
70	1.49	1.51	0.258	0.0356	100	116	0.2019	1.36
71	1.53	1.51	0.292	0.01872	100	100	0.2462	0.535
72	1.53	1.50	0.293	0.01865	100	120	0.2473	0.531
73	1.52	1.50	0.294	0.01345	100	80	0.2585	0.374
75	1.495	1.498	0.293	0.01059	100	55	0.2544	0.291
76	1.494	1.52	0.290	0.0068	100	64	0.2581	0.180
77	1.514	1.500	0.4899	0.0254	100	100	0.3135	0.5698
80	1.507	1.510	0.4229	0.0340	100	100	0.2874	0.8366
81	1.497	1.511	0.7180	0.0341	100	100	0.3557	0.6786
82	1.490	1.482	0.9489	0.0284	100	100	0.3991	0.4942
83	1.495	1.485	0.9266	0.0267	100	100	0.3977	0.4670
99	1.513	1.515	0.5568	0.0281	100	100	0.3271	0.6112

TABLE XXIII (continued)

EXPERIMENTAL DATA

Steady-State Transfer of Uranyl Nitrate

Temp. = 25° C ± 0.3° C

Transfer Direction Water ⟶ TBP

Run	Flow Rates cc/min Aqueous	Organic	Uranyl Nitrate Concentration Molar Aqueous	Organic	Stirring Rates RPM Aqueous	Organic	Driving Force Molar	Overall Mass Transfer Coefficient $K_{os} \times 10^3$ cm/sec
100	1.515	1.515	0.1448	0.0157	100	100	0.0894	1.2520
101	1.5400	1.515	0.1831	0.0185	100	100	0.1336	0.9871

Transfer Direction TBP ⟶ Water

84	1.519	1.515	0.0249	0.4371	100	100	0.4364	0.4070
85	1.530	1.521	0.0161	0.3187	100	100	0.3192	0.3631
86	1.520	1.520	0.0132	0.2163	100	100	0.2169	0.4339
87	1.488	1.518	0.0080	0.1076	100	100	0.1080	0.5185
88	1.634	1.545	0.0241	0.3127	100	100	0.3121	0.4070
89	1.498	1.503	0.0241	0.2023	100	100	0.2017	0.4062
90	1.508	1.498	0.0257	0.1094	100	100	0.1085	0.4796
91	1.503	1.498	0.2248	0.4185	100	100	0.2177	0.5610
92	1.509	1.497	0.2300	0.4503	100	100	0.2439	0.5250
93	1.489	1.435	0.2392	0.3285	100	100	0.1125	0.6482
94	1.496	1.494	0.1293	0.4454	100	100	0.3590	0.3809
95	1.50	1.492	0.1289	0.2103	100	100	0.1242	0.5272

APPENDIX C

TABLE XXIV

CALCULATED RESULTS

Steady-State Transfer of Uranyl Nitrate

Run	Reynolds Number Aqueous	Reynolds Number Organic	Schmidt Number x 10^3 Aqueous	Schmidt Number x 10^3 Organic	$(C_S^* - C_S)$ Molar	$(A_W - A_S)$	K_{os}/ν x 10^2 cm^{-1}	K_{os}/ν_2 x 10^2 cm^{-1}
43	2150	1088	1.423	12.48	0.2210	0.118	3.38	6.33
44	2130	1100	1.415	12.30	0.2257	0.104	2.76	5.99
45	2140	1070	1.410	12.60	0.1912	0.096	6.39	12.73
46	2140	1042	1.405	13.02	0.1650	0.080	12.01	28.70
47	2150	1083	1.425	12.43	0.2112	0.123	3.42	5.87
49	2140	1088	1.410	12.45	0.2129	0.100	3.91	8.32
50	2135	1081	1.412	12.45	0.214	0.102	4.20	8.77
51	2142	1088	1.410	12.43	0.219	0.102	3.78	8.12
56	2140	1062	1.408	12.85	0.176	0.092	9.48	18.06
57	2139	1060	1.409	12.85	0.184	0.097	10.32	19.56
60	2135	1078	1.412	12.52	0.219	0.099	5.78	12.81
62	1405	427	1.420	10.80	0.251	0.107	1.21	2.84
63	1422	676	1.410	11.20	0.203	0.100	5.92	12.02
64	1422	1033	1.41	11.20	0.203	0.100	5.92	12.02
65	1403	287	1.43	12.05	0.271	0.148	0.168	0.31
66	1407	476	1.42	12.12	0.264	0.148	0.811	1.45
67	1409	566	1.42	12.25	0.260	0.130	1.63	1.26
68	1409	650	1.43	12.41	0.244	0.126	2.88	5.56
69	1409	499	1.43	12.30	0.257	0.130	1.80	3.56
70	1420	706	1.41	12.60	0.201	0.100	6.13	12.37
71	1410	625	1.43	12.32	0.246	0.125	2.46	4.86

TABLE XXIV (continued)

CALCULATED RESULTS

Steady-State Transfer of Uranyl Nitrate

Run	Reynolds Number		Schmidt Number x 10^3		$(C_s^* - C_s)$	$(A_w - A_s)$	K_{os}/v x 10^2	K_{os}/v_2 x 10^2
	Aqueous	Organic	Aqueous	Organic	Molar		cm^{-1}	cm^{-1}
72	1410	750	1.42	12.32	0.247	0.125	2.43	4.80
73	1407	503	1.42	12.25	0.253	0.126	1.71	3.45
75	1408	348	1.42	12.25	0.254	0.129	1.34	2.64
76	1399	407	1.42	12.13	0.258	0.144	0.84	1.61
77	1360	616	0.94	12.1	0.313	0.251	2.57	3.23
80	1388	610	1.10	12.23	0.287	0.200	3.75	5.38
81	1257	610	0.552	12.23	0.356	0.426	3.04	2.54
82	1148	614	0.338	12.17	0.399	0.693	2.22	1.29
83	1158	615	0.354	12.15	0.398	0.280	2.11	1.26
99	1331	613	0.802	12.16	0.327	0.300	2.75	2.99
100	1479	621	1.885	12.02	0.089	0.054	5.71	9.36
101	1470	620	1.809	12.05	0.134	0.056	4.48	10.80
84	1500	396	1.553	18.88	0.436 *	0.861 **	1.18	0.599
85	1501	450	1.449	16.59	0.319 *	0.218 **	1.20	1.744
86	1501	504	1.408	14.82	0.217 *	0.118 **	1.60	2.936
87	1502	566	1.322	13.18	0.108 *	0.060 **	2.15	3.878
88	1500	453	1.544	16.48	0.312 *	0.209 **	1.35	2.020
89	1500	512	1.544	14.59	0.202 *	0.315 **	1.524	1.183
90	1500	565	1.560	13.21	0.108 *	0.0478 **	1.99	4.514

* $(C_s - C_s^*)$

** $(A_s - A_w)$

TABLE XXIV (continued)

CALCULATED RESULTS

Steady-State Transfer of Uranyl Nitrate

Run	Reynolds Number Aqueous	Reynolds Number Organic	Schmidt Number x 10^3 Aqueous	Schmidt Number x 10^3 Organic	$(C_s - C_s^*)$ Molar	$(A_s - A_w)$	K_{os}/ν x 10^2 cm^{-1}	K_{os}/ν_2 x 10^2 cm^{-1}
91	1458	404	1.694	18.50	0.218	0.625	1.66	0.058
92	1457	390	1.679	19.15	0.244	1.090	1.502	0.034
93	1454	445	1.651	16.77	0.112	0.1375	2.117	1.732
94	1483	392	1.902	19.05	0.359	0.941	1.095	0.042
95	1483	507	1.902	14.72	0.124	0.0585	1.961	4.164

TABLE XXV

Variation of Mass Transfer Coefficient with Molecular Diffusivity

$\frac{K_{os}}{\nu(C_s^* - C_s)}$ x 10^2 cm-l/sec-mole	D x 10^6 cm^2/sec
8.2	7.3
13.0	6.8
8.56	8.73
5.56	9.25
8.40	7.55
5.29	9.15
63.7	4.83
33.45	4.93
11.61	5.65
9.95	5.63

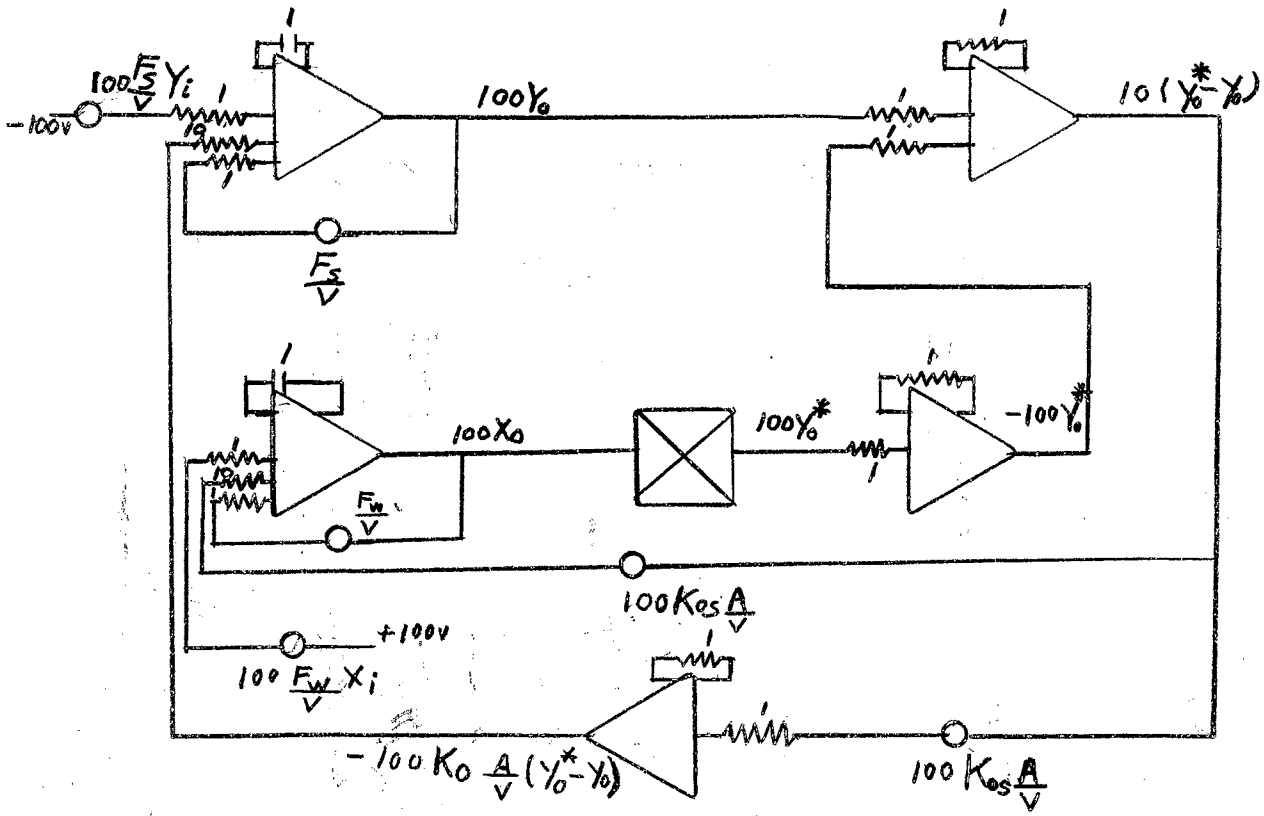

Figure 23.

Analog Computer Simulation
of Mass Transfer Cell

APPENDIX D

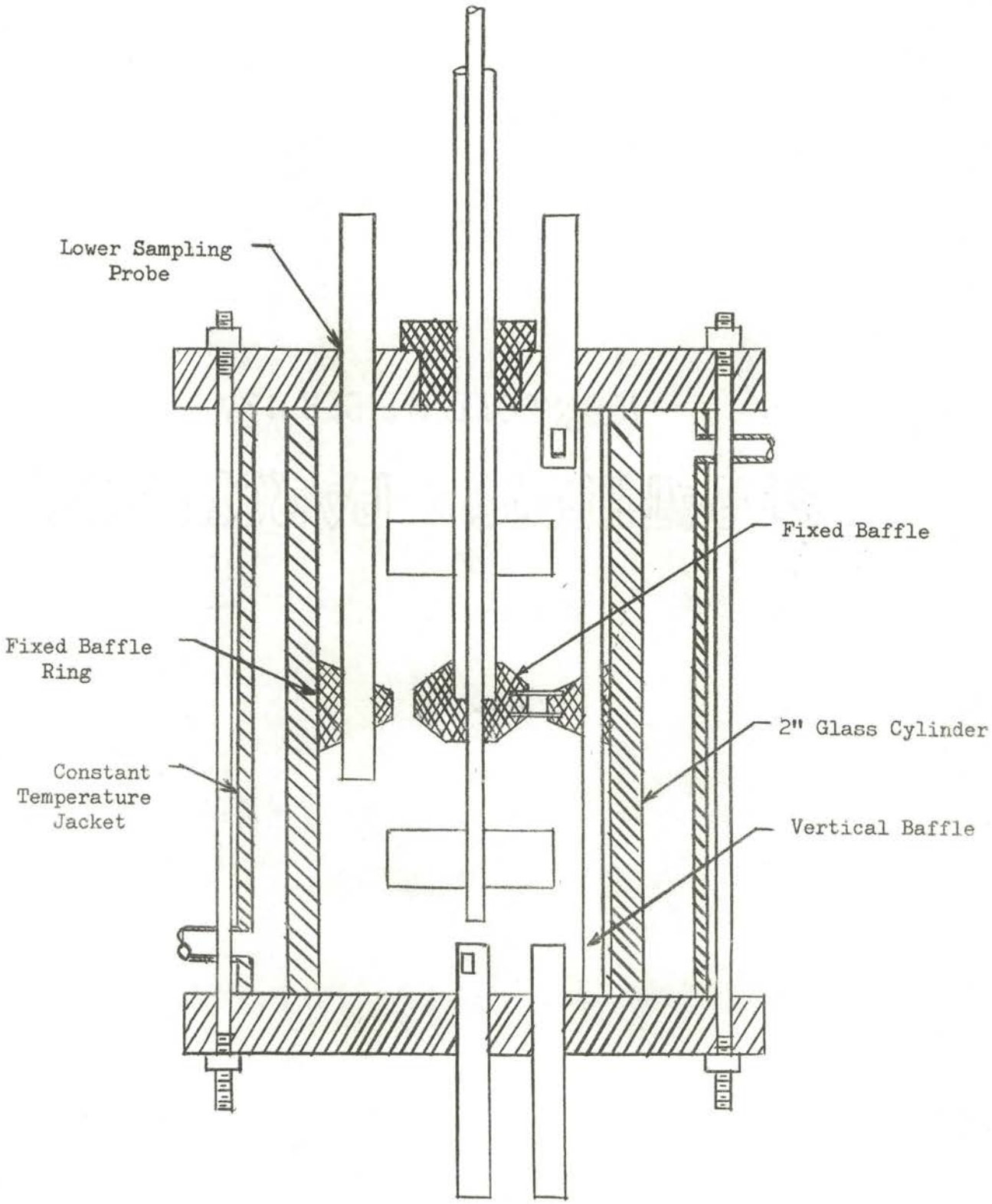

Figure 24.

Stirred Extraction Cell Schematic

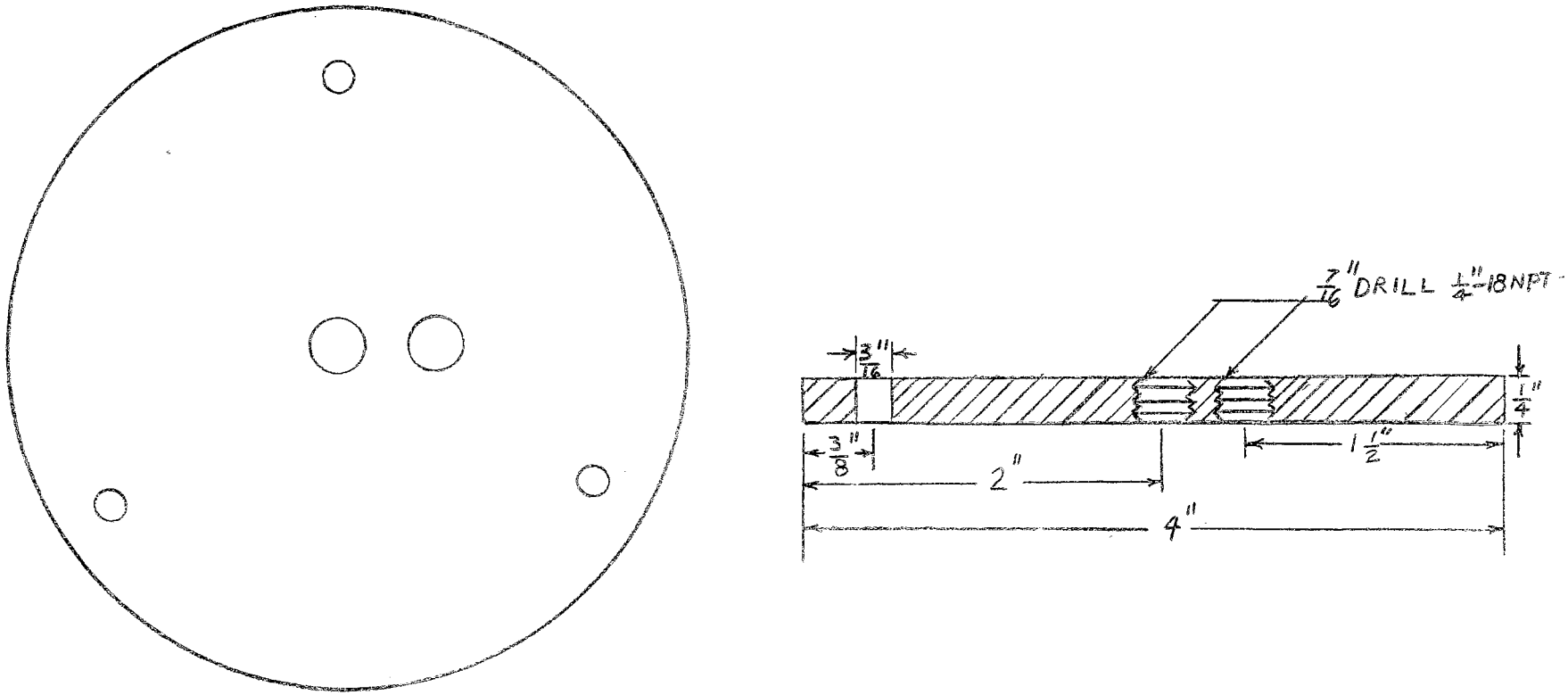

Figure 25.

Cell Bottom Plate Design

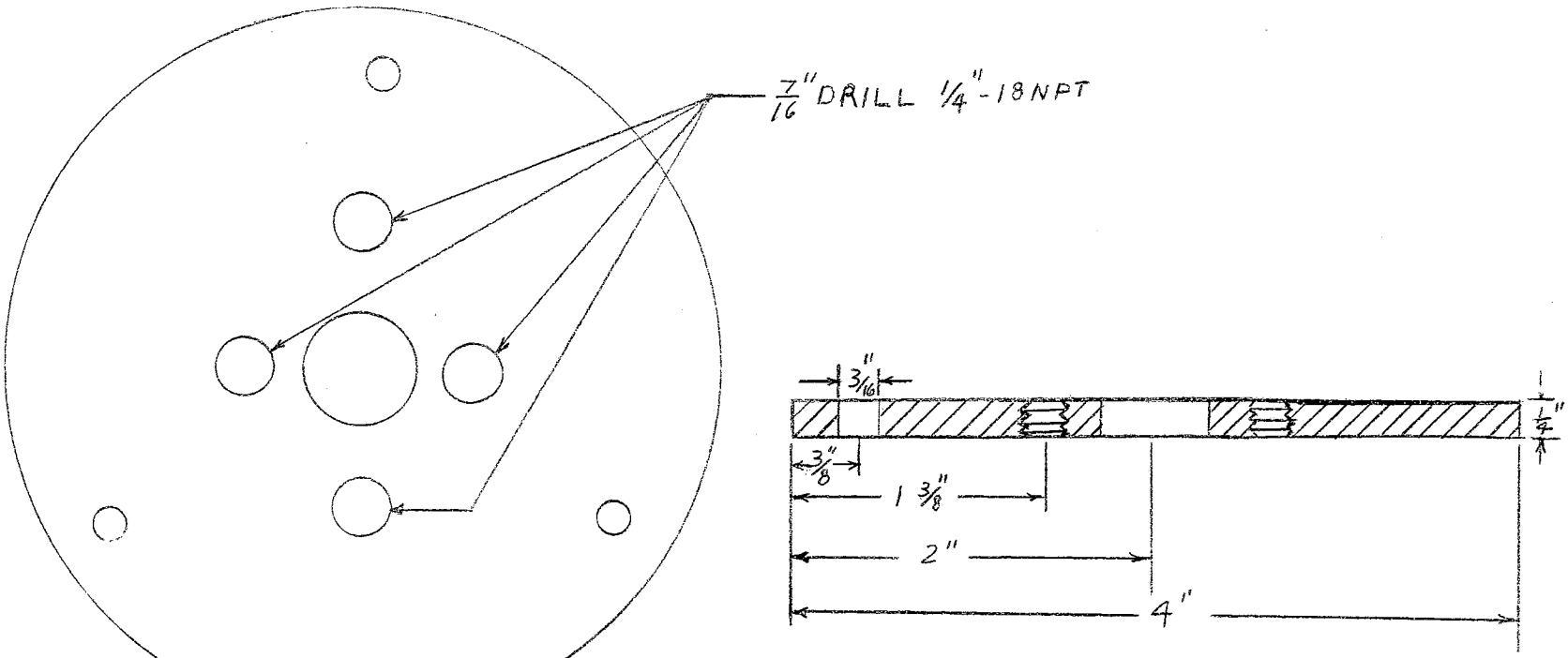

Figure 26.

Cell Top Plate Design

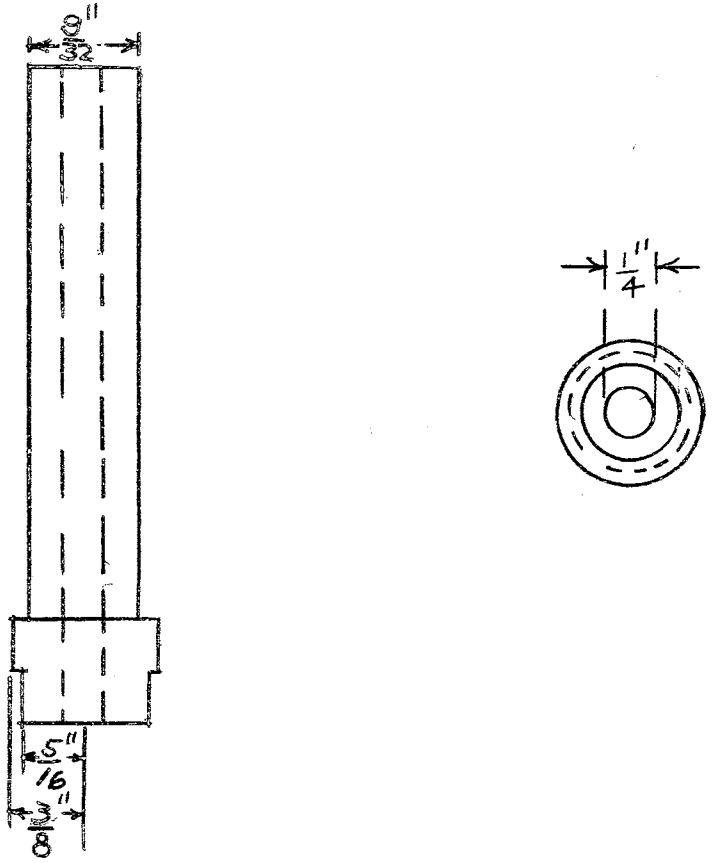

Figure 27.

Upper Stirrer Bearing Design

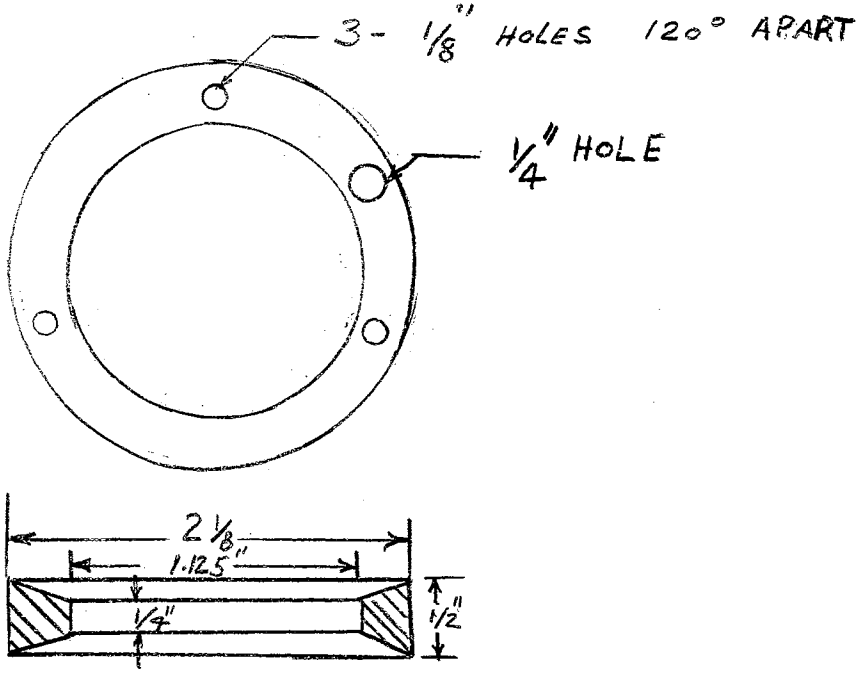

Fixed Baffle

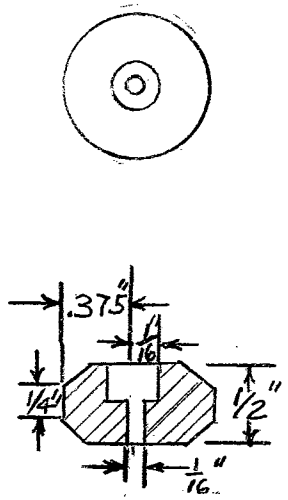

Center Baffle

Figure 28.

Fixed and Center Baffle Design

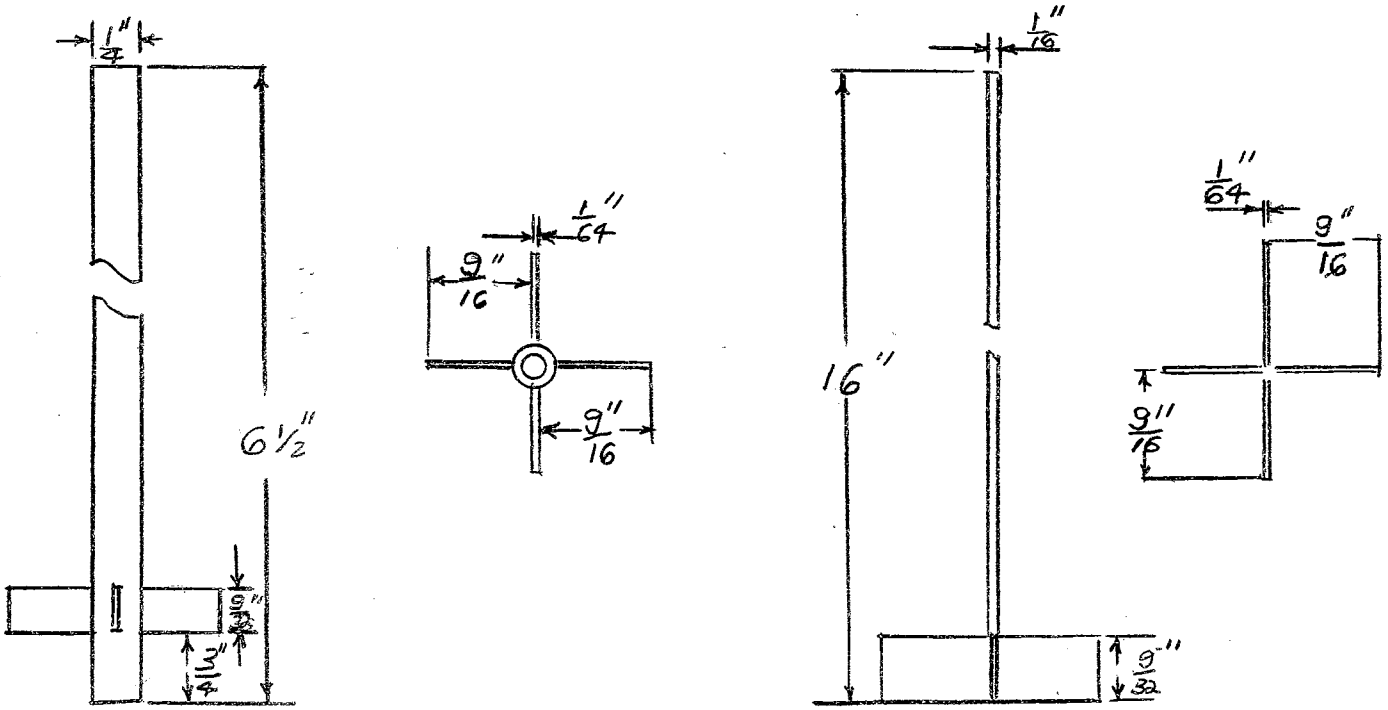

Upper Stirrer

Lower Stirrer

Figure 29.

Upper and Lower Stirrer Design

VITA

Dale Edward Bush

Candidate for the degree of

Doctor of Philosophy

Thesis: EFFECT OF CONCENTRATION DIFFERENCE ON THE RATES OF TRANSFER OF URANYL NITRATE BETWEEN WATER AND TBP

Major Field: Chemical Engineering

Biographical:

Person Data: Born in Detroit, Michigan, November 4, 1937, the son of Edward F. and Evelyn I. Bush.

Education: Attended grade school in Detroit, Michigan; graduated in 1955 from Cooley High School, Detroit, Michigan; received the Bachelor of Science in Chemical Engineering from the Michigan Technological University in 1959; received the Master of Science in Nuclear Engineering from the Michigan Technological University in 1960; completed the requirements for the Doctor of Philosophy degree in May, 1966.

Professional Experience: Summer employment in the Chemical Engineering Division of the Argonne National Laboratory, Argonne, Illinois, June to September 1959. At present, an engineer in the Research and Engineering Section of the Douglass United Nuclear Corporation. Membership in scholarly or professional societies includes Tau Beta Pi, Sigma Xi, Phi Kappa Phi, Phi Lambda Upsilon, Omega Chi Epsilon, and the American Institute of Chemical Engineers.